
Masters Theses

Student Theses and Dissertations

Fall 1984

Thermally stimulated current studies of barium titanate capacitors

Patrick Donald Martin

Follow this and additional works at: https://scholarsmine.mst.edu/masters_theses



Part of the [Ceramic Materials Commons](#)

Department:

Recommended Citation

Martin, Patrick Donald, "Thermally stimulated current studies of barium titanate capacitors" (1984). *Masters Theses*. 222.

https://scholarsmine.mst.edu/masters_theses/222

This thesis is brought to you by Scholars' Mine, a service of the Missouri S&T Library and Learning Resources. This work is protected by U. S. Copyright Law. Unauthorized use including reproduction for redistribution requires the permission of the copyright holder. For more information, please contact scholarsmine@mst.edu.

THERMALLY STIMULATED CURRENT STUDIES
OF BARIUM TITANATE CAPACITORS

BY

PATRICK DONALD MARTIN, 1958-

A THESIS

Presented to the Faculty of the Graduate School of the

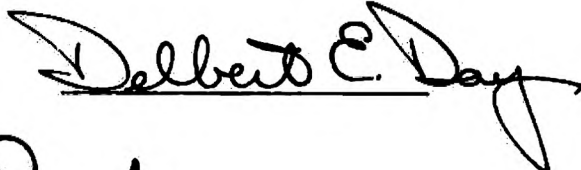
UNIVERSITY OF MISSOURI-ROLLA

In Partial Fulfillment of the Requirements of the Degree

MASTER OF SCIENCE IN CERAMIC ENGINEERING

1984

Approved by

 (Advisor) 


ABSTRACT

Thermally stimulated polarization current (TSPC) and thermally stimulated depolarization current (TSDC) measurements were used to study sample current behavior based on the thermally activated release of trapped charges and polarization mechanisms. Samples studied included laboratory-prepared barium titanate samples (the barium to titanium ratio ranging from 0.96 to 1.04) and commercial ceramic capacitors. Both TSPC and TSDC showed the current spectra of the barium titanate samples were a function of crystal structure and the Ba/Ti ratio. The TSPC/TSDC results of the ceramic capacitors showed differences between capacitor formulations. TSPC/TSDC results also showed differences between good capacitors (physically and electrically) and capacitors having failed under test conditions. The usefulness of the TSPC/TSDC measurement technique to determine capacitor reliability was also shown.

ACKNOWLEDGEMENT

This research was funded by the Office of Naval Research under Contract no. ONR N00014-82-K-0294 and its support is gratefully acknowledged.

TABLE OF CONTENTS

	Page
ABSTRACT.....	ii
ACKNOWLEDGEMENT.....	iii
TABLE OF CONTENTS.....	iv
LIST OF ILLUSTRATIONS.....	vi
LIST OF TABLES.....	ix
I. INTRODUCTION.....	1
II. LITERATURE REVIEW.....	3
A. TSPC/TSDC REVIEW AND RELATED STUDIES.....	3
B. REVIEW OF RELATED WORK ON BARIUM TITANATE.....	7
C. FERROELECTRICITY AND BARIUM TITANATE.....	10
D. CAPACITOR RELIABILITY.....	16
III. EXPERIMENTAL PROCEDURE.....	18
A. DESCRIPTION OF EQUIPMENT.....	18
B. SAMPLE PREPARATION.....	21
C. TSPC/TSDC MEASUREMENT PROCEDURE.....	24
IV. RESULTS AND DISCUSSION.....	26
A. BARIUM TITANATE CURRENT SPECTRA.....	26
1. Rhombohedral to Orthorhombic Structure.....	26
2. Orthorhombic to Tetragonal Structure.....	35
3. Tetragonal to Cubic Structure.....	41
4. Sample Microstructure.....	43
5. Activation Energy/Resistivity.....	50
B. CAPACITOR EXAMINATION THROUGH TSPC/TSDC.....	54
1. Formulation Description.....	54

2. NPO Capacitor Results.....	58
3. Z5U Capacitor Results.....	61
4. BX Capacitor Results.....	61
5. Reliability Determination-TSPC/TSDC.....	70
V. CONCLUSION.....	74
REFERENCES.....	75
VITA.....	78
APPENDIX: ADDITIONAL ILLUSTRATIONS.....	79

LIST OF ILLUSTRATIONS

Figure	Page
1. Graph of Dielectric Constant versus Temperature for A and C Axes of Barium Titanate (Merz-Reference #17).....	9
2. Illustration of Ferroelectric Hysteresis Loop (Kingery-Reference #16).....	11
3. Spontaneous Polarization of Barium Titanate as a Function of Temperature (Merz-Reference #17).....	15
4. TSC Test Chamber. a) copper wire to electrodes, b) alumina tube, c) Teflon insulation, d) thermocouple, e) O-ring, f) helium inlet, g) vacuum gauge, h) inner copper tube, i) thermocouple spaghetti, j) screw, k) Teflon insulation, l) test sample, m) metal frame, n) set screw, o) electrodes, p) spring, q) set screw, r) exhaust outlet, s) vacuum outlet, and t) stainless steel container (Hong and Day-Reference #3).....	19
5. TSPC Graph of Barium Titanate (Ba/Ti = 1.00) with Field of 250 V/cm and Heating Rate of 0.07 K/s.....	27
6. TSPC Graph of Barium Titanate (Ba/Ti = 1.00) with Field of 250 V/cm and Heating Rate of 0.07 K/s.....	28
7. TSPC Graph of Barium Titanate (Single Crystal) with Field of 1250 V/cm and Heating Rate of 0.07 K/s.....	29
8. TSPC Graph of Barium Titanate (Single Crystal) with Field of 1250 V/cm and Heating Rate of 0.07 K/s.....	30
9. TSPC Graph of Barium Titanate (Ba/Ti = 0.98) with Field of 250 V/cm and Heating Rate of 0.07 K/s.....	31
10. TSPC Graph of Barium Titanate (Ba/Ti = 0.98) with Field of 250 V/cm and Heating Rate of 0.07 K/s.....	32
11. TSPC Graph of Barium Titanate (Ba/Ti = 1.02) with Field of 250 V/cm and Heating Rate of 0.07 K/s.....	33
12. TSPC Graph of Barium Titanate (Ba/Ti = 1.02) with Field of 250 V/cm and Heating Rate of 0.07 K/s.....	34
13. TSDC Graph of Barium Titanate (Ba/Ti = 1.00 and Single Crystal) with No Field and Heating Rate of 0.07 K/s.....	36
14. TSDC Graph of Barium Titanate (Ba/Ti = 1.00 and Single Crystal) with No Field and Heating Rate of 0.07 K/s.....	37

Figure	Page
15. TSDC Graph of Barium Titanate (Ba/Ti = 1.02 and 0.98) with No Field and Heating Rate of 0.07 K/s.....	38
16. TSDC Graph of Barium Titanate (Ba/Ti = 1.02 and 0.98) with No Field and Heating Rate of 0.07 K/s.....	39
17. SEM Photograph of Barium Titanate (Ba/Ti = 1.04) at Magnification of 3900 X.....	44
18. SEM Photograph of Barium Titanate (Ba/Ti = 1.02) at Magnification of 3900 X.....	45
19. SEM Photograph of Barium Titanate (Ba/Ti = 0.98) at Magnification of 500 X.....	46
20. SEM Photograph of Barium Titanate (Ba/Ti = 0.96) at Magnification of 500 X.....	47
21. SEM Photograph of Barium Titanate (Ba/Ti = 1.00) at Magnification of 3900 X.....	48
22. TSPC/TSDC Graph of NPO Multilayer Capacitor (Sample #1) with Field of 7200 V/cm and Heating Rate of 0.07 K/s.....	59
23. TSPC/TSDC Graph of NPO Multilayer Capacitor (Sample #2) with Field of 7200 V/cm and Heating Rate of 0.07 K/s.....	60
24. TSPC/TSDC Graph of Z5U Multilayer Capacitor with Field of 7200 V/cm and Heating Rate of 0.07 K/s.....	62
25. TSPC/TSDC Graph of Z5U Multilayer Capacitor with Field of 7200 V/cm and Heating Rate of 0.07 K/s.....	63
26. TSPC/TSDC Graph of BX Multilayer Capacitor (Sample #1) with Field of 7200 V/cm and Heating Rate of 0.07 K/s.....	65
27. TSPC/TSDC Graph of BX Multilayer Capacitor (Sample #1) with Field of 7200 V/cm and Heating Rate of 0.07 K/s.....	66
28. TSPC Graph of BX Multilayer Capacitors (Samples #2 and #3) with Field of 7200 V/cm and Heating Rate of 0.07 K/s.....	68
29. TSPC Graph of BX Multilayer Capacitors (Samples #4 and #5) with Field of 7200 V/cm and Heating Rate of 0.07 K/s.....	69
30. TSPC/TSDC Graph of BX Multilayer Capacitor (Sample #6) with Field of 7200 V/cm and Heating Rate of 0.07 K/s.....	71

Figure	Page
31. TSPC Graph of BX Multilayer Capacitor (Sample #7) with Field of 7200 V/cm and Heating Rate of 0.07 K/s.....	72
APPENDIX	
32. TSPC Graph of Barium Titanate (Ba/Ti = 0.96) with Field of 250 V/cm and Heating Rate of 0.07 K/s.....	80
33. TSPC Graph of Barium Titanate (Ba/Ti = 0.97) with Field of 250 V/cm and Heating Rate of 0.07 K/s.....	81
34. TSPC Graph of Barium Titanate (Ba/Ti = 0.99) with Field of 250 V/cm and Heating Rate of 0.07 K/s.....	82
35. TSPC Graph of Barium Titanate (Ba/Ti = 0.995) with Field of 250 V/cm and Heating Rate of 0.07 K/s.....	83
36. TSPC Graph of Barium Titanate (Ba/Ti = 1.005) with Field of 250 V/cm and Heating Rate of 0.07 K/s.....	84
37. TSPC Graph of Barium Titanate (Ba/Ti = 1.01) with Field of 250 V/cm and Heating Rate of 0.07 K/s.....	85
38. TSPC Graph of Barium Titanate (Ba/Ti = 1.03) with Field of 250 V/cm and Heating Rate of 0.07 K/s.....	86
39. TSPC Graph of Barium Titanate (Ba/Ti = 1.04) with Field of 250 V/cm and Heating Rate of 0.07 K/s.....	87
40. TSDC Graph of Barium Titanate (Ba/Ti = 1.04 and 0.96) with No Field and Heating Rate of 0.07 K/s.....	88
41. TSDC Graph of Barium Titanate (Ba/Ti = 1.03 and 0.97) with No Field and Heating Rate of 0.07 K/s.....	89
42. TSDC Graph of Barium Titanate (Ba/Ti = 1.01 and 0.99) with No Field and Heating Rate of 0.07 K/s.....	90
43. TSDC Graph of Barium Titanate (Ba/Ti = 1.005 and 0.995) with No Field and Heating Rate of 0.07 K/s.....	91

LIST OF TABLES

Table	Page
1. DENSITY AND POROSITY DATA FOR BaTiO ₃ SAMPLES.....	22
2. ACTIVATION ENERGIES/CURRENT MAGNITUDES.....	51
3. SAMPLE RESISTIVITY.....	53
4. EIA CAPACITOR DESIGNATIONS.....	55
5. CAPACITOR SPECIFICATIONS.....	56

I. INTRODUCTION

The stability of insulators based upon barium titanate (BaTiO_3) to DC fields is regarded as one of the important factors in determining the quality of BaTiO_3 -based ceramic capacitors. The gradual increase in electrical conductivity of an insulator stressed by DC fields at levels below the breakdown strength is called degradation. Since degradation is a common problem to the ceramic capacitor industry, many degradation studies have been made over the past three decades. The studies have tried to do the following:

- a) Learn the source(s) and solution(s) of degradation (upgrade capacitor reliability).
- b) Develop short term tests to detect degradation.

Investigations on the electrical degradation of BaTiO_3 by Keck¹ and a study of material problems involving ceramic capacitors by Buessem and Prokopowicz² are just two of many studies on the subject.

One method not extensively used to examine the current behavior of ceramic dielectrics involves the use of thermally stimulated polarization and depolarization current measurements (TSPC/TSDC). For this investigation, the TSPC/TSDC measurement experiments involved laboratory prepared BaTiO_3 samples at various Ba/Ti ratios (0.96 to 1.04) and commercial ceramic multilayer capacitors of different formulations (NP0, BX, and Z5U).

TSPC/TSDC measurement techniques have been shown to be very sensitive to both polarization processes and trapping states. The purpose of the study was to see if this high sensitivity could yield information regarding the physical and chemical state of a material.

In particular, the desire was to see if the TSPC/TSDC technique could give information on structural defects, phase transitions, chemical inhomogeneities, and dielectric degradation. From examination of both BaTiO_3 and capacitor samples, the usefulness of the TSPC/TSDC measurement technique to determine the reliability of ceramic capacitors was evaluated.

II. LITERATURE REVIEW

A. TSPC/TSDC REVIEW AND RELATED STUDIES

Thermally stimulated polarization and depolarization current measurements (TSPC/TSDC) have been used extensively to study charge motion in insulators. These measurements are based on the thermally activated release of trapped charges (ions, holes, or electrons) or from polarization mechanisms. If these sources exist in a material, current peaks or maxima appear during heating.

The TSPC technique examines the current behavior of a material subjected to a constant DC field and heated at a constant rate from low temperature. If the material contains trapping states, peaks or maxima are observed in the current when the temperature becomes high enough for trapped charges to be released. The current release during this process is represented by Equation 1³:

$$I(T) = A \exp(-E_a/kT) \exp[-B \int_{T_0}^T \exp(-E_a/kT')dT'] \quad (1)$$

where

E_a = activation energy or trapped depth
 k = Boltzmann constant
 T_0 to T = heating temperature range
 A, B = constants depending upon current sources (from trapped charges, dipole polarization or others) and measurement conditions (electrode area, heating rate, etc.)

The TSDC technique, which is used primarily to study dipole polarization, differs slightly from the TSPC method. The TSDC process involves measuring the charge release from an already polarized material as it is heated from low temperature. During heating, the discharge current occurs from dipole depolarization and emptying of trapped

states. The current produced by random dipole reorientation is represented by Equation 2³:

$$I(T) = (N_d u^2 a E_p/k T_p t_0) \exp(-E_a/kT) \\ * \exp[(-1/b t_0) \int_{T_0}^T \exp(-E_a/kT') dT'] \quad (2)$$

where

T_p = polarization temperature
 N_d = dipole concentration
 u = dipole moment
 t_0 = dipole relaxation time
 a = factor of dipole orientation freedom
 b = heating rate
 E_p = applied field

with the other terms being defined previously.

Chen⁴ reviewed methods for the kinetic analysis of thermally stimulated processes. These methods included thermoluminescence (TL), thermally stimulated current (TSC), ionic thermocurrents (ITC), and thermally stimulated electron emission (TSEE). Shindo⁵ reviewed formula derivations for the spectral peaks occurring in TSPC/TSDC measurements, and recognized the spectra caused by reorientation of permanent dipoles were similar to those caused by ion transference.

Hong and Day⁶ studied the ionic motion in certain glasses using TSPC/TSDC methods. The polarization peaks found in the glasses were attributed to bulk polarization and were dependent upon glass composition. A type of dipole orientational polarization involving sodium ion movement around nonbridging oxygen ions was also found. Similar work done by Agarwal and Day⁷ was concerned with investigating alkali ion motion in both single alkali-silicate glasses (using various alkali ions) and in mixed alkali glasses to determine polarization and conduction mechanisms.

Bucci and Fieschi⁸ investigated the thermally activated release of dielectric polarization using the ITC technique. Measurements including the determination of activation energy and impurity solubility were made on Sr- and Ca-doped NaCl. Also, qualitative measurements were completed on Teflon, calcite and quartz to illustrate polarization in nonferroelectric dielectrics. McKeever and Hughes⁹ observed the polarization current of alkali halides via TSPC methods comparing their results to those of Bucci and Fieschi⁸. The observed current was due to polarization of impurity/vacancy dipoles in alkali halides doped with divalent metallic impurities. In related studies, Hino¹⁰ made thermally stimulated measurements on solid dielectrics such as organic polymers, ZnTe, and an Al-SiO₂-Si MOS composition. Through his measurements, Hino described dipolar relaxation time, trap levels, and ionic space charge polarization.

Morin and Oliver¹¹ used thermally stimulated current measurements on strontium titanate (SrTiO₃). Their measurements located the energy levels associated with iron and aluminum impurities in the band gap of SrTiO₃. Morin and Oliver assigned energy level values to items within the band gap of SrTiO₃. Examples of energy level values include the following: oxygen ion vacancy donors 0.085 eV below the conduction band, Al⁺³ acceptors 0.18 eV below conduction band, and Fe⁺³ acceptors 0.075 eV below the conduction band. Siegarth and Morrow¹² made TSC measurements on SrTiO₃ ceramics with and without V and Nb impurities. The observed current peaks were not due to ferroelectric or antiferroelectric transitions but to the presence of a thermoelectric state existing for permanent dipoles in the material. Lebedeva,

et. al.¹³, investigated the SrTiO₃ current behavior using TSC techniques to measure both filled and partially filled electron traps. The thermal activation energies of the trap levels from TSC determination ranged from 0.50 eV to 0.92 eV.

B. REVIEW OF RELATED WORK ON BARIUM TITANATE

Chynoweth¹⁴ developed a dynamic measurement method to study the pyroelectric effect in BaTiO₃ single crystals. The method proved to be a sensitive, nondestructive technique for studying the polarization state of BaTiO₃ single crystals. Chynoweth showed that the transient currents produced in BaTiO₃ single crystals, which were subjected to flashes of light, were pyroelectric. He concluded from hysteresis loop measurements that the temperature dependent current was associated with dipole polarization.

Chynoweth¹⁵ also investigated surface space-charge layers in BaTiO₃ single crystals. From wave form studies of the pyroelectric current above the Curie point, Chynoweth concluded space-charge layers (up to 10⁻⁵cm thick) resided at the BaTiO₃ crystal surface with the surface charges producing a field through the crystal interior. Also, the space-charge field influenced the polarization direction of the BaTiO₃ crystal domains when the crystal was cooled through the Curie point. The space-charge field affected dielectric constant measurements above the Curie point and influenced the actual transition temperature. Chynoweth finally concluded that the space-charge fields were important to the domain nucleation process in BaTiO₃.

The electrical degradation study made by Keck¹ on BaTiO₃ was of particular importance to this investigation. Keck made current-field and current-temperature measurements on BaTiO₃ to determine the current injection mechanism responsible for degradation. Keck observed through transient current measurements the occurrence of current maxima in the region of the tetragonal-cubic transition temperature. He related the

peaks to the temperature dependence of the dielectric constant^{16,17} (temperature dependence of the dielectric constant for BaTiO₃ illustrated in Figure 1¹⁷). Keck also showed that the peaks were related to the charge release due to dipole elimination at the Curie point.

Mathematically, Keck¹ represented the current behavior during the tetragonal to cubic transition by considering the negative current (capacitance current) of the BaTiO₃ samples and the positive current (resistance current). The equation for the capacitance current is as follows¹:

$$J_c = (\epsilon_0 E) \left(\frac{\partial k}{\partial T} \right) \left(\frac{\partial T}{\partial t} \right) \quad (3)$$

where

J_c = capacitance current
 E = applied field
 $\frac{\partial k}{\partial T}$ = slope of dielectric constant vs temperature curve
 $\frac{\partial T}{\partial t}$ = heating rate
 ϵ_0 = permittivity of free space

Keck¹ did not expand on these pseudo-TSC measurements since they were not the focal point of his research. However, Keck did show TSC-type measurements could reveal some details about the ferroelectric/paraelectric transformation in BaTiO₃. Based on his current-field studies, Keck determined that the degradation resistance in BaTiO₃ was related to the Ba/Ti ratio. Low degradation resistance was detected in samples having a Ba/Ti ratio < 1.00, while degradation resistance was observed when the Ba/Ti ratio exceeded 1.00. For BaTiO₃ samples showing signs of degradation, space charge limited current was prevalent. When no degradation occurred, the current injection mechanism exhibited by BaTiO₃ samples was ohmic.

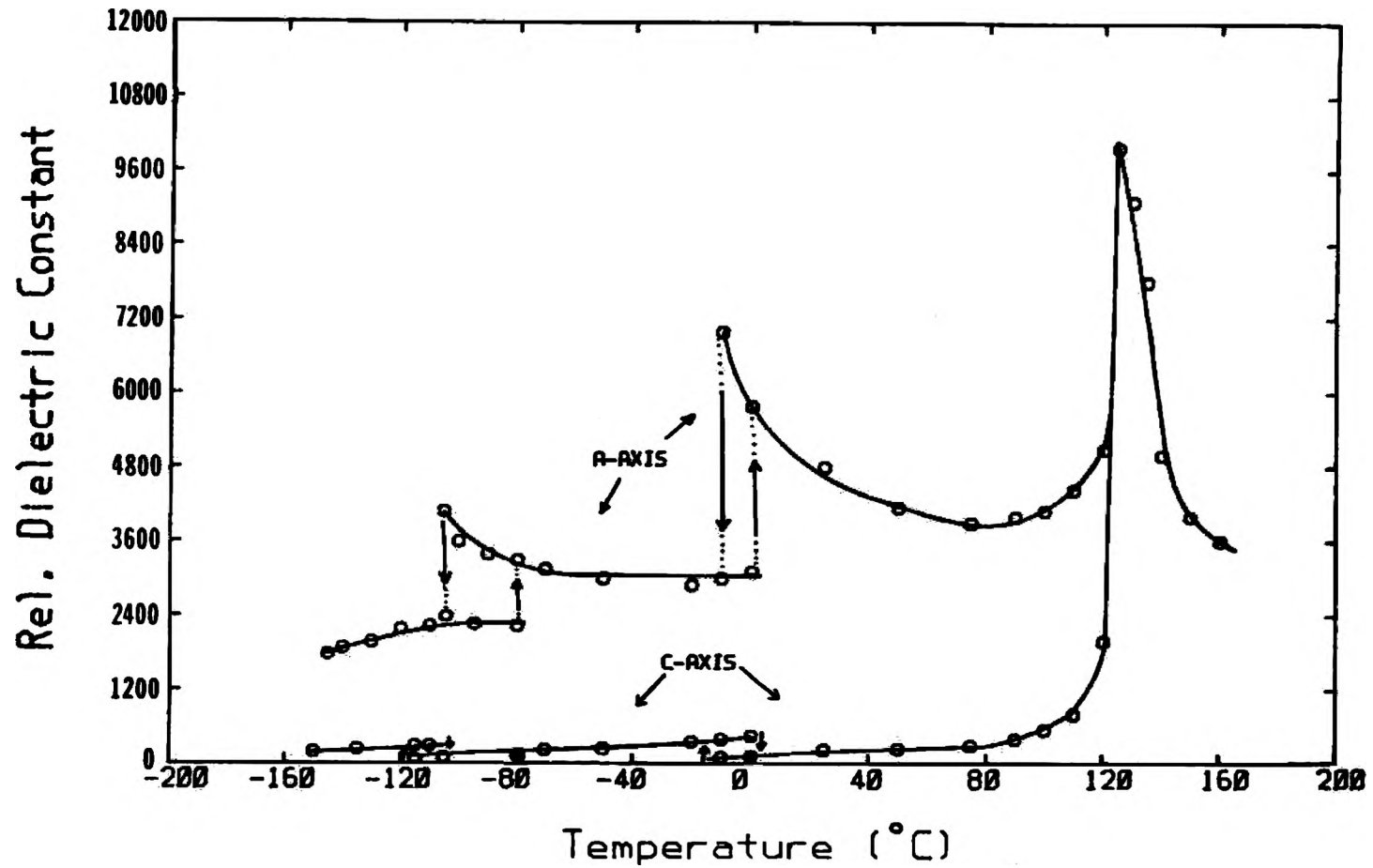


Figure 1. Graph of Dielectric Constant versus Temperature for A and C Axes of Barium Titanate (Merz-Reference # 17).

C. FERROELECTRICITY AND BARIUM TITANATE

Ferroelectricity is defined as the spontaneous polarization (or alignment) of a crystal's electric dipoles by their mutual interaction with an external field absent. The direction of spontaneous polarization within the crystal is called the polar axis. The spontaneous polarization value, however, is temperature dependent. If the temperature of the ferroelectric crystal is altered, a change in the polarization occurs. Electric charges are observed on those crystal faces that are perpendicular to the polar axis. The temperature dependence of spontaneous polarization is known as the pyroelectric effect. Therefore, ferroelectric crystals having spontaneous polarization are known as pyroelectric crystals.

The polarization direction of a pyroelectric crystal can be reversed by applying a sufficiently large external field. Also, the spontaneous polarization of a ferroelectric crystal can be reversed by means of an external field, as shown by hysteresis loop measurements (Figure 2¹⁶). Thus, ferroelectricity can be stated as the effect produced in a pyroelectric crystal where reversible polarization occurs.

The general source of spontaneous polarization in a ferroelectric crystal (or material) is described through the equation for static field polarization¹⁶:

$$\text{where } P = (k' - 1) \epsilon_0 E = N \alpha E' \quad (4)$$

k' = dielectric constant
 ϵ_0 = dielectric permittivity
 E = external field
 N = dipole number/unit volume
 α = atomic polarizability
 E' = internal dipole field

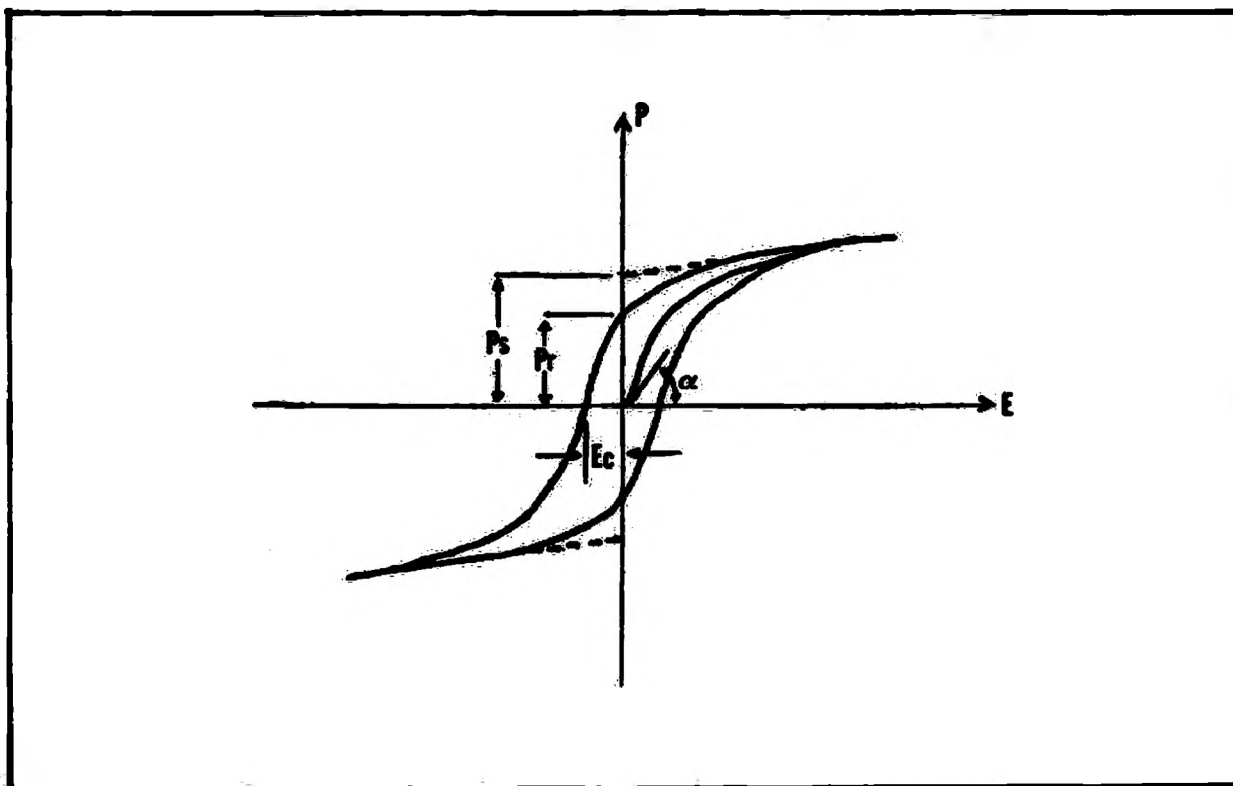


Figure 2. Illustration of Ferroelectric Hysteresis Loop (Kingery-Reference #16).

Since the orientational polarizability of a dipole is inversely proportional to temperature and spontaneous polarization begins at a critical temperature (T_C), the relationship between spontaneous polarization and the dielectric constant can be represented by the following equation¹⁶:

$$\frac{P}{\epsilon_0 E} = k' - 1 = \frac{3 T_C}{T - T_C} \quad (5)$$

The linear dependence of the dielectric constant on the reciprocal of $(T - T_C)$ is called the Curie-Weiss Law, with T_C being the Curie temperature.

Because of spontaneous polarization, very high dielectric constants together with hysteresis effects appear in ferroelectric crystals. The hysteresis effects, shown through a hysteresis loop, are similar to the effects observed for ferromagnetic materials. Electric dipole alignment may extend over only a region of the crystal while in another region the spontaneous polarization direction may be reversed. Such regions of uniform polarization are called domains, a term borrowed again from ferromagnetism. The boundaries between ferroelectric domains are oriented crystallographic domain walls. As an example, BaTiO_3 has domain walls with 90° and 180° orientation.

At low field strengths in unpolarized materials, the polarization is initially reversible and nearly linear, as illustrated by the hysteresis loop (Figure 2). The initial slope of the hysteresis curve gives the initial dielectric constant, k' . At higher fields, the polarization increase for a given increase in field lessens, corresponding to saturation polarization. When saturation polarization occurs, all domains of like orientation aligned in the direction of the

electric field. The saturation polarization (P_S) can be found through curve extrapolation of the hysteresis loop (to where $E = 0$).

When the external field is removed, the polarization does not go to zero but remains at a finite value. This value is known as the remanent polarization (P_r). The remanent polarization results from the oriented domains being unable to return to their original random state without an additional energy input by an oppositely directed field; that is, energy is required to change domain orientation. The electric field strength required to return the polarization to zero is known as the coercive field (E_C).

Among ferroelectric materials, $BaTiO_3$ has been most extensively investigated. Above the Curie point ($125^\circ C$) $BaTiO_3$ has the cubic (perovskite) structure and is no longer ferroelectric. The structure of $BaTiO_3$ becomes a symmetric atomic array with no polar axis. With the loss of all ferroelectric behavior above the Curie point, $BaTiO_3$ is said to be paraelectric (analogous to paramagnetism). The transition from ferroelectric to paraelectric behavior also destroys dipole existence.

As the temperature passes below the Curie point, the crystal structure becomes slightly stretched parallel to one cubic edge. The new structure is tetragonal, and the stretched edge becomes the new polar axis. Since there are six equivalent $\langle 100 \rangle$ axes in the original cubic structure, the new polar axis can be parallel to any one of the six equivalent directions resulting in six possible directions of spontaneous polarization.¹⁸ The tetragonal structure of $BaTiO_3$ is stable from the Curie point to about $5^\circ C$.

Between 5°C and -90°C, the BaTiO₃ structure becomes orthorhombic by stretching slightly the original cubic structure along one face diagonal and compressing the cubic structure along the other face diagonal. The two face diagonals are the new orthorhombic axes with one of the face diagonals becoming the new polar axis. Again, since there are twelve equivalent <110> directions in the original cubic structure, there are twelve possible directions of the spontaneous polarization in the orthorhombic structure¹⁸.

A third structural change occurs in BaTiO₃ below -90°C. The new rhombohedral structure is formed by slightly stretching the original cube along its body diagonal. The body diagonal subsequently becomes the new polar axis. As there are eight equivalent <111> axes in the original cubic structure, there are eight allowed directions of the spontaneous polarization in the rhombohedral structure¹⁸.

The temperature dependence of the spontaneous polarization of BaTiO₃ single crystals, which was measured by Merz¹⁷ with a Sawyer-Tower circuit, is shown in Figure 3. (Merz noted that the measured polarization was the component of the spontaneous polarization normal to the surface of the crystal coinciding with the cubic face.) As the polar axis changes from the cubic edge to the face diagonal and then to the body diagonal, the polarization value changes from P_s to $P_s/\sqrt{2}$ and then to $P_s/\sqrt{3}$.¹⁹ Because of the multiple polar directions, more complicated domain patterns are possible in BaTiO₃ than in other ferroelectric materials (such as KH₂PO₄ and tri-glycine sulfate). The effect of domain orientation on the TSPC/TSDC spectra of BaTiO₃ will be discussed in more detail in the Results and Discussion section.

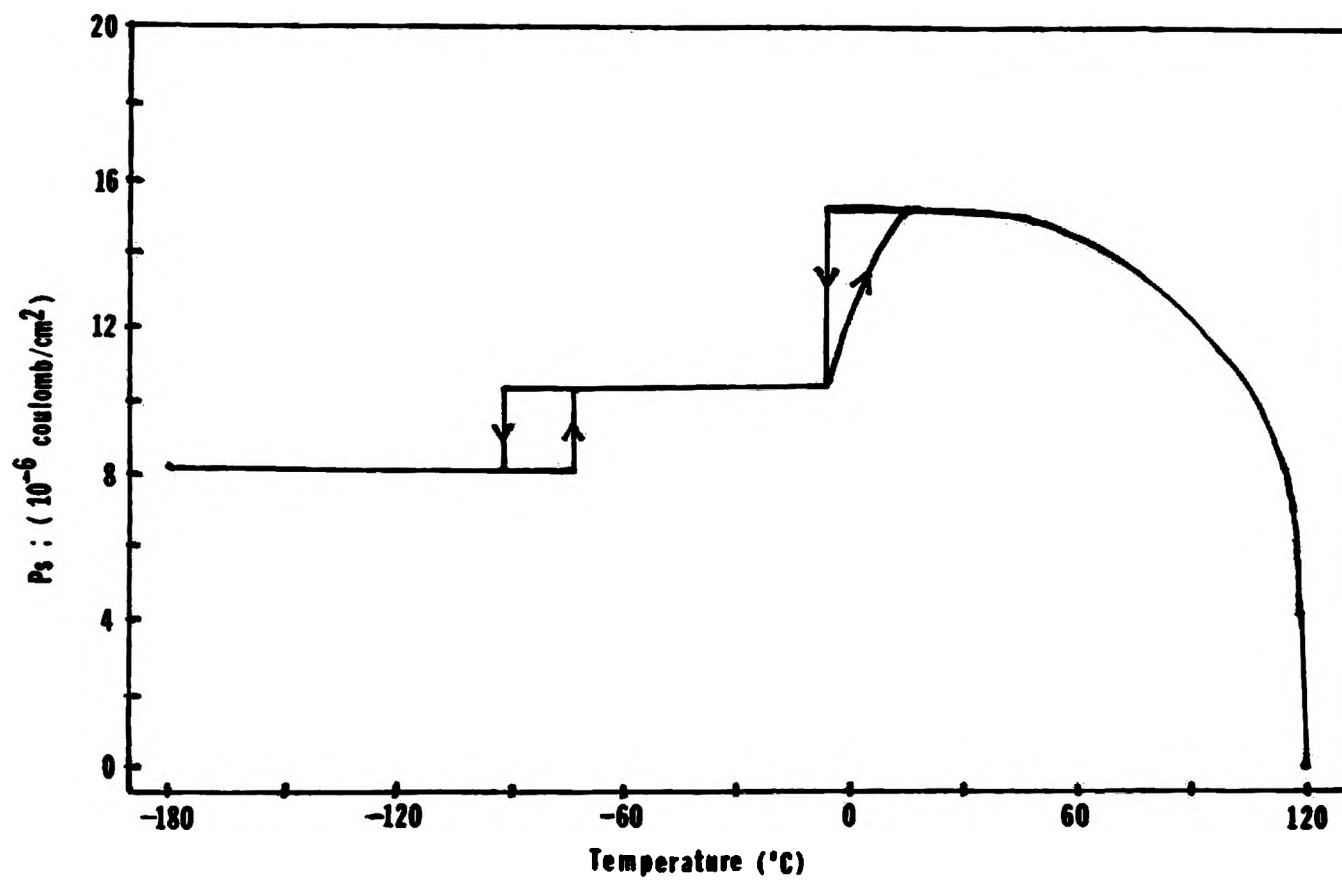


Figure 3. Spontaneous Polarization of Barium Titanate as a Function of Temperature (Merz-Reference #17).

D. CAPACITOR RELIABILITY

Ceramic dielectric materials are generally quite durable and are extensively used for multilayer capacitors. Of all ceramic dielectric materials, barium titanate (BaTiO_3) is the most important ingredient to multilayer capacitors. The stability of BaTiO_3 to high DC fields has long been recognized as an important factor in determining capacitor quality. In contrast, factors influencing the degradation process of BaTiO_3 -base capacitors include the Ba/Ti ratio, dopant additions, and hydroxyl content.

In recent years, ceramic capacitors have been under great scrutiny due to questions concerning ceramic capacitor reliability. Studies by many investigators on capacitor reliability focus upon two areas: physical and electrical defects in capacitors and the role of ceramic dielectrics in intrinsic and extrinsic reliability failures.

Brennan²⁰ concluded that ceramic capacitor failures, due to low insulation resistance (IR), could occur at low voltages (< 10 VDC) despite previous accelerated electrical screening. However, many capacitor failures recovered as voltage was increased. Brennan found capacitor electrical failure was from voids, delaminations, and unagglomerated ceramic powder within the voids, instead of contamination. Similar findings concerning capacitor failures related to low IR were made by others^{21,22} using a recently developed lifetesting procedure. The test procedure (incorporated into military specification MIL-C-123) involves the exposure of capacitor sample lots to 85°C, 85% relative humidity, and a 1.5 VDC bias for 168 hours or longer. Chittick, et al.²³, however, developed a different technique involving a

nondestructive methanol screening of encapsulated and unencapsulated capacitors to detect possible low voltage failures.

Sato, et. al.²⁴, discovered a possible mechanism to explain why ceramic capacitors fail insulation resistance testing at DC voltages far below the capacitors' rated voltage. Using improved microanalysis techniques and electrochemical methods, they found capacitor failure occurring from electromigration of Pd electrode material in the dielectric. The migration was through voids or cracks generated in the capacitor manufacturing process. The Pd electrode material was electrolyzed by an aqueous solution containing Cl^- ions.

W. Payne²⁵ discussed the impact of ceramic dielectrics on multilayer capacitor reliability. He considered it feasible that the dielectric formulation could influence the formation of extrinsic physical defects. W. Payne mentions voids and porosity as undesirable physical defects and places blame on these defects for some multilayer capacitor failures. He also suggested some dielectric formulations inherently have greater porosity than other and that specific manufacturing processes and lot to lot formulation variations also influenced porosity.

Finally, D. Payne²⁶ found a correlation between the reliability of BaTiO_3 -based capacitors and their equilibrium current-voltage characteristics based on the amount of ionic charge transport. D. Payne suggested the current-voltage behavior could be used as a simple, quick, nondestructive test for reliability with the unreliable units showing a current-voltage relationship similar to Schottky emission.

III. EXPERIMENTAL PROCEDURE

A. DESCRIPTION OF EQUIPMENT

The measurement system used for TSPC/TSDC measurements had a sensitivity of 10^{-14} amps. The sensitivity was achieved by shielding the test chamber using coaxial cable and using a battery-powered electrometer that was free of AC interference.

The TSC test chamber⁶ (shown in Figure 4) consisted of an outer metal container made of stainless steel with a removable inner core assembly that contained the spring loaded electrode contacts and monitoring thermocouples. Teflon inserts and alumina tubing were used to prevent electrode or thermocouple contact with the metallic parts of the chamber. Three sets of valved tubing were connected to the outer metal container to supply vacuum, inert atmosphere, and exhaust for the interior of the test chamber. A mechanical vacuum pump provided the vacuum for the chamber with vacuum monitored by an attached vacuum gauge. Dry helium gas was passed through the test chamber to purge the chamber of moisture and to provide good thermal contact to the sample.

The instrumentation used for the TSPC/TSDC measurements consisted of a battery-powered electrometer (Keithly model 602) coupled to a X-Y plotter (Linseis model L1800). The DC voltage supply (external field) was supplied by a battery bank that could be varied from 45 to 225 volts DC. The heat source for the chamber was provided by heating tape controlled through a solid state temperature controller (Eurotherm).

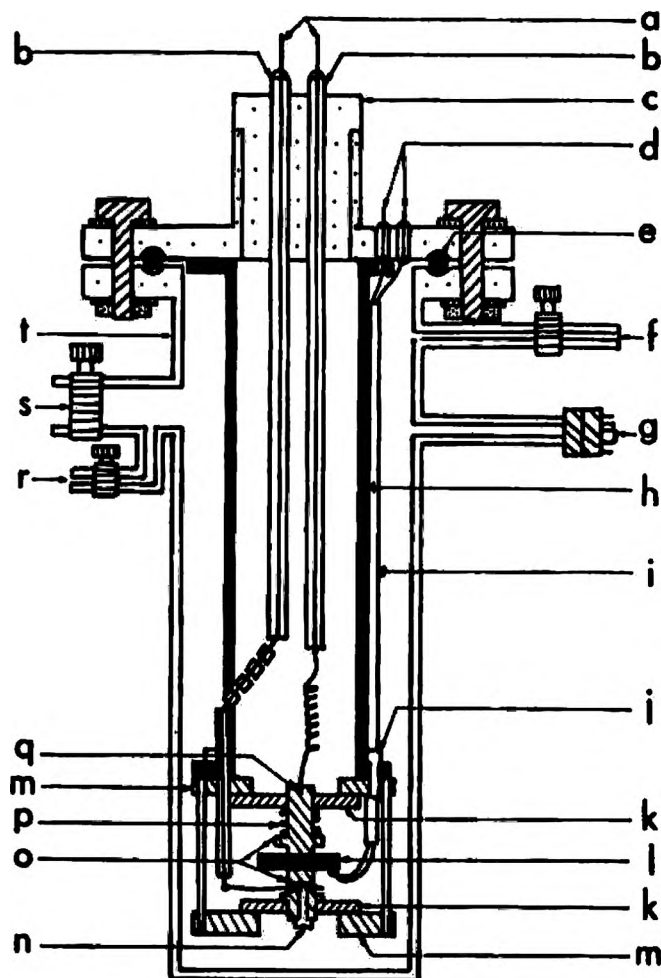


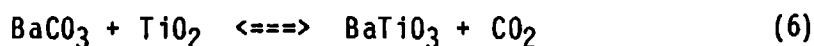
Figure 4. TSC Test Chamber. a) copper wire to electrodes, b) alumina tube, c) Teflon insulation, d) thermocouple, e) O-ring, f) helium inlet, g) vacuum gauge, h) inner copper tube, i) thermocouple spaghetti, j) screw, k) Teflon insulation, l) test sample, m) metal frame, n) set screw, o) electrodes, p) spring, q) set screw, r) exhaust outlet, s) vacuum outlet, and t) stainless steel container. (Hong and Day-Reference #3).

The influence of external stimuli (not including the external field and heat source) was not investigated in this study. However, the influence of various external stimuli (including light at various wavelengths, alpha and gamma radiation, thermal and mechanical stress, and magnetic polarization) has been studied by other investigators⁴.

B. SAMPLE PREPARATION

Except for the commercial ceramic capacitors and the single crystalline and polycrystalline samples obtained from outside sources, most of the barium titanate (BaTiO_3) samples were prepared in the laboratory by a method described by Pechini²⁷. The process, known as the 'liquid mix process', essentially involves the quantitative mixing and dissolution of the desired cations in a citric acid/ethylene glycol solution. The solution is evaporated into an amorphous polymer and subsequent calcination yielded the desired powdered compound.

Conventionally, BaTiO_3 is formed by the solid state reaction²⁸:



However, the reaction is diffusion controlled, which will never go to completion, resulting in a chemically inhomogeneous powder. In contrast, the liquid mix process has no precipitation occurring. The cations of the base material and any desired dopant are randomly distributed throughout the powdered compound yielding a homogeneous material.

Prior to powder compaction, a polyvinyl alcohol/water solution (6 to 12 weight % PVA) was added to the powder and mixed-in by shaking with plastic beads in a vibratory mill. The powder was then pressed into discs approximately 2.00 to 3.00 mm thick in a 1.25 cm diameter stainless steel die at a compaction pressure of 3500 kg/cm².

The BaTiO_3 discs used for TSPC/TSDC measurements were densified by sintering at 1400°C for four hours (densities of BaTiO_3 samples listed in Table I). To minimize the introduction of impurities in the sintering operation, the discs were placed on a zirconia plate covered

TABLE I
DENSITY AND POROSITY DATA FOR BaTiO₃ SAMPLES

<u>Ba/Ti Ratio</u>	<u>Porosity(%)</u>	<u>Bulk Density(g/cm³)</u>	<u>Theoretical Density (%)</u>
0.96	5.67	5.28	88.0
0.97	5.12	5.22	87.0
0.98	4.13	5.34	89.0
0.99	3.45	5.66	94.3
0.995	4.27	5.29	88.2
1.00	2.03	5.62	93.7
1.005	5.51	5.30	88.3
1.01	4.94	5.52	92.0
1.02	3.01	5.58	93.0
1.03	2.97	5.64	94.0
1.04	3.83	5.54	92.3

Average sample diameter--> 1.13 cm

Average thickness--> 0.18 cm

Electrode diameter--> 0.82 cm

Electrode area--> 0.52 cm²

Firing Temperature--> 1400°C for 4 hrs.

Theoretical density for BaTiO₃--> 6.0 g/cm³

Note: Porosity and bulk density determined using ASTM C-20-83 procedure. (Xylene used as immersing medium.)

with pure BaTiO_3 powder and air-fired in an alumina muffle tube furnace. The electrode material used for all fired BaTiO_3 sample discs was an unfritted platinum paste. A stencil was used as a guide in painting the electrode material onto the discs. The samples were first placed in a drying oven to remove the organic solvents from the electrode material and subsequently fired to 800°C for at least four hours to assure electrode adhesion to the sample discs.

The other group of samples tested were commercial ceramic capacitors. The capacitors varied in formulation, with either NPO, BX, or Z5U characteristics and were either encapsulated or unencapsulated. The capacitor termination material was fritted silver which for some capacitors was solder coated. To facilitate testing, wire leads were attached to all unleaded capacitors. (The encapsulated capacitors came with leads.)

C. TSPC/TSDC MEASUREMENT PROCEDURE

The following is a synopsis of the procedure used in making the thermally stimulated current (TSPC/TSDC) measurements:

- a) The sample was placed between the spring loaded brass electrodes of the sample holder (inner assembly) and was inserted into the test chamber (Figure 4).
- b) The chamber was sealed, with all electrical leads to the instrumentation connected, except for the external field.
- c) The sealed chamber was evacuated to about 0.001 torr and was heated to 165°C for two to six hours to aid in the removal of moisture from both the sample and the chamber.
- d) The test chamber was then purged with dry helium gas and was cooled to around -100°C through immersion in liquid nitrogen.
- e) After cooling to -100°C, the 1st polarization measurement began, first by starting the heating cycle, and second by applying the external field. The temperature range of the heating cycle was from -100 to 165°C, while the external field ranged from 45 to 225 volts DC.
- f) The chamber was then heated at a constant rate of 4 degrees/minute with the electrometer monitoring the current passing through the circuit.
- g) Once the 1st polarization measurement was completed, the sample was re-cooled to -100°C, with the external field still applied and a 2nd polarization measurement was executed.
- h) Following the 2nd polarization measurement, the sample was again re-cooled, the external field removed, and reheated to measure the depolarization current.

In most of the measurements, poling occurred during the 1st polarization. Subsequent polarizations did not change the current spectra of these samples except for the BaTiO₃ samples which had to be subjected to a second polarization in order to stabilize the current.

Therefore, with the exception of the BaTiO_3 samples, only one TSPC spectral measurement was reported. Since TSDC measurements were not a function of poling, the depolarization of these samples yielded reproducible spectra.

Four samples were measured for each Ba/Ti ratio, while the number of commercial capacitors examined depended upon the capacitor formulation (8, 24, and 75 for Z5U, NPO, and BX formulations, respectively). Certain capacitors were subjected to special conditions that will be discussed in detail later.

The TSC data was collated by use of a Hewlett Packard micro-computer (model HP-85) and plotted by a Bosch and Lomb graphics plotter (model DMP-29). Transitions between negative and positive currents were shown on the graphs by a dotted line. Each current spectral graph presented was a representation of all samples within a particular sample group examined through TSPC/TSDC.

Also, two graph types were used to represent the BaTiO_3 current spectra. One type was a log current versus inverse temperature graph which was used to distinguish between the 1st and 2nd polarization, to denote the current maxima, and to determine activation energy values. The other type was a log current versus temperature graph, used to illustrate the current spectra more clearly. For the capacitor samples, a current versus temperature graph was also used in order to better illustrate some of the TSPC/TSDC deviations occurring with compositional variation.

IV. RESULTS AND DISCUSSION

A. BARIUM TITANATE CURRENT SPECTRA

1. Rhombohedral to Orthorhombic Structure. At -100°C , where TSPC examination was initiated, all BaTiO_3 samples (Figures 5-12, 32-39) were in the rhombohedral crystal phase. During the 1st polarization, a positive current (leakage current) was initially observed for all the unpoled BaTiO_3 samples. The applied external field, similar to the coercive field of a hysteresis loop, prevented internal current release (from the dipoles). As the rhombohedral/orthorhombic transition temperature was approached, polarization (domain reorientation) caused a current maximum to occur in each BaTiO_3 sample. The current spectra of the BaTiO_3 samples remained in the positive current region through the orthorhombic structure.

In the 2nd polarization measurement, the BaTiO_3 samples were poled. As the rhombohedral/orthorhombic structural change occurred, negative current maxima were observed in the BaTiO_3 current spectra (an exception was BaTiO_3 single crystal). The current change was due to domain reorientation and the increase in the number of possible spontaneous polarization directions from eight (rhombohedral structure) to twelve (orthorhombic structure). The increase of spontaneous polarization directions lessened the dominance of the external field and the resulting leakage current from the samples. Also, the switching of the 180° domains allowed the negative internal field (formed by dipoles) to dominate the BaTiO_3 current spectra. This negative current dominance occurred from the transition temperature through the orthorhombic structure.

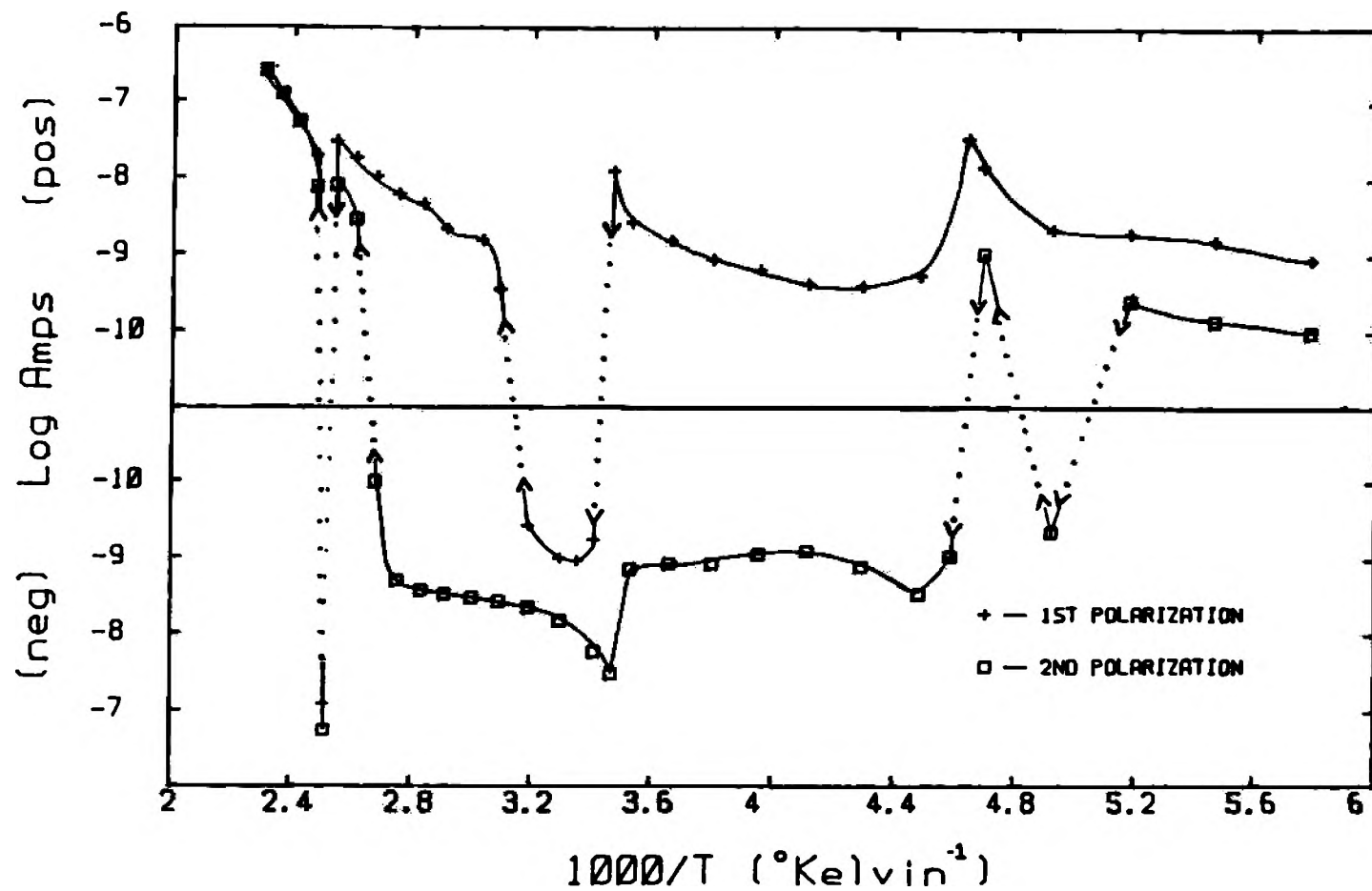


Figure 5. TSPC Graph of Barium Titanate (Ba/Ti = 1.00) with Field of 250 V/cm and Heating Rate of 0.07 K/s.

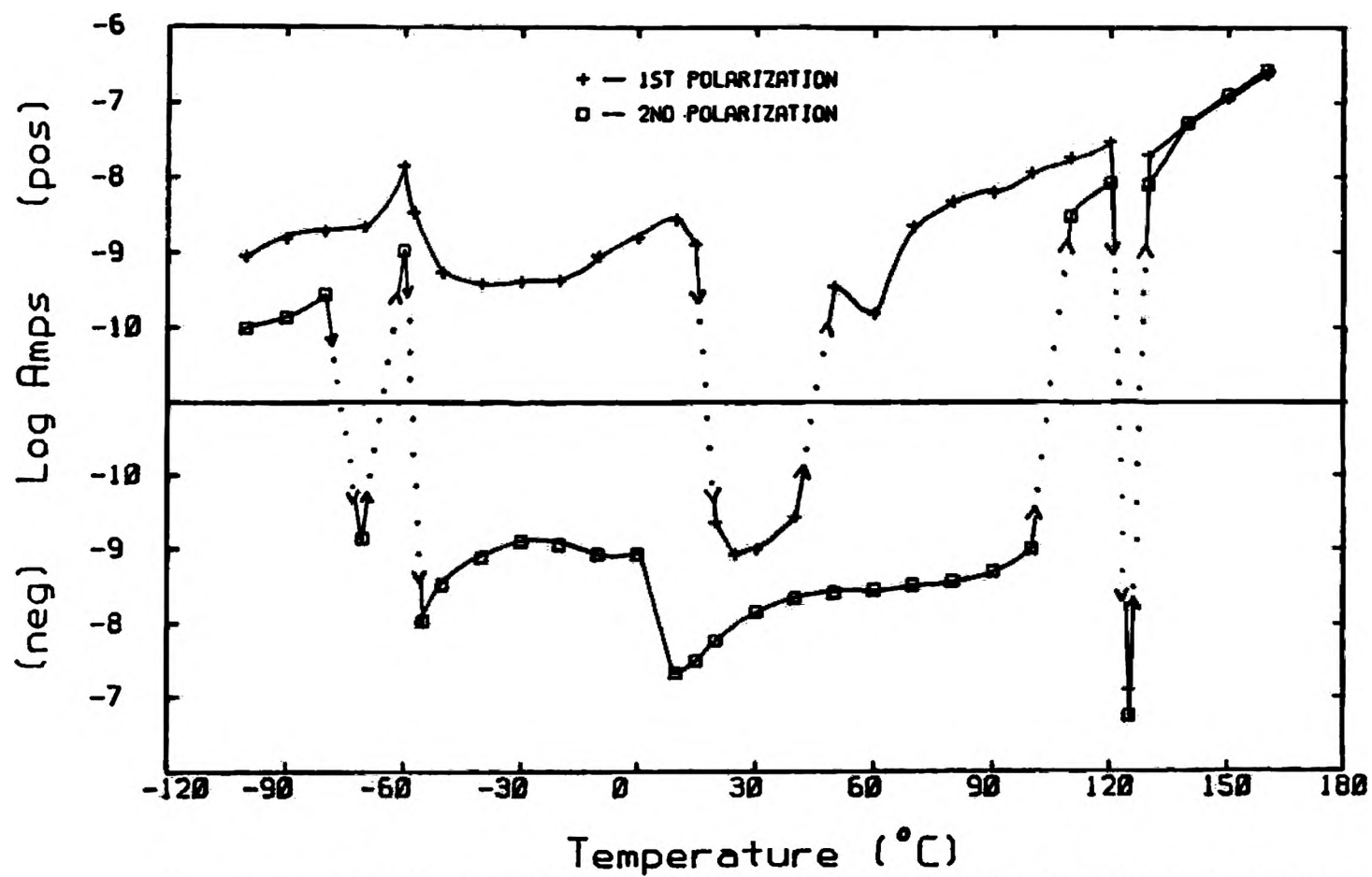


Figure 6. TSPC Graph of Barium Titanate (Ba/Ti = 1.00) with Field of 250 V/cm and Heating Rate of 0.07 K/s.

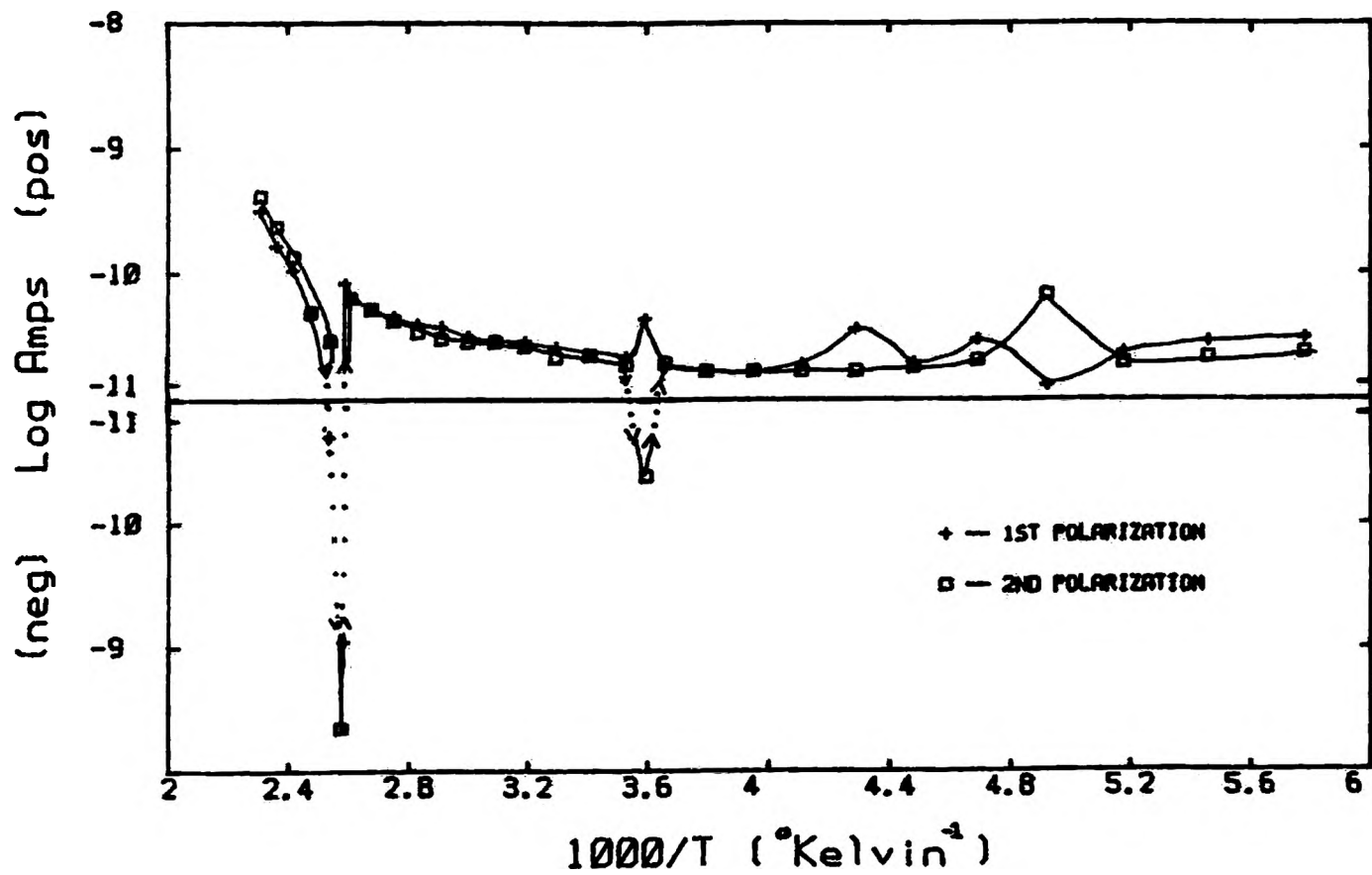


Figure 7. TSPC Graph of Barium Titanate (Single Crystal) with Field of 250 V/cm and Heating Rate of 0.07 K/s.

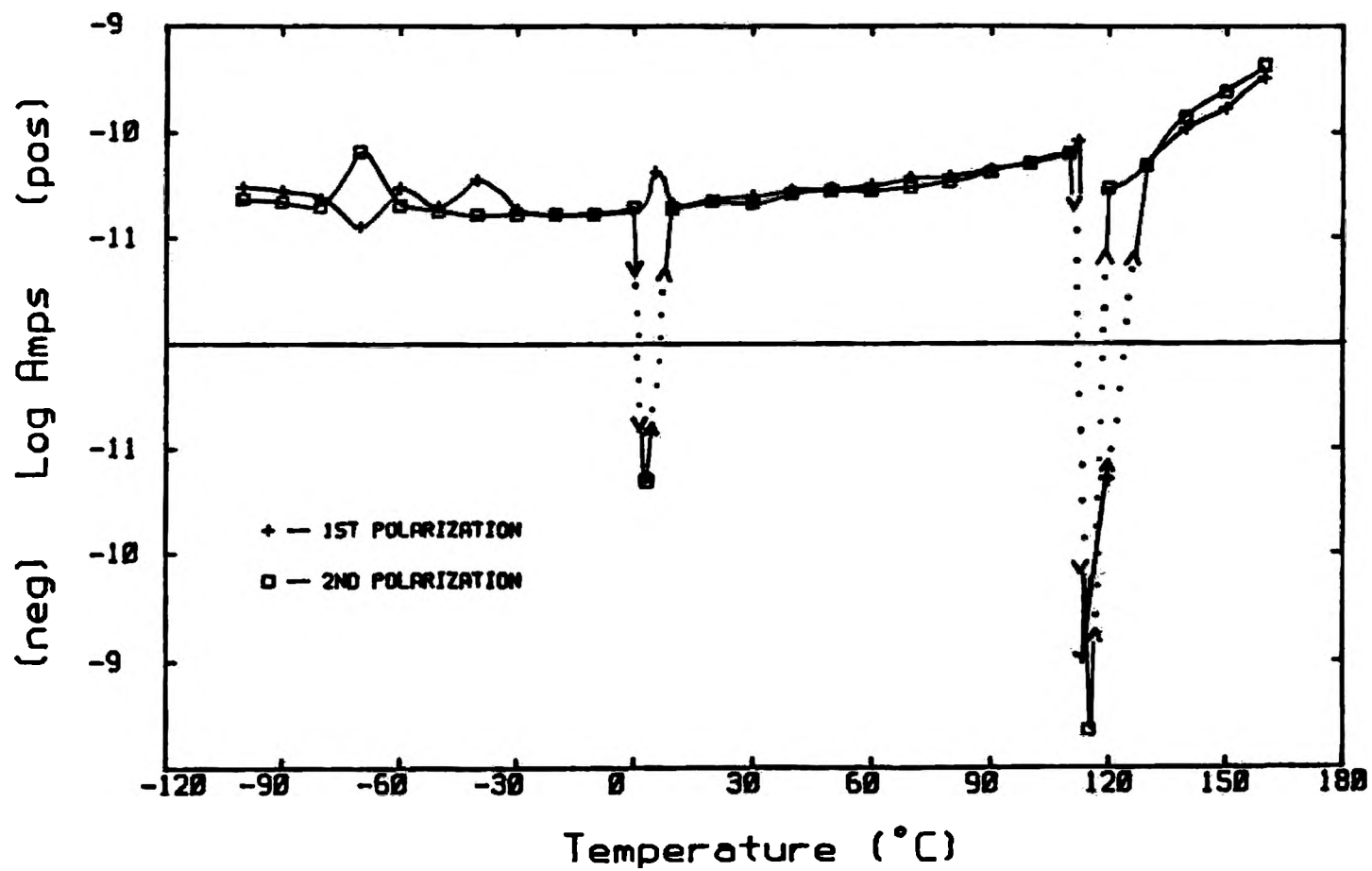


Figure 8. TSPC Graph of Barium Titanate (Single Crystal) with Field of 250 V/cm and Heating Rate of 0.07 K/s.

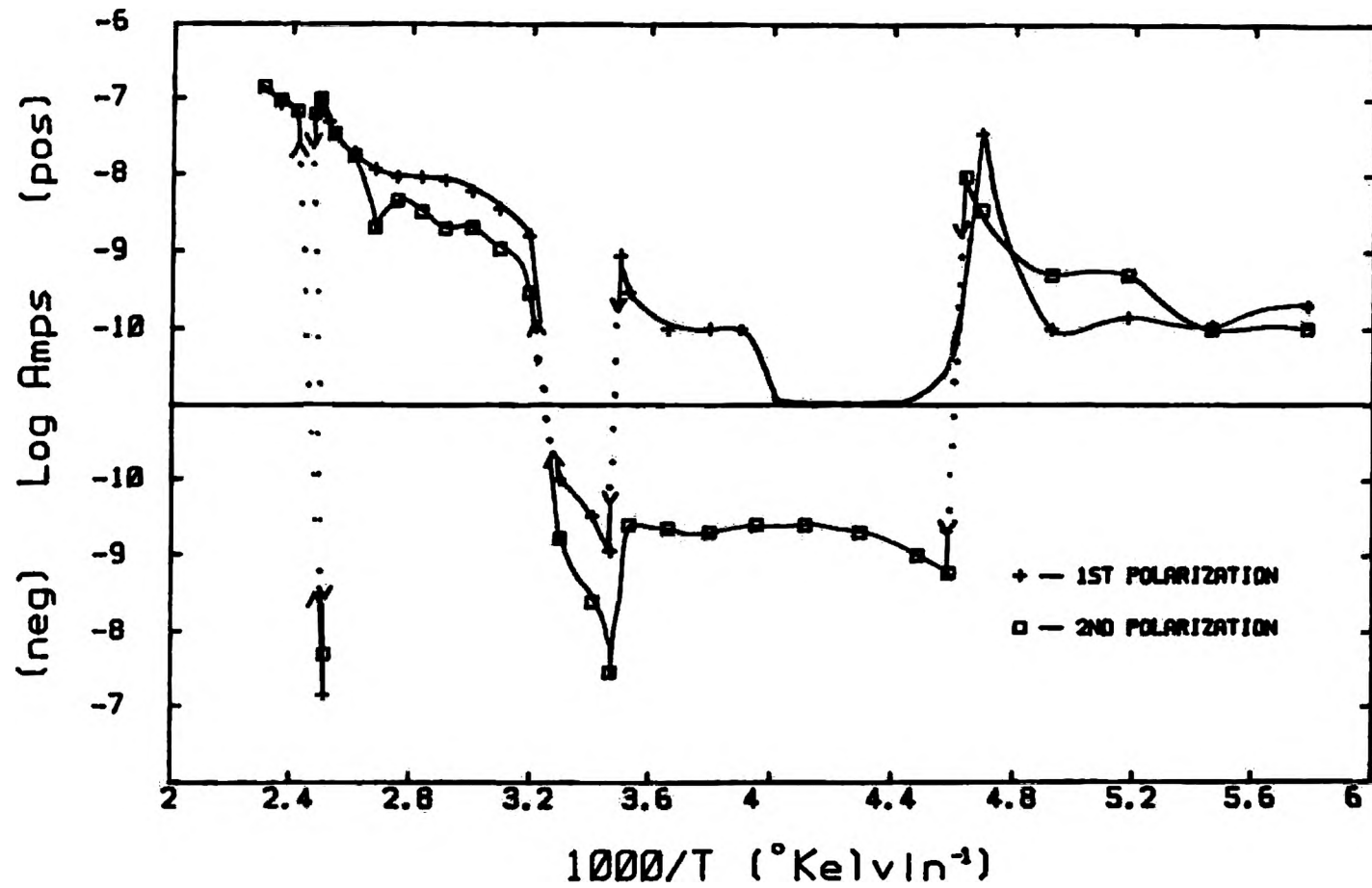


Figure 9. TSPC Graph of Barium Titanate (Ba/Ti = 0.98) with Field of 250 V/cm and Heating Rate of 0.07 K/s.

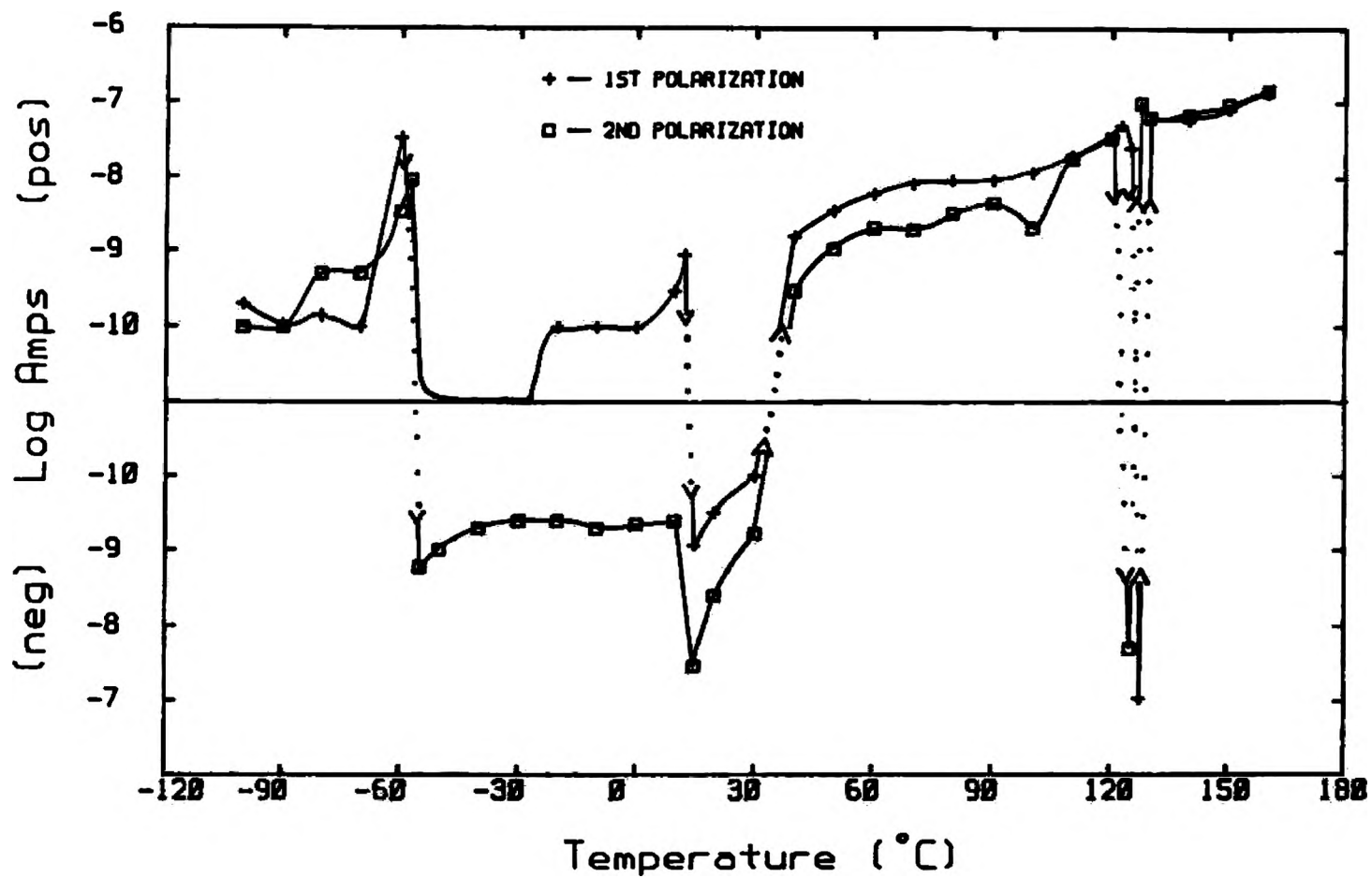


Figure 10. TSPC Graph of Barium Titanate (Ba/Ti = 0.98) with Field Of 250 V/cm and Heating Rate of 0.07 K/s.

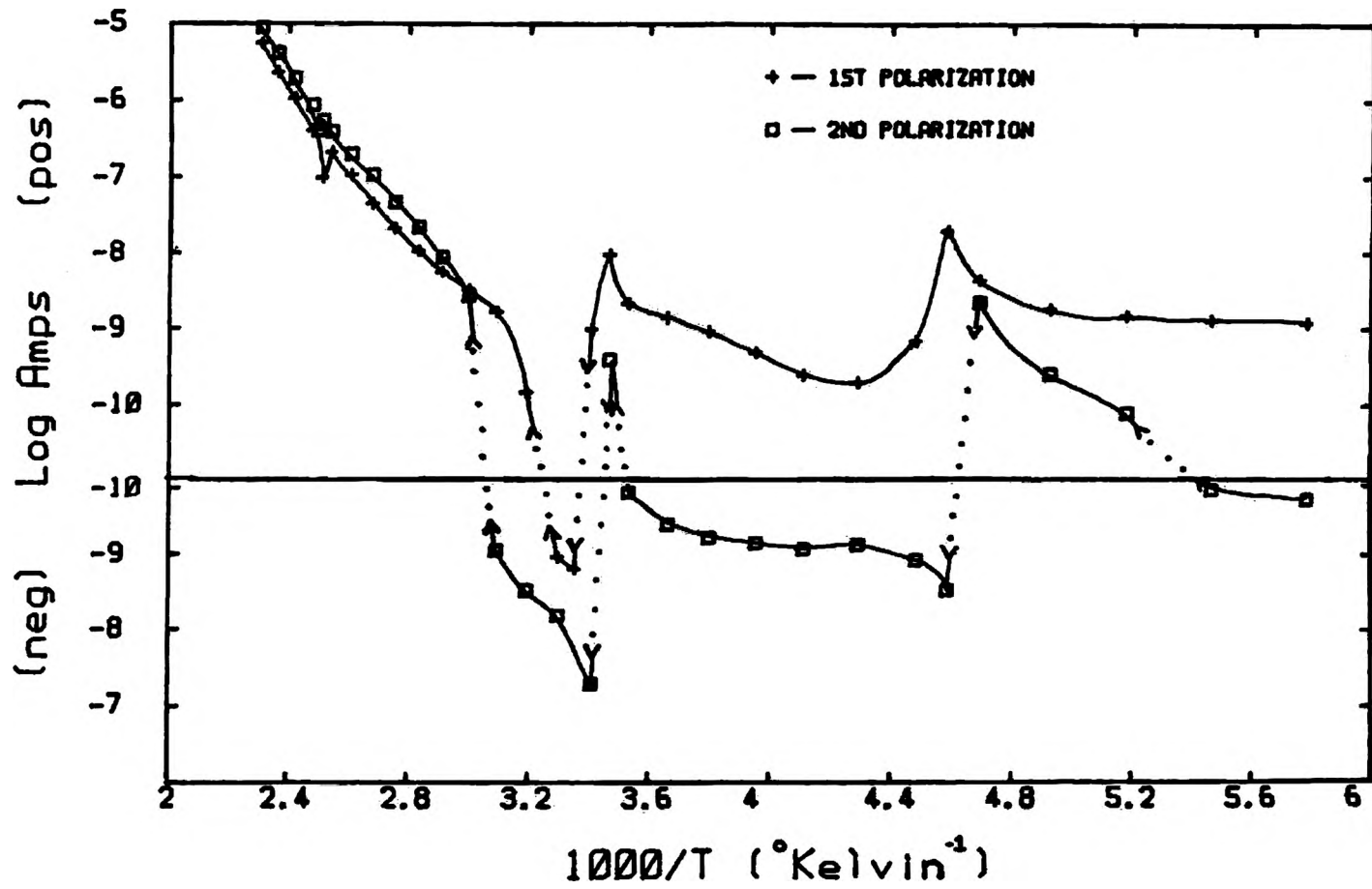


Figure 11. TSPC Graph of Barium Titanate (Ba/Ti = 1.02) with Field of 250 V/cm and Heating Rate of 0.07 K/s.

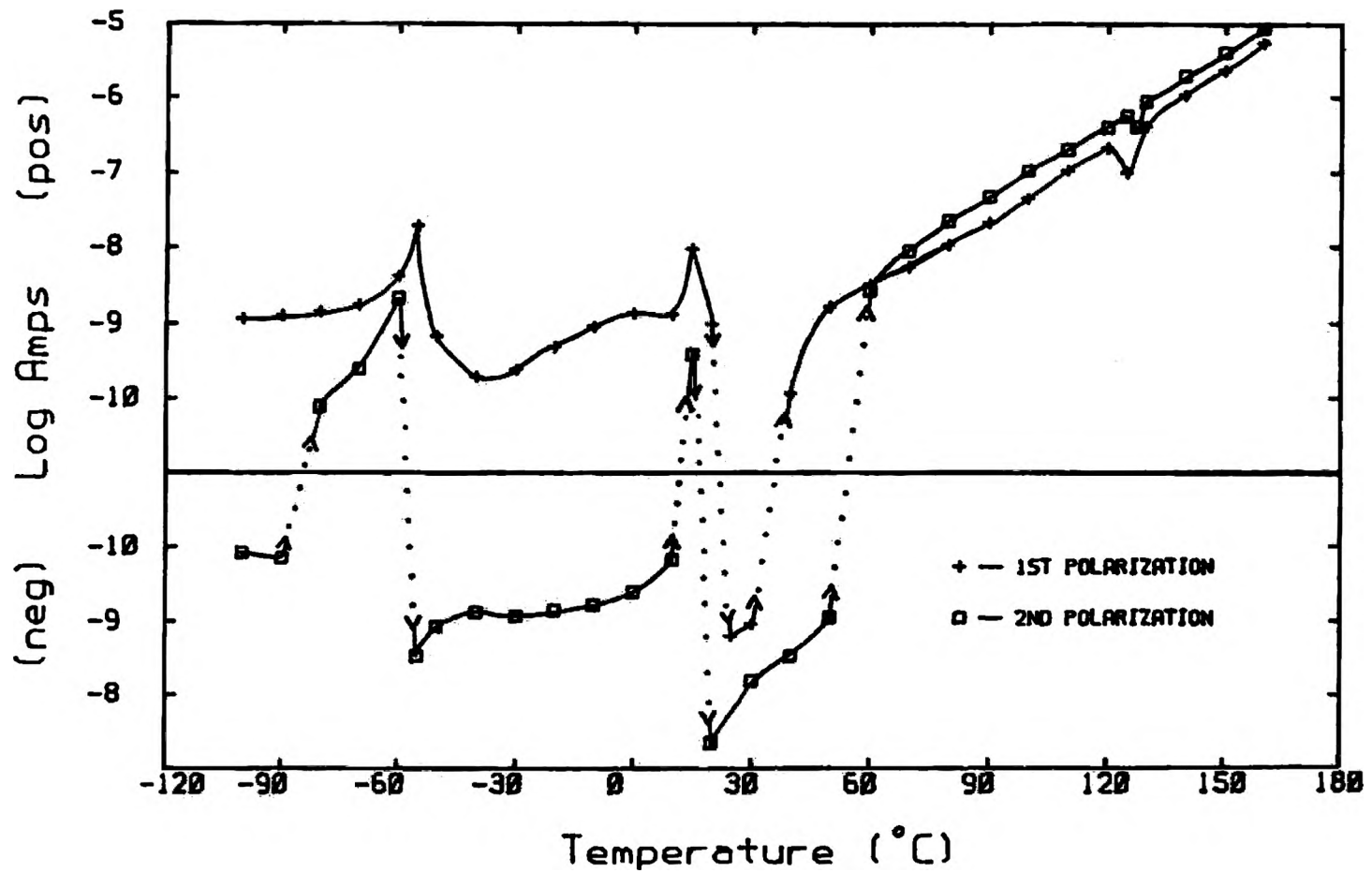


Figure 12. TSPC Graph of Barium Titanate (Ba/Ti = 1.02) with Field of 250 V/cm and Heating Rate of 0.07 K/s.

During 2nd polarization, the BaTiO₃ single crystal showed only a positive current maximum during the rhombohedral/orthorhombic transition. This was probably due to the application of an insufficient field to pole the BaTiO₃ single crystal. Complete reorientation of the domain structure did not occur, which led to the dipole charge release being masked by the leakage current.

The depolarization current spectra for all BaTiO₃ samples (Figures 13-16, 40-43) showed negative current maxima at the transition temperature as the samples discharged. Domain reorientation allowed more dipole current release during the transition. The current discharge before and after the transition temperature was relatively constant.

The current maxima observed in the BaTiO₃ spectra were directly related to the maximum value of the dielectric constant. In addition, the dielectric constant value was related to the amount of domain reorientation. The dielectric constant values for BaTiO₃ have been investigated by many authors¹⁶⁻¹⁹ and are illustrated in Figure 1¹⁷. Comparison of Figure 1 to the BaTiO₃ current spectra showed a direct relationship of the current maxima to the dielectric constant maximum value at the structural transition temperature. This relationship will be seen at the other crystallographic transitions.

2. Orthorhombic to Tetragonal Structure. During the 1st polarization, the BaTiO₃ samples showed partial poling effects at the transition temperature. The current spectra showed a positive maxima, then briefly switched into the negative current region. The change to negative current was due to a dipole charge release as the 180° domains were reoriented. The current spectra switched back to the positive

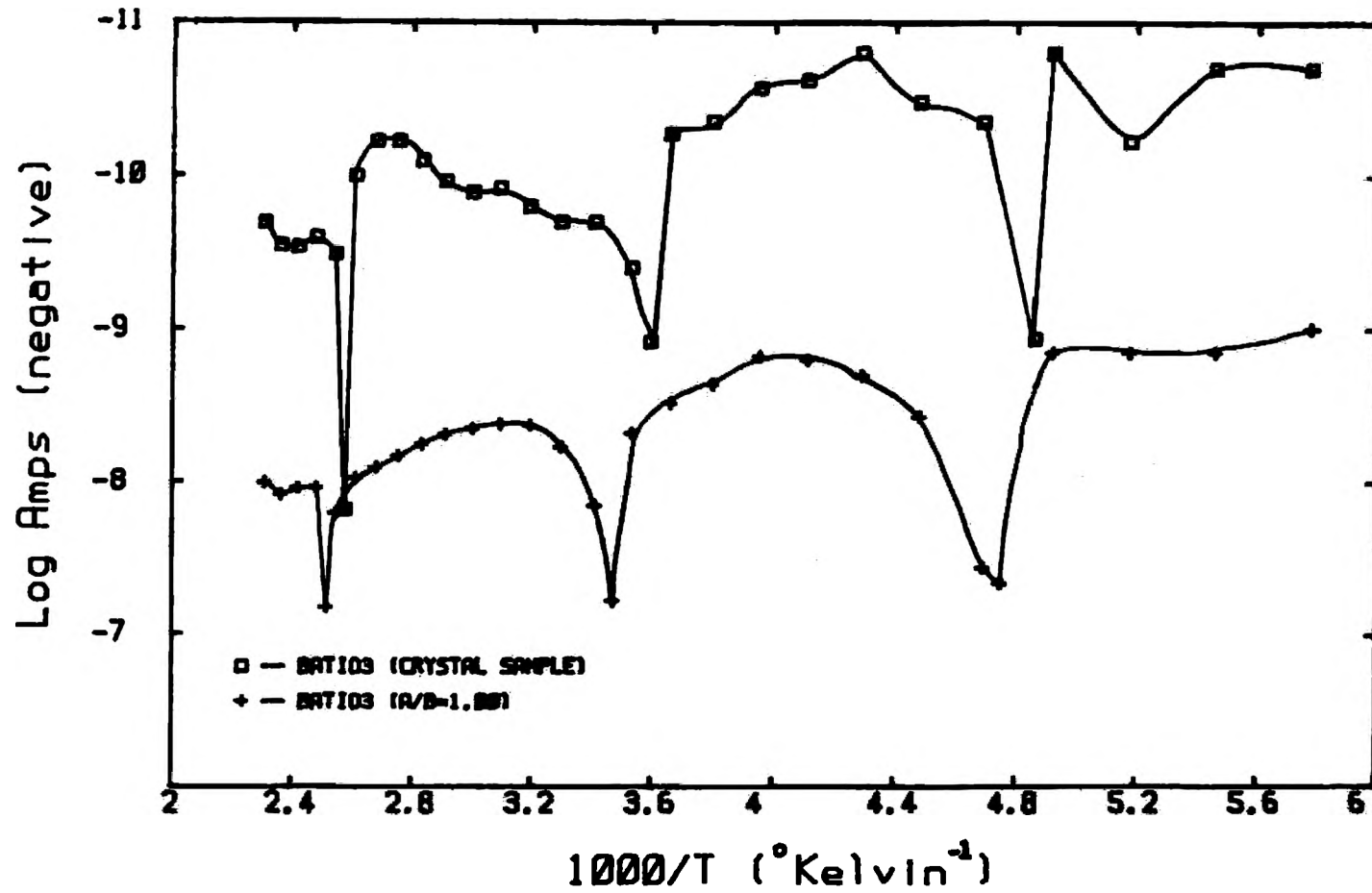


Figure 13. TSDC Graph of Barium Titanate ($\text{Ba/Ti} = 1.00$ and Single Crystal) with No Field and Heating Rate of 0.07 K/s .

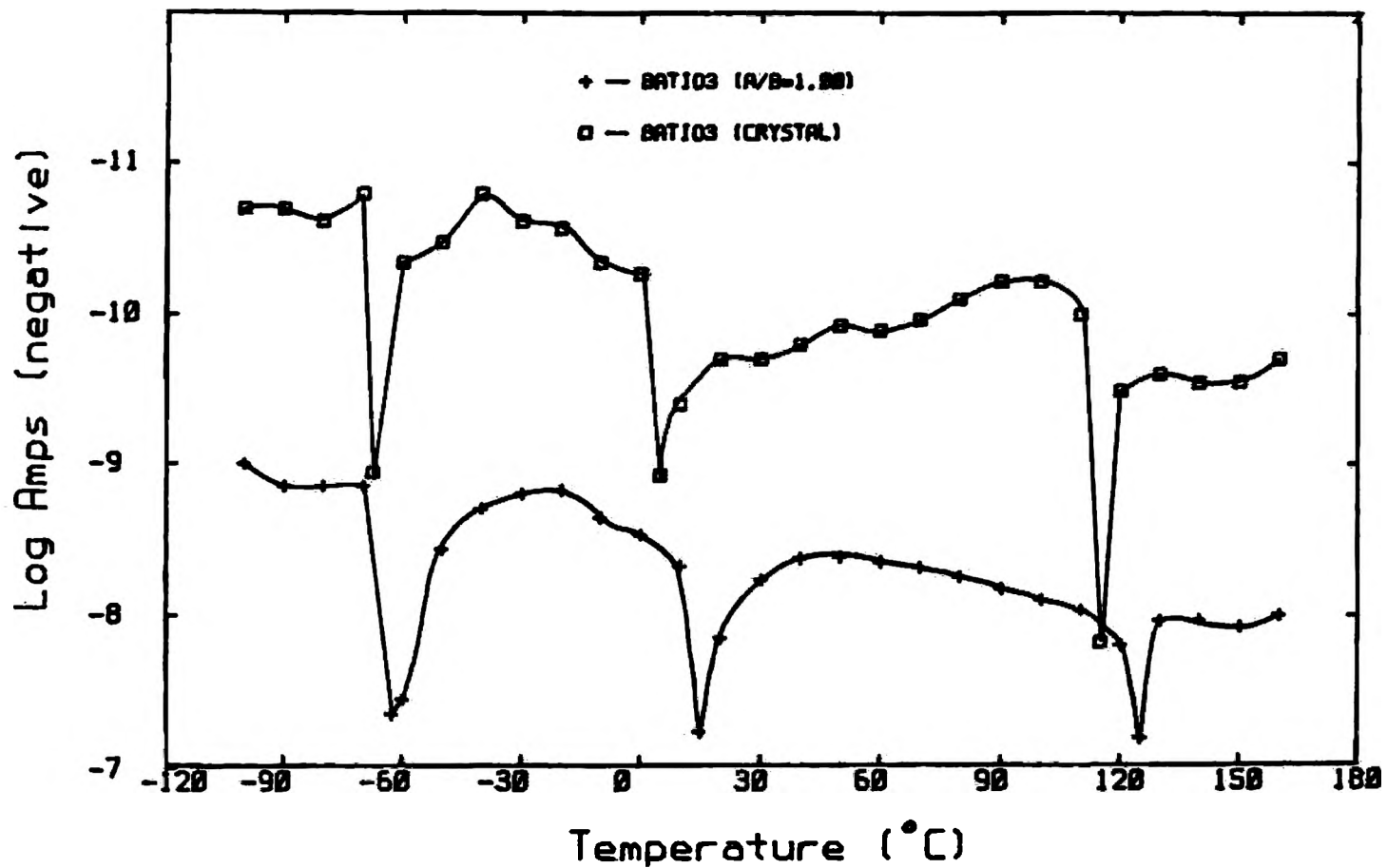


Figure 14. TSDC Graph of Barium Titanate (Ba/Ti = 1.00 and Single Crystal) with No Field and Heating Rate of 0.07 K/s.

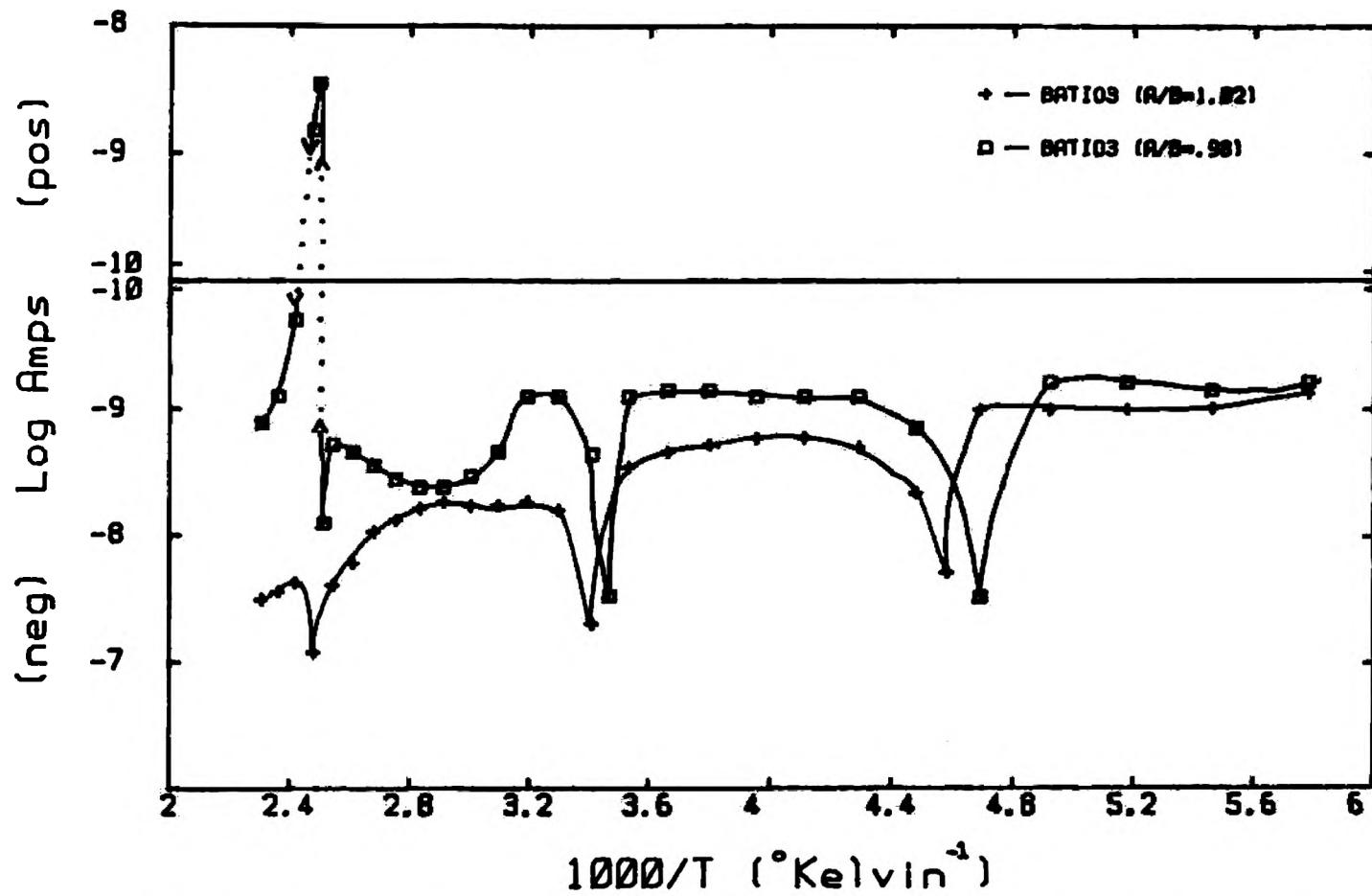


Figure 15. TSDC Graph of Barium Titanate (Ba/Ti = 1.02 and 0.98) with No Field and Heating Rate of 0.07 K/s.

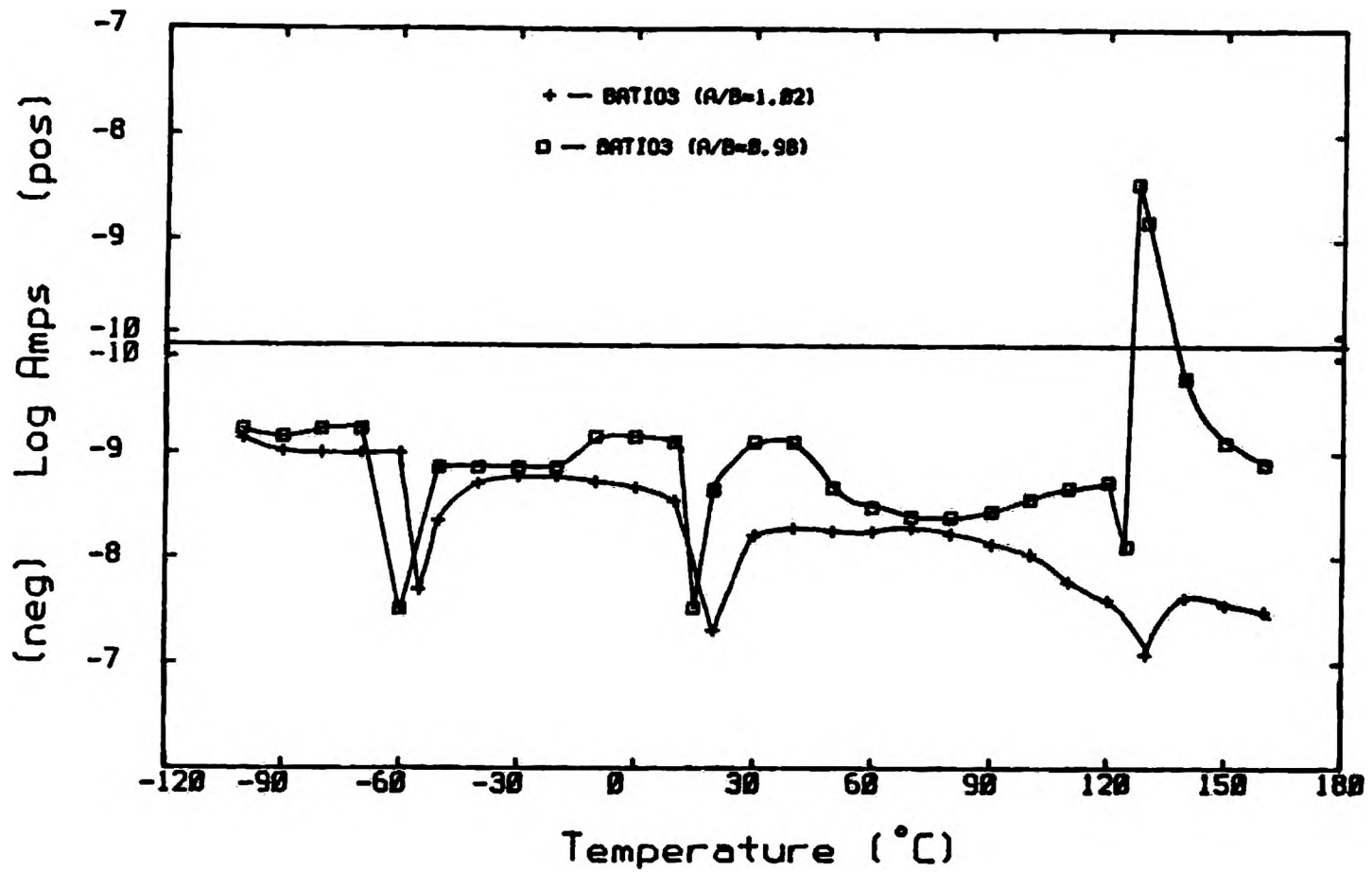


Figure 16. TSDC Graph of Barium Titanate (Ba/Ti = 1.02 and 0.98) with No Field and Heating Rate of 0.07 K/s.

current region when polarization reversal (saturation) was completed and the dipoles were fully polarized. The process of polarization reversal (saturation), as it affects domain orientation, has been explained by Jona and Shirane¹⁸ through three mechanisms:

- a) Nucleation of antiparallel domains.
- b) 180° domain wall motion in the polar axis direction.
- c) 180° domain wall motion perpendicular to the polar axis.

The 90° domains in the BaTiO₃ samples are not readily affected by an external field (based upon past studies^{18,29}) and were a small factor in domain reorientation.

Since polarization was completed, the current spectra for the BaTiO₃ samples remained positive throughout the tetragonal structure region. Again, the BaTiO₃ single crystal was the exception at the orthorhombic/tetragonal structural transition. Evidently, little polarization occurred at the low temperatures so no charge release was seen at the rhombohedral/orthorhombic transition.

The effects of sample poling and Ba/Ti ratio were seen in the 2nd polarization current spectra. For samples with Ba/Ti ratios ≤ 1.00 , the current spectra showed a negative maxima during the orthorhombic/tetragonal transition as charge was released during domain reorientation. In contrast, the current spectra of samples with Ba/Ti ratios > 1.00 briefly showed current maxima due to the abrupt change in dielectric constant. However, the magnitude of the charge release occurring with domain reorientation brought the current back into the negative current region. The BaTiO₃ single crystal showed poling effects with a

brief negative current maximum at the transition temperature. The return to the positive current region was due to polarization saturation.

For all BaTiO_3 polycrystalline samples, complete polarization saturation took place in the tetragonal structure. As the samples were heated, the current spectra switched into the positive current region and remained in the region up to the Curie point.

The depolarization current spectra for all BaTiO_3 samples showed similar negative current maxima during the orthorhombic/tetragonal transition similar to that observed at the rhombohedral/orthorhombic transition.

3. Tetragonal to Cubic Structure. During the tetragonal/cubic structural transition, the BaTiO_3 current spectra were mainly affected by changes in the Ba/Ti ratio. The current spectra were also affected by the change from ferroelectric to paraelectric behavior at the Curie point. The atomic structure of BaTiO_3 changed from a nonsymmetric atomic array (consisting of dipoles and domains) to a symmetric array where dipoles, spontaneous polarization, domain orientation, and a polar axis cannot exist. Also, as the atomic structure was reoriented, the dielectric constant for BaTiO_3 reached its maximum value.

As the tetragonal/cubic structural transition occurred for samples with Ba/Ti ratio ≤ 1.00 and the BaTiO_3 single crystal, a final domain reorientation during 1st and 2nd polarization allowed the internal electric dipole field to dominate the current spectra. Because of internal field domination, negative current maxima were observed in the samples with Ba/Ti ratios ≤ 1.00 and the single crystal. After

completion of the phase change, paraelectric behavior prevailed in the cubic structure and the current spectra remained in the positive current region due to leakage current.

The depolarization spectra for samples with Ba/Ti ratios ≤ 1.00 showed a positive current maxima due to charge release at the Curie point. During depolarization, the positive current due to a rapidly changing dielectric constant (see Equation 3) and the internal field dominated the negative charge release until the structure became cubic. Since the atomic array changed from nonsymmetric to symmetric during the tetragonal/cubic structural transition, the strongest release of charge was at the structural transition.

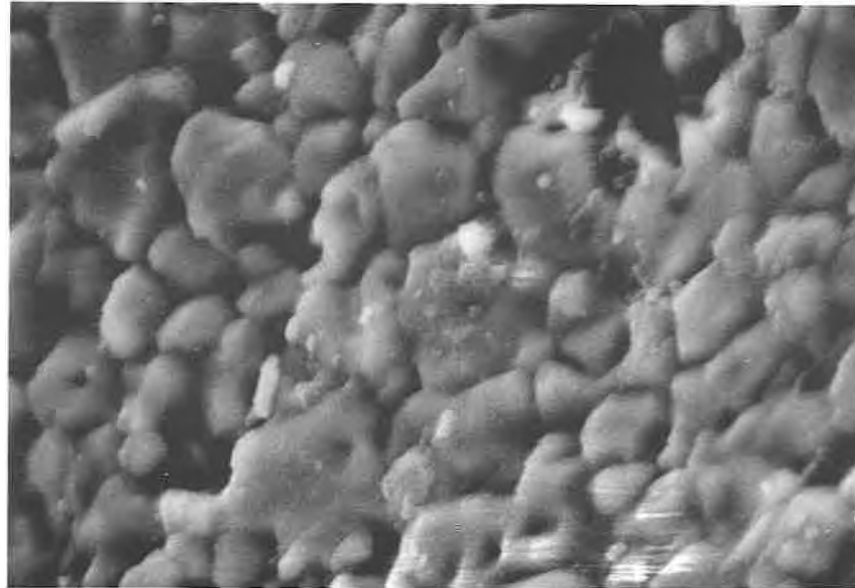
For BaTiO_3 samples with Ba/Ti ratios > 1.00 , the electrical behavior during 1st polarization also changed from ferroelectric to paraelectric at the Curie point. However, the polarization current spectra showed no switching to the negative current region or very little positive current deviation through the transition temperature. Apparently, complete polarization saturation had occurred gradually at temperatures below the Curie point. Therefore, no abrupt charge release was observed at the Curie temperature. This gradual release of charge was related to domain clamping by internal stresses (a function of grain size). Thus, no negative currents were observed and the current spectra remained in the positive current region to the end of TSPC examination. Further explanation of the current spectra at the Curie point, as related to sample grain size, will be discussed in the next section.

The depolarization spectra for samples with Ba/Ti ratios > 1.00 (including single crystal) showed only a small negative current maxima at the Curie point. Due to small grain size, domains were clamped and abrupt charge release at the transition temperature was suppressed. The grain structure effect will be discussed in the next section.

4. Sample Microstructure. The effect of grain size on the BaTiO₃ current spectra was most pronounced at the Curie point. The grain size changed as the Ba/Ti ratio was changed. The BaTiO₃ sample grain size was examined through a scanning electron microscope (SEM).

Very fine grains (1-8 μm) were observed in samples with Ba/Ti ratios > 1.00 . This is illustrated in Figures 17 and 18 which are photomicrographs of samples with Ba/Ti ratios of 1.04 and 1.02, respectively. However, when the Ba/Ti ratio exceeded 1.00, the microstructure coarsened to 20-80 μm , as illustrated in Figures 19 and 20, which are photomicrographs of samples with Ba/Ti ratios of 0.98 and 0.96, respectively. A mixture of fine and coarse grains were seen when the Ba/Ti ratio = 1.00 and is illustrated in Figure 21. Similar microstructural results were shown by Jaffe, et. al.³⁰

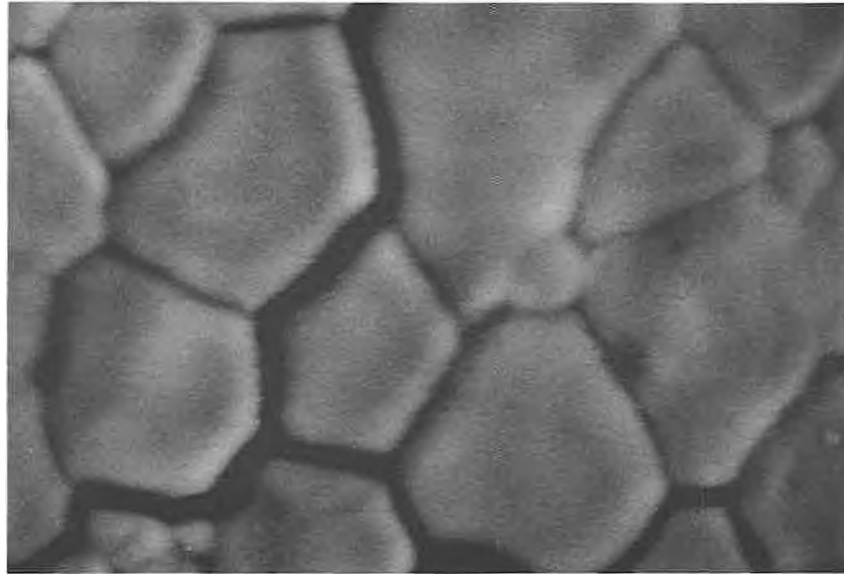
Miller³¹ established that at low external fields, polarization reversal (saturation) occurred more rapidly in fine-grained BaTiO₃ than in coarse-grained BaTiO₃. In the fine grain structure case, each grain acts as an individual domain surrounded by other single domain grains. Thus, the local field acting on the fine grains can be much higher than on the larger grains of a coarse-grained BaTiO₃ sample since the coarse grains can be partially shielded by adjacent antiparallel domains. Due to high fields, Miller concluded polarization reversal (saturation) is



25 KV 3900 X Ba/Ti = 1.04

10 μ m

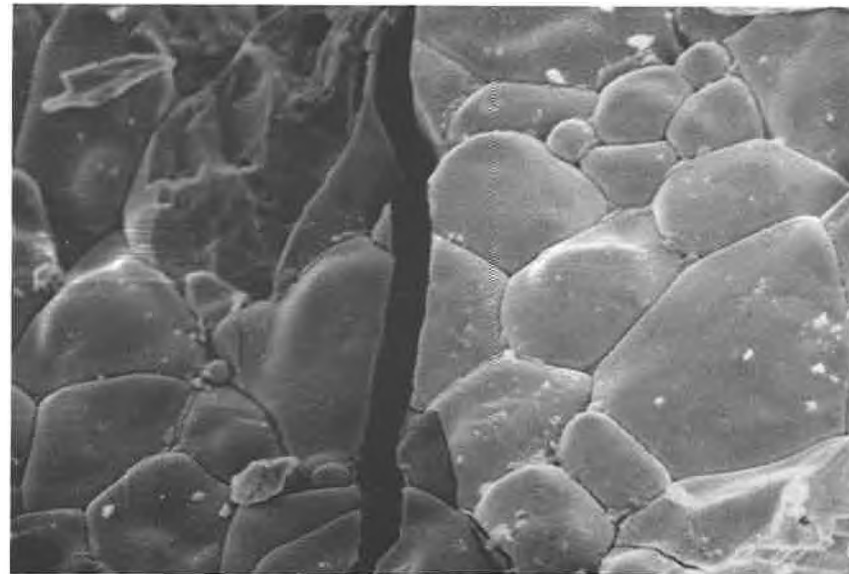
Figure 17. SEM Photograph of Barium Titanate (Ba/Ti = 1.04) at Magnification of 3900 X.



25 KV 3900 X Ba/Ti = 1.02

10 μm 

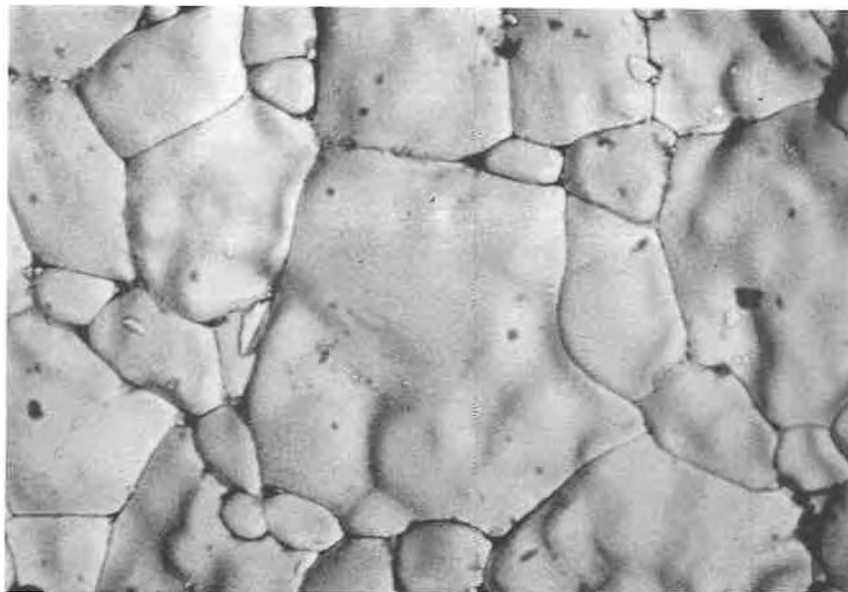
Figure 18. SEM Photograph of Barium Titanate (Ba/Ti = 1.02) at Magnification of 3900 X.



25 KV 500 X Ba/Ti = 0.98

10 μm —

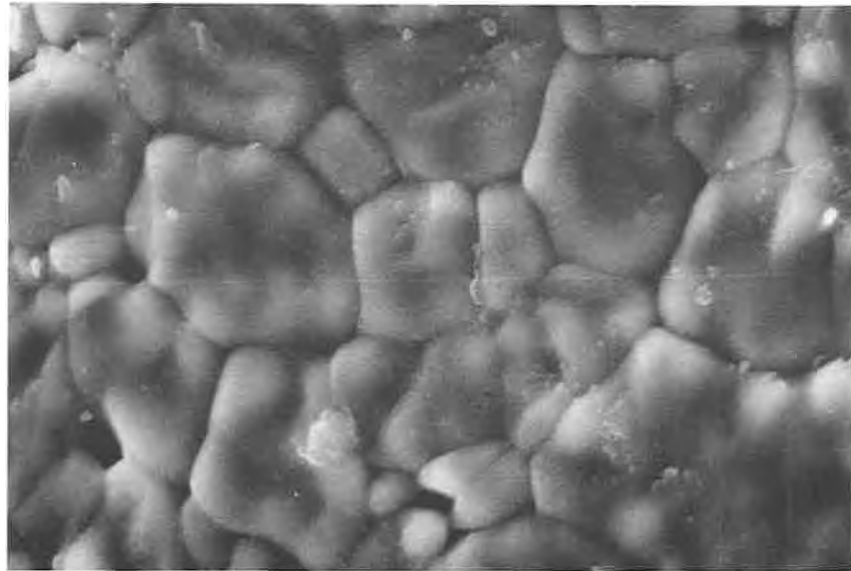
Figure 19. SEM Photograph of Barium Titanate (Ba/Ti = 0.98) at Magnification of 500 X.



25 KV 500 X Ba/Ti = 0.96

10 μ m —

Figure 20. SEM Photograph of Barium Titanate (Ba/Ti = 0.96) at Magnification of 500 X.



25 KV 3900 X Ba/Ti = 1.00

10 μ m 

Figure 21. SEM Photograph of Barium Titanate (Ba/Ti = 1.00) at Magnification of 3900 X.

more energetically favored in fine-grained BaTiO₃ than in coarse-grained BaTiO₃. Miller also concluded that this explanation helped to explain, in part, why fine-grained BaTiO₃ had a higher dielectric constant than coarse-grained BaTiO₃.

Other authors have also studied the effects of grain size to the dielectric constant of BaTiO₃³²⁻³⁶. Of particular interest was the study done by Kinoshita and Yamaji³⁶ on the grain size effects on the dielectric properties of BaTiO₃. Kinoshita and Yamaji showed that the dielectric constant depended strongly on the grain size in the ferroelectric state while being almost independent of grain size in the paraelectric state. Moreover, in the ferroelectric state, they showed that the dependence of the dielectric constant on grain size was different in each crystallographic phase of BaTiO₃.

Specifically, for the tetragonal phase, Kinoshita and Yamaji³⁶ found that the finer the grain size, the higher the dielectric constant. However, in the rhombohedral and orthorhombic phases, the K of the finer-grained BaTiO₃ ceramics was not always higher than that of coarser-grained ceramics due to different dependence on temperature. When grain size was reduced smaller than 3 μm, K decreased rapidly with lowering temperature. As a result, the dielectric constant of 1.1 μm grained ceramics was almost identical to that of 53 μm at -140°C, although the former has a dielectric constant about four times as high as that of the latter in the tetragonal phase. In contrast, Kinoshita and Yamaji found that in the paraelectric state, K follows the Curie-Weiss law, which meant that the behavior of K was not influenced by grain size above T_C.

The conclusions by Miller³¹ also help to explain the occurrence of no maxima in BaTiO₃ current spectra with Ba/Ti ratios > 1.00 (fine grains) and the occurrence of maxima in BaTiO₃ samples with Ba/Ti ratios ≤ 1.00 (coarse grains) and the BaTiO₃ single crystal. Complete polarization saturation and gradual charge release occurred before the Curie point was reached in samples with Ba/Ti ratios > 1.00 allowing the external field to dominate the current spectra. The result was only a small maxima being observed in the TSPC/TSDC current spectra in samples with Ba/Ti ratios > 1.00. However, polarization saturation was completed abruptly at the Curie point in samples with Ba/Ti ratios ≤ 1.00 (including the single crystal). This resulted in charge release and a negative maxima in the TSPC current spectra for Ba/Ti ratios ≤ 1.00.

5. Activation Energy/Resistivity. The activation energies for the BaTiO₃ samples were determined from the current spectra over a temperature range of 50 to 160°C. The slope of the log current versus inverse temperature graph determined the activation energy of the sample. Table II lists the activation energies for BaTiO₃ samples.

BaTiO₃ samples with Ba/Ti ratios < 1.00 had activation energy values ranging from 0.5 to 0.8 eV while samples with Ba/Ti ratios ≥ 1.00 had values ranging from 0.9 to 1.2 eV. Keck¹ observed similar activation energies for the same Ba/Ti ratios. He also found electrical degradation resistance was higher in samples with Ba/Ti ratios > 1.00 while samples with Ba/Ti ratios < 1.00 were more susceptible to degradation. Thus, it appears that the results of this investigation compare well with those made by Keck, although measurements at higher

TABLE II
ACTIVATION ENERGIES/CURRENT MAGNITUDES

<u>Sample Description</u>	<u>Activation Energy(eV)</u>	<u>Temperature Range(°C)</u>	<u>Log Current Magnitude Change</u>
BaTiO ₃ (a/b=1.04)	1.0	50-160	6
BaTiO ₃ (a/b=1.03)	1.0	100-160	5
BaTiO ₃ (a/b=1.02)	1.0	60-160	5
BaTiO ₃ (a/b=1.01)	0.9	60-160	5
BaTiO ₃ (a/b=1.005)	1.0	70-160	5
BaTiO ₃ (a/b=1.00)	1.2	110-160	4
BaTiO ₃ (a/b=0.995)	0.7	70-160	4
BaTiO ₃ (a/b=0.99)	0.8	80-160	4
BaTiO ₃ (a/b=0.98)	0.5	50-160	4
BaTiO ₃ (a/b=0.97)	0.5	60-160	3
BaTiO ₃ (a/b=0.96)	0.6	60-160	3
Z5U Capacitor	1.5	70-160	6
NPO Cap(sample #1)	1.2	80-160	4
NPO Cap(sample #2)	1.0	80-160	4
BX Cap (sample #1)	1.4	120-160	3
BX Cap (sample #2)	failure @ 40°C		9
BX Cap (sample #3)	1.3	120-160	3
BX Cap (sample #4)	failure @ 60°C		6
BX Cap (sample #5)	1.2	100-160	4
BX Cap (sample #6)	1.3	110-160	4
BX Cap (sample #7)	failure @ -20°C		8

Note: Activation energy calculation error --> ± 0.1 eV

fields would be needed to make a direct correlation.

The resistivities of the BaTiO_3 samples were also determined from their current spectra. Table III lists the initial and final resistivity values for the samples measured. The greatest amount of resistivity change was seen with BaTiO_3 samples with Ba/Ti ratios ≥ 1.00 . The amount of resistivity change seen with these samples was on the average six orders of magnitude. The lowest resistivity value (5×10^5 ohm-cm) was seen with a sample with a Ba/Ti ratio of 1.04. In contrast, the samples with Ba/Ti ratios < 1.00 showed higher resistivities and lesser amounts of magnitude change. The magnitude of the resistivity changes occurring between -100 and 160°C were directly attributed to the activation energy for conduction of each composition. That is, the largest changes occurred for samples having the higher activation energies, which was related to the Ba/Ti ratio.

TABLE III
SAMPLE RESISTIVITY

<u>Sample Description</u>	<u>Temperature Range(°C)</u>	<u>Resistivity(ohm-cm)</u>	
		<u>Initial</u>	<u>Final</u>
BaTiO ₃ (a/b=1.04)	-100 to 160	1 x 10 ¹⁰	5 x 10 ⁵
BaTiO ₃ (a/b=1.03)	-100 to 160	1 x 10 ¹⁰	4 x 10 ⁵
BaTiO ₃ (a/b=1.02)	-100 to 160	1 x 10 ¹⁰	5 x 10 ⁵
BaTiO ₃ (a/b=1.01)	-100 to 160	1 x 10 ¹⁰	4 x 10 ⁵
BaTiO ₃ (a/b=1.005)	-100 to 160	1 x 10 ¹⁰	3 x 10 ⁵
BaTiO ₃ (a/b=1.00)	-100 to 160	1 x 10 ¹⁰	3 x 10 ⁵
BaTiO ₃ (a/b=0.995)	-100 to 160	1 x 10 ¹¹	6 x 10 ⁷
BaTiO ₃ (a/b=0.99)	-100 to 160	1 x 10 ¹¹	6 x 10 ⁷
BaTiO ₃ (a/b=0.98)	-100 to 160	1 x 10 ¹¹	6 x 10 ⁷
BaTiO ₃ (a/b=0.97)	-100 to 160	1 x 10 ¹¹	4 x 10 ⁷
BaTiO ₃ (a/b=0.96)	-100 to 160	1 x 10 ¹¹	4 x 10 ⁷
Z5U Capacitor	70 to 160	3 x 10 ⁸	5 x 10 ³
NPO Cap(sample #1)	70 to 160	1 x 10 ¹¹	5 x 10 ⁷
NPO Cap(sample #2)	70 to 160	1 x 10 ¹¹	2 x 10 ⁷
BX Cap(sample #1)	80 to 160	1 x 10 ¹⁰	1 x 10 ⁷
BX Cap(sample #2)	-100 to 160	7 x 10 ⁹	8.0
BX Cap(sample #3)	80 to 160	1 x 10 ¹⁰	2 x 10 ⁷
Bx Cap(sample #4)	80 to 160	2 x 10 ⁷	1 x 10 ³
BX Cap(sample #5)	100 to 160	1 x 10 ¹⁰	1 x 10 ⁵
BX Cap(sample #6)	100 to 160	1 x 10 ⁹	2 x 10 ⁶
BX Cap(sample #7)	-20 to 160	2 x 10 ¹¹	6 x 10 ³

B. CAPACITOR EXAMINATION THROUGH TSPC/TSDC.

1. Formulation Description. Barium titanate (BaTiO_3) is the most important and widely used single component for multilayer ceramic capacitors. In the previous section, the current spectra of BaTiO_3 were discussed. This section will discuss the TSPC/TSDC spectra of BaTiO_3 -based ceramic capacitors. Before detailed discussion can begin, however, a brief explanation of capacitor formulations and their characteristics is needed.

Of all capacitor formulations used, all can be classified under one of two specific dielectric classifications, as set by the Electronic Industries Association (EIA)²⁵. The classes are:

- a) Class I dielectrics.
- b) Class II dielectrics.

In general, most Class I dielectric capacitors have the designation "NPO" while the most popular designations for Class II dielectrics included "Z5U" and "X7R" (military equivalent "BX"). Table IV lists the possible designations for both Class I and II dielectrics. Table V lists the electrical properties of the three most popular capacitor formulations; NPO, X7R/BX, and Z5U.

Class I dielectrics are defined by the EIA as follows²⁵:

Components of this classification are temperature-compensating, fixed, ceramic dielectric capacitors of a type suited for resonant circuit application where high Q and stability of capacitance are required.

As stated previously, the NPO dielectrics are the most popular Class I dielectrics used in ceramic capacitor manufacture. The two most important properties of this class of dielectric are:

TABLE IV
EIA CAPACITOR DESIGNATIONS

Class I Designations

<u>Designation</u>	<u>Cap. Change Limit</u>	<u>Temp. Limits</u>
NPO	+ 30 ppm/°C	-55 to 125°C
COG	(same as NPO)	

Class II Designations

<u>Lower Temp. Limit (°C)</u>	<u>Reference</u>	<u>Upper Temp. Limit (°C)</u>	<u>Reference</u>	<u>Cap. Change Limit (%)</u>	<u>Reference</u>
+10	Z	+45	2	+1.0	A
-30	Y	+65	4	+1.5	B
-55	X	+105	5	+2.2	C
		+125	7	+3.3	D
				+4.7	E
				+7.5	F
				+10.0	P
				+15.0	R
				+22.0	S
				+22.0, -33.0	T
				+22.0, -56.0	U
				+22.0, -82.0	V

Example: Y5R
 Cap. Change = 0+15%
 From -30°C
 to +85°C

Note: Capacitance changes referenced at 25°C.

TABLE V
CAPACITOR SPECIFICATIONS

<u>Type of Capacitor</u> --->	<u>Z5U</u>	<u>X7R(BX)</u>	<u>NPO</u>
<u>Properties</u>			
Temp. Range (°C)	+10 to 85	-55 to 125	-55 to 125
Max. Cap % Change Allowed over Temp. Range (no bias)	+22%,-56%	<u>+15%</u>	0 <u>+ 30 ppm/°C</u>
Dissipation Factor (%) @ 1kHz	2.5% max.	2.5% max.	2.5% max
Insulation Resistance Mega-ohms (ohm-farad) @ 25°C	100K (500-1000)	100K (1000)	100K (1000)
Rated Voltage (volts DC)	25-100	50-200	50-200
Flash Test Voltage (DWV) (Dielectric Strength)	2X to 3X rated	2.5 X rated	2.5X to 4X rated
Max. Cap% Change over Temp. Range at Rated Voltage (100 V--BX only)		+15 % -25 %	
Life Test Parameter	1000 hrs. @ 1.5X rated voltage @ 85°C	1000 hrs. @ 2X rated voltage @ 125°C	1000 hrs. @ 2X rated voltage @ 125°C

a) Class I dielectrics show neither piezoelectric nor ferroelectric properties; rather, paraelectric (linear) dielectric properties.

b) Class I dielectrics are relatively unaffected by the environment or imposed operating conditions.

Because of its paraelectric properties, Class I dielectrics generally have low K (dielectric constant) values ranging from 10 to 80. For example, most NPO formulations contain a mixture of BaTiO_3 and TiO_2 with possible additions of ZrO_2 or $\text{Nd}(\text{CO}_3)_4$ ³⁷.

Class II dielectrics have the following description as defined by the EIA²⁵:

Components of this classification are fixed, ceramic dielectric capacitors of a type suited for bypass and coupling application or for frequency discriminating circuits where Q and stability of capacitance characteristic are not of major importance.

Class II ceramic dielectric exhibit a predictable capacitance change with time and voltage. Compensation for the aging effect is made by referencing capacitance limits to a future time deemed to be most useful to the buyer; 1000 hours is normally chosen, but other arrangements may be negotiated between buyer and seller. Voltage will also cause a temporary capacitance change and test sequence should be such that capacitance measurements are not affected by previous voltage tests.

Although both Z5U and X7R/BX formulations are Class II dielectrics, each formulation has different electrical properties (Tables IV and V) and different K values determined by the addition of certain additives. To achieve the high K values (5500-7000) over a narrow temperature range (around room temperature) for a Z5U formulation, an additive to shift and slightly depress the Curie point dielectric constant peak of BaTiO_3 is needed. Additives for this purpose contain either Sr, Zr, or Sn (in the form of SrTiO_3 , BaZrO_3 , CaZrO_3 , or CaSnO_3 ,

as examples)³⁷. To achieve the moderate K values (1200-3000) over a wide temperature range for a X7R/BX formulation, an additive to suppress or flatten the Curie point dielectric constant peak of BaTiO₃ is used. Possible additives to achieve Curie point suppression include Bi₂O₃ and Nb₂O₅³⁷.

2. NPO Capacitor Results. The current spectra of two different NPO capacitor samples are illustrated in Figures 22 and 23. The good NPO capacitor was subjected to no accelerated electrical testing (sample #1-Figure 22) while the other NPO capacitor (sample #2-Figure 23) had failed accelerated lifetesting (using MIL-C-123 test conditions for 1000 hours).

NPO capacitor sample #1 showed a polarization spectrum with a gradual linear increase in positive (leakage) current as the temperature increased (above 85°C). The small amount of positive current seen in the first half of the current spectrum was probably from residual charges on the capacitor surface; otherwise no current would have been observed. The depolarization spectrum of sample #1 showed a gradually increasing negative (discharge) current with increasing temperature (above 85°C). Both TSPC/TSDC spectra of the NPO formulation illustrated typical paraelectric behavior which is to be expected since the formulation compositions are paraelectric.

NPO capacitor sample #2 showed a similar TSPC/TSDC spectra to that of sample #1 even though sample #2 had failed accelerated lifetesting. The behavior can be explained in this manner:

- a) All moisture was removed from the sample prior to testing (as set by the procedures).

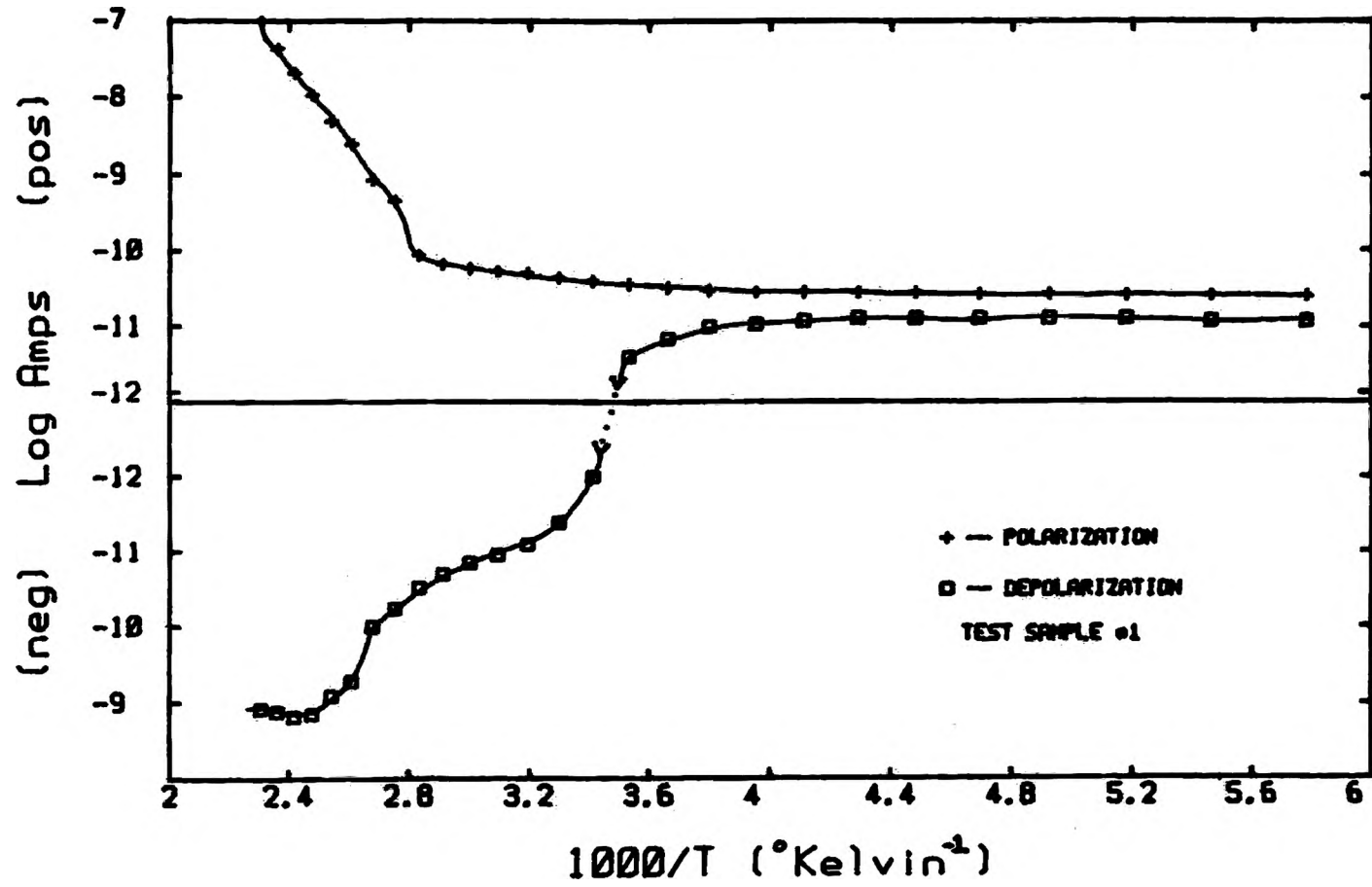


Figure 22. TSPC/TSDC Graph of NPO Multilayer Capacitor (Sample #1) with Field of 7200 V/cm and Heating Rate of 0.07 K/s.

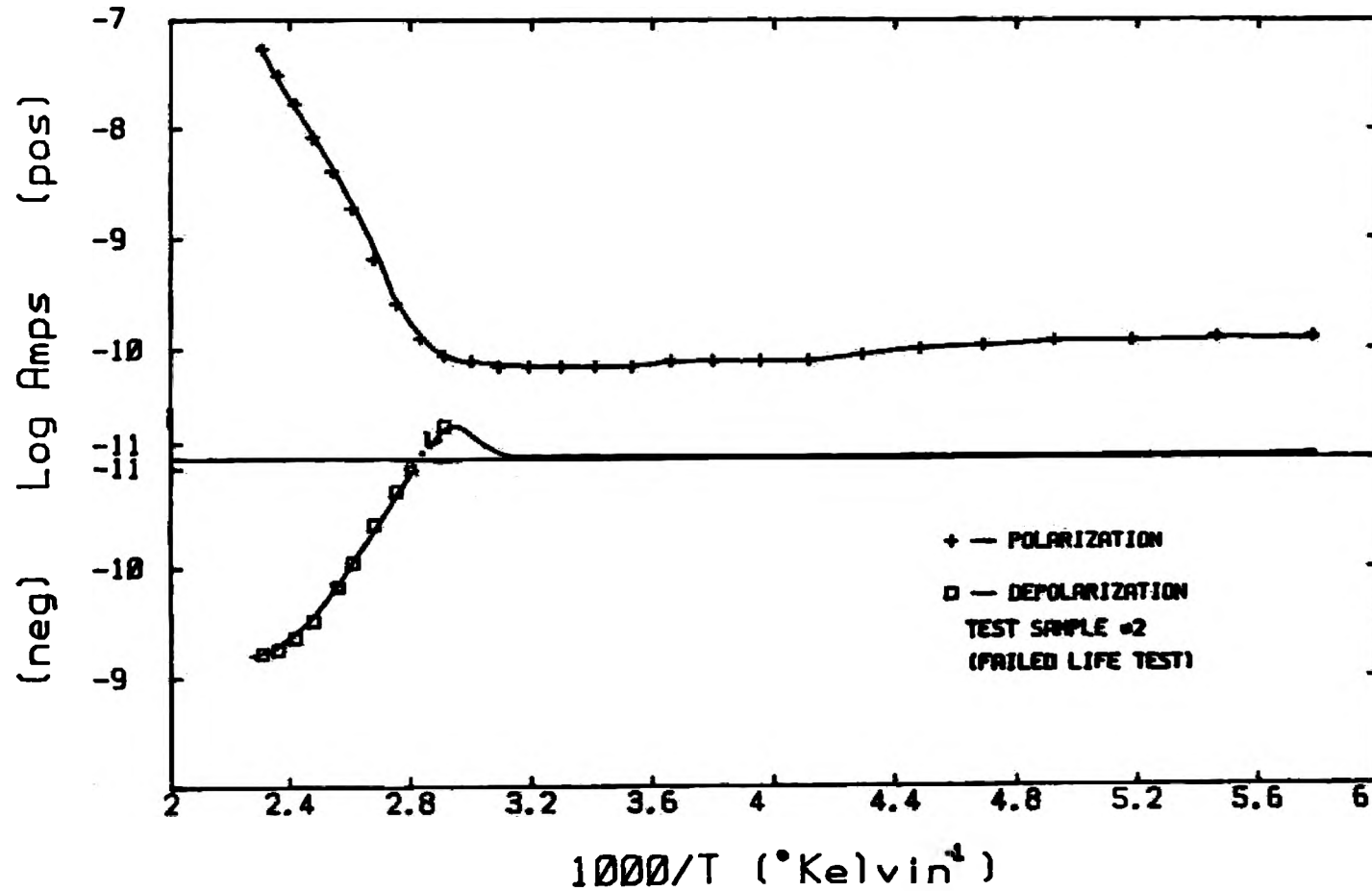


Figure 23. TSPC/TSDC Graph of NPO Multilayer Capacitor (Sample #2) with Field of 7200 V/cm and Heating Rate of 0.07 K/s.

b) TSPC/TSDC examination was performed in a moisture-free, inert atmosphere.

c) The failed sample partially recovered before TSPC/TSDC examination began.

3. Z5U Capacitor Results. The current spectra of the Z5U capacitor formulation (Figures 24 and 25) showed the effect of shifting the structural transitions in BaTiO_3 (especially the tetragonal-cubic transition) to lower temperatures by the addition of cations (like Sr^{+2} , Zr^{+2} , and Sn^{+2}) as substitutes for Ba^{+2} and Ti^{+4} cations in the BaTiO_3 lattice. For Z5U characteristics, sufficient additives are used to shift the maximum dielectric constant of BaTiO_3 from 125°C to lower temperatures (normally 25 to 40°C). The current spectra for the Z5U capacitor sample (Figures 24 and 25) showed a shifted Curie point around 40°C and a orthorhombic/tetragonal transition which shifted from approximately 15°C to about -40°C . Polarization effects seen in the Z5U capacitor spectra were similar to those observed in the BaTiO_3 samples discussed previously (especially samples with Ba/Ti ratios ≤ 1.00). Domain switching had taken place during the phase transitions resulting in the occurrence of a negative current maxima. As the temperature exceeded the shifted Curie point, complete charge release occurred. The spectra returned to the positive current region and the leakage current prevailed afterwards.

The depolarization spectra of the Z5U capacitor showed small negative (discharge) current maxima during charge release as the temperature passed through the shifted Curie temperature.

4. BX Capacitor Results. The X7R/BX capacitor formulation was the most extensively studied formulation in this investigation. The

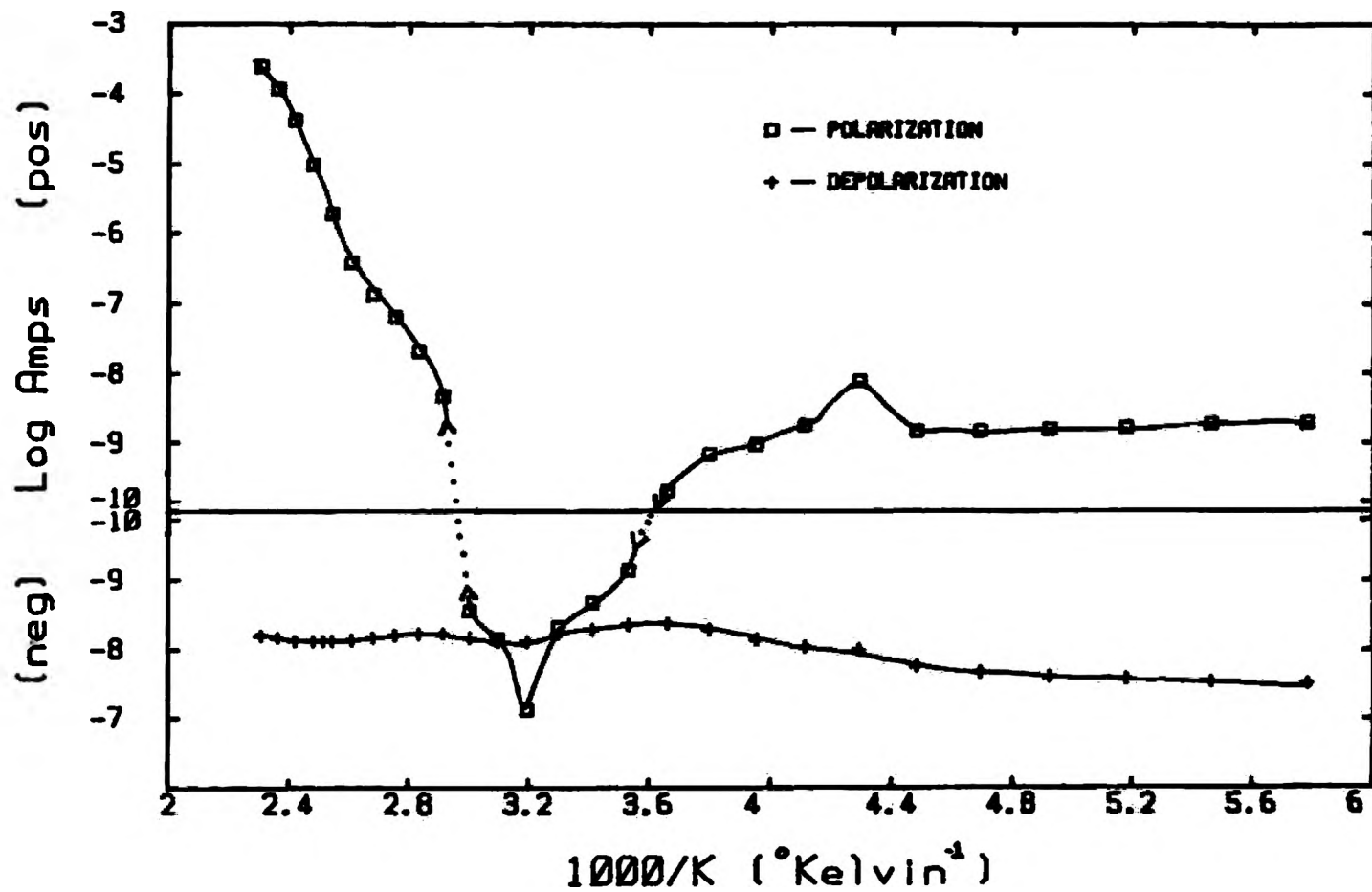


Figure 24. TSPC/TSDC Graph of Z5U Multilayer Capacitor with Field of 7200 V/cm and Heating Rate of 0.07 K/s.

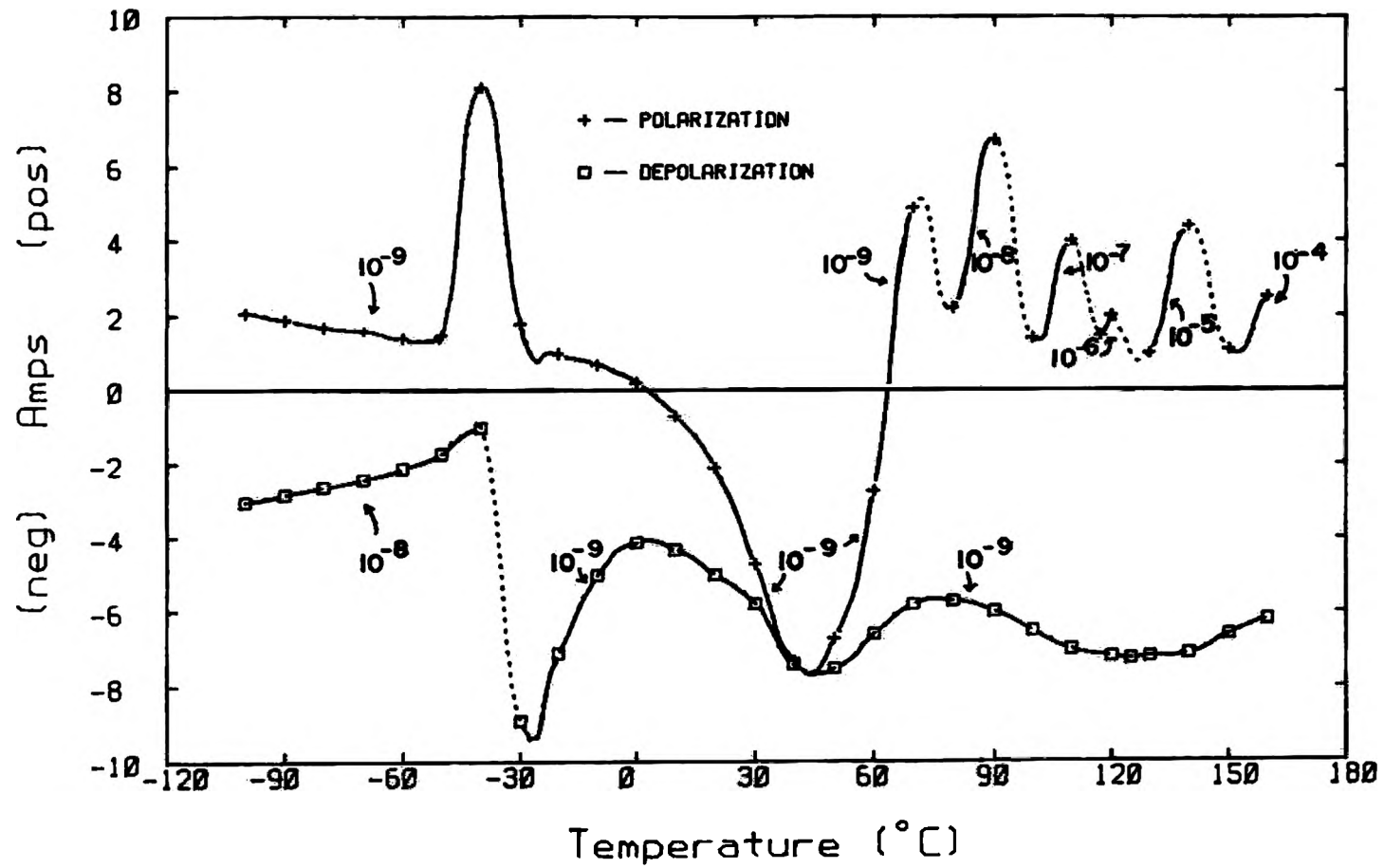


Figure 25. TSPC/TSDC Graph of Z5U Multilayer Capacitor with Field of 7200 V/cm and Heating Rate of 0.07 K/s.

capacitors examined (excluding NPO and Z5U capacitors) met the military capacitor designation 'BX' and shall be referred to as BX capacitors (see Table V for specifications). TSPC/TSDC behavior of BX capacitor samples are illustrated in Figures 26-31 (samples #1-7).

The current spectra of the BX capacitor formulation (Figures 26 and 27-sample #1) showed the effect of shifting and broadening the tetragonal/cubic structural transition (Curie point) of BaTiO_3 by shifter-type additives. The changes in the phase transition led to a flattened and broadened the dielectric constant maximum over a wide temperature range. As stated earlier, the additives used to achieve this behavior are typically Bi_2O_3 and Nb_2O_5 .

The result of flattening and broadening the tetragonal/cubic transition over a large temperature range also affected the current behavior of sample #1. The polarization spectra (Figures 26 and 27) showed a negative current with small distortions (or peaks) up to 120°C . Polarization saturation took place in the capacitor resulting in the current spectra returning to the positive current region. The large current maximum usually seen in BaTiO_3 at the Curie point (and the corresponding dielectric constant maximum) appear to have dispersed into a series of smaller peaks. The small peaks were probably due to charge release by regions of the chemically nonhomogeneous capacitors as their particular Curie temperatures were exceeded. The depolarization spectra for BX capacitor sample #1 also showed a series of partial charge releases which tends to agree that chemical nonhomogeneities prevail in the BX formulation.

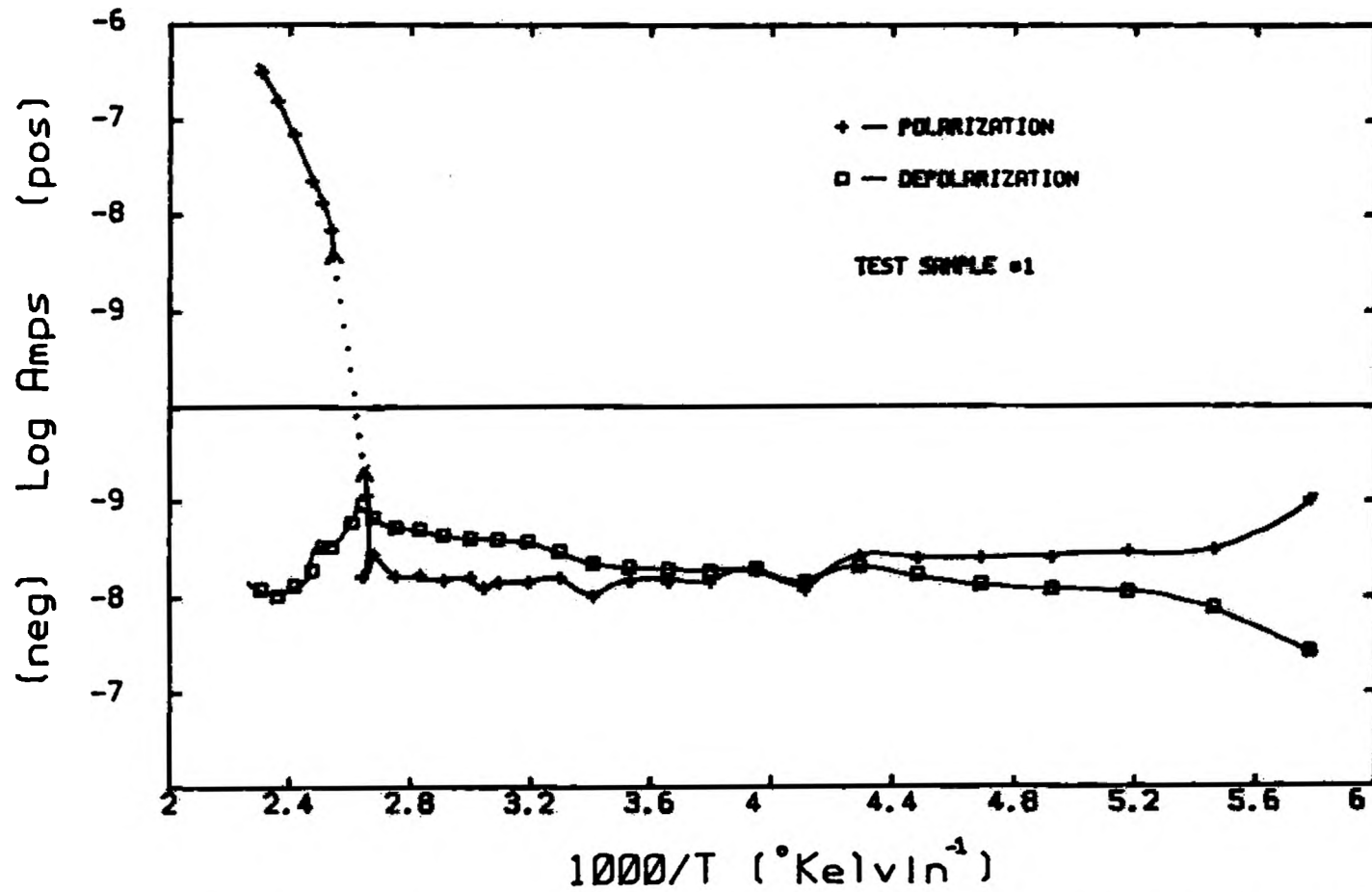


Figure 26. TSPC/TSDC Graph of BX Multilayer Capacitor (Sample #1) with Field of 7200 V/cm and Heating Rate of 0.07 K/s.

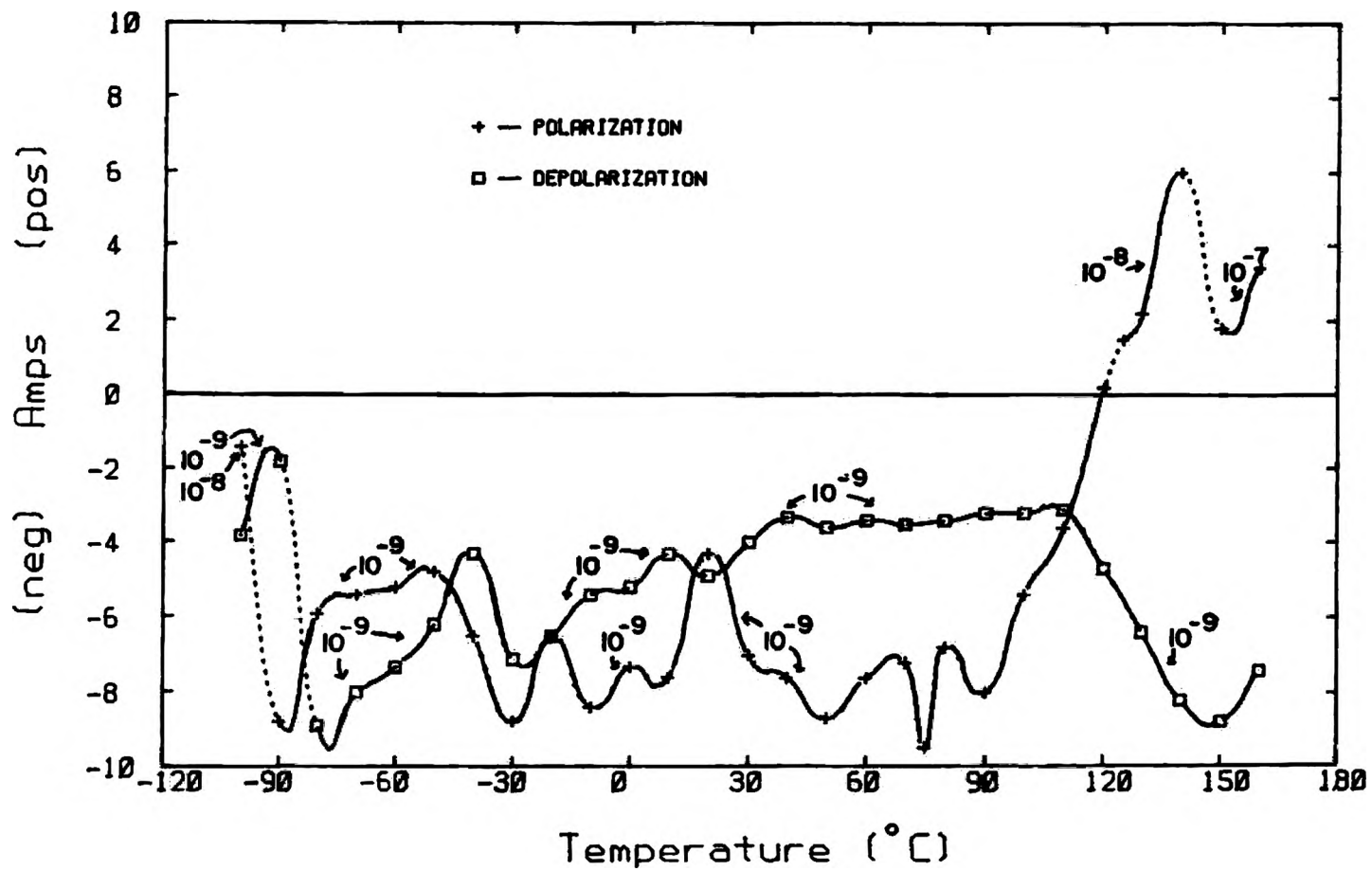


Figure 27. TSPC/TSDC Graph of BX Multilayer Capacitor (Sample #1) with Field of 7200 V/cm and Heating Rate of 0.07 K/s.

For the remaining BX capacitor samples, the polarization spectra will be the main focus of the discussion. Other depolarization spectra to be shown were similar to the spectra illustrated by sample #1. No depolarization spectra were detected with failed BX capacitor samples since no current could be stored within the failed capacitors. Most capacitor failures involved electrical shorting within the capacitor. Also, the activation energies of the BX capacitor samples (excluding failures) showed little change from sample to sample.

Current spectra for BX capacitor samples #2 through #5 (Figures 28-29) showed the effects of lifetesting on the capacitor samples prior to TSPC/TSDC measurements. Samples #2 and #3 were tested under modified lifetest conditions (Sample # 2 subjected to 190°C, 1000 VDC for 17 hours; Sample #3 subjected to 200°C, 800 VDC for 42 hours). Samples #4 and #5 were lifetested using conditions specified in MIL-C-123 for 1000 hours.

BX capacitor samples #3 and #5 survived lifetesting and both showed normal polarization spectra typical of the BX capacitor formulation. On the other hand, BX capacitor samples #2 and #4 showed only positive current throughout their current spectra. Sample #2 had a large current jump around 60°C with resistivity dropping 9 orders of magnitude indicating failure. Samples #4 initially showed low resistivity levels that continued to drop with increasing temperature signifying capacitor failure during lifetesting. The failures in samples #2 and #4 were probably due to electrical shorting within the capacitor at a weak point or hole in a dielectric layer, as seen in the past by other authors²⁰⁻²². Attempts to detect failures through repeated

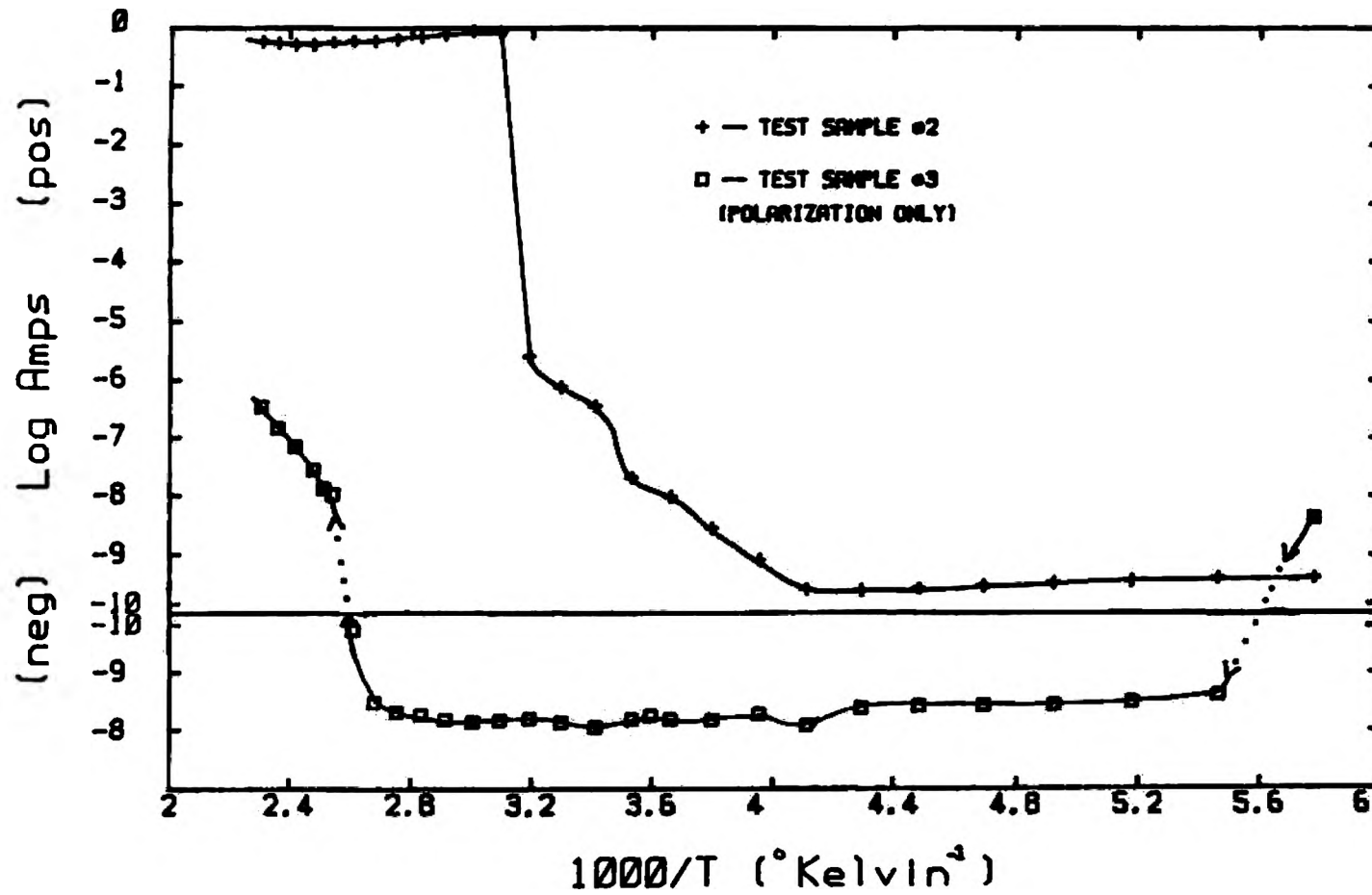


Figure 28. TSPC Graph of BX Multilayer Capacitors (Samples #2 and #3) with Field of 7200 V/cm and Heating Rate of 0.07 K/s.

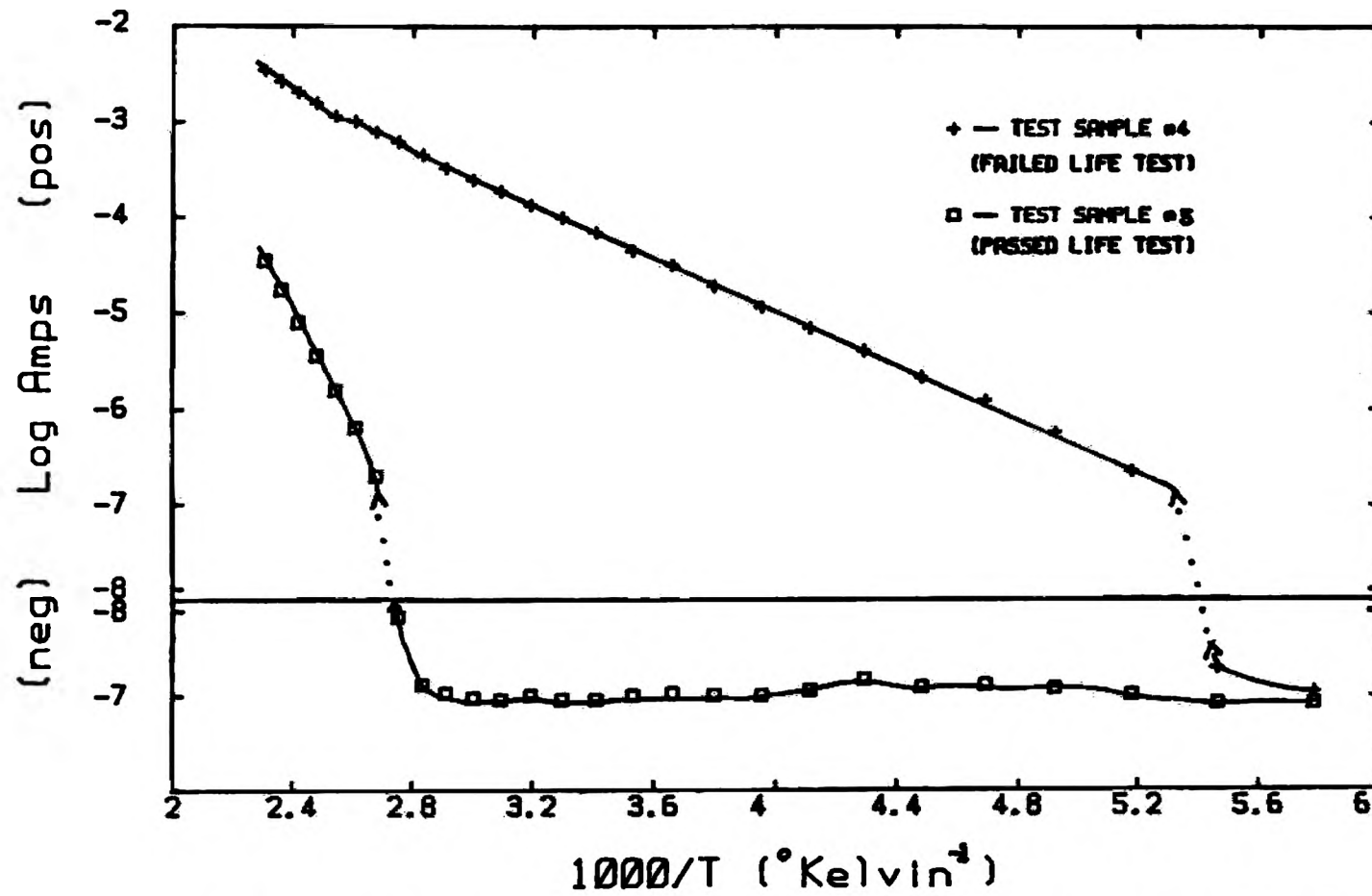


Figure 29. TSPC Graph of BX Multilayer Capacitors (Samples #4 and #5) with Field of 7200 V/cm and Heating Rate of 0.07 K/s.

TSPC/TSDC measurements only showed that the BX capacitor spectra was reproducible.

The methanol screening technique developed by Chittick²³ indicated that sample #6 (Figure 30) should fail accelerated lifetesting (MIL-C-123). The TSPC/TSDC current spectra of sample #6, showed normal BX capacitor current behavior. Since this capacitor was encapsulated, the methanol screening technique apparently indicated surface resistance changes of the sample due to encapsulation flaws instead of internal flaws. Thus, the TSPC/TSDC measurements did not show abnormalities in the capacitor tested.

The current spectrum of a BX capacitor which failed during commercial use (sample #7) is shown in Figure 31. The 1st polarization spectrum for sample #7 was similar to the current spectra of BX capacitor sample #2 except failure began in sample #7 around -20°C. The 2nd polarization spectrum showed that the capacitor failed with low resistivity being measured throughout the spectrum (Table III).

5. Reliability Determination-TSPC/TSDC. One of the main objectives of this study was to see if TSPC/TSDC measurement techniques could distinguish between reliable and unreliable capacitors. The results showed that:

- 1) Differences between a 'good' and a 'failed' capacitor could be distinguished.
- 2) Tendencies of capacitor failure were observed.
- 3) Actual predictions of failure could not be made since typical capacitor failures were erratic and unpredictable with a dependence on formulation and physical defects.

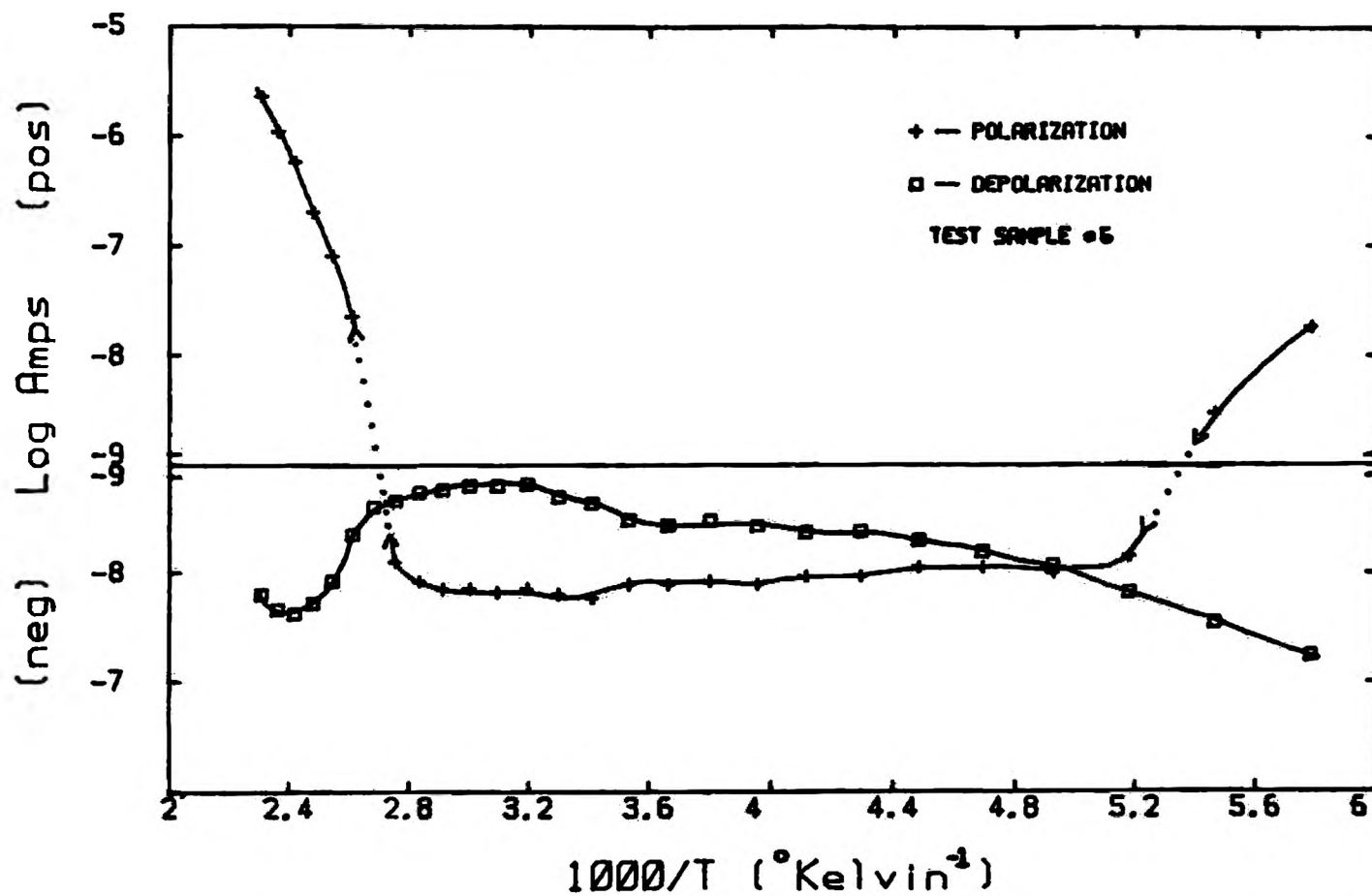


Figure 30. TSPC/TSDC Graph of BX Multilayer Capacitor (Sample #6) with Field of 7200 V/cm and Heating Rate of 0.07 K/s.

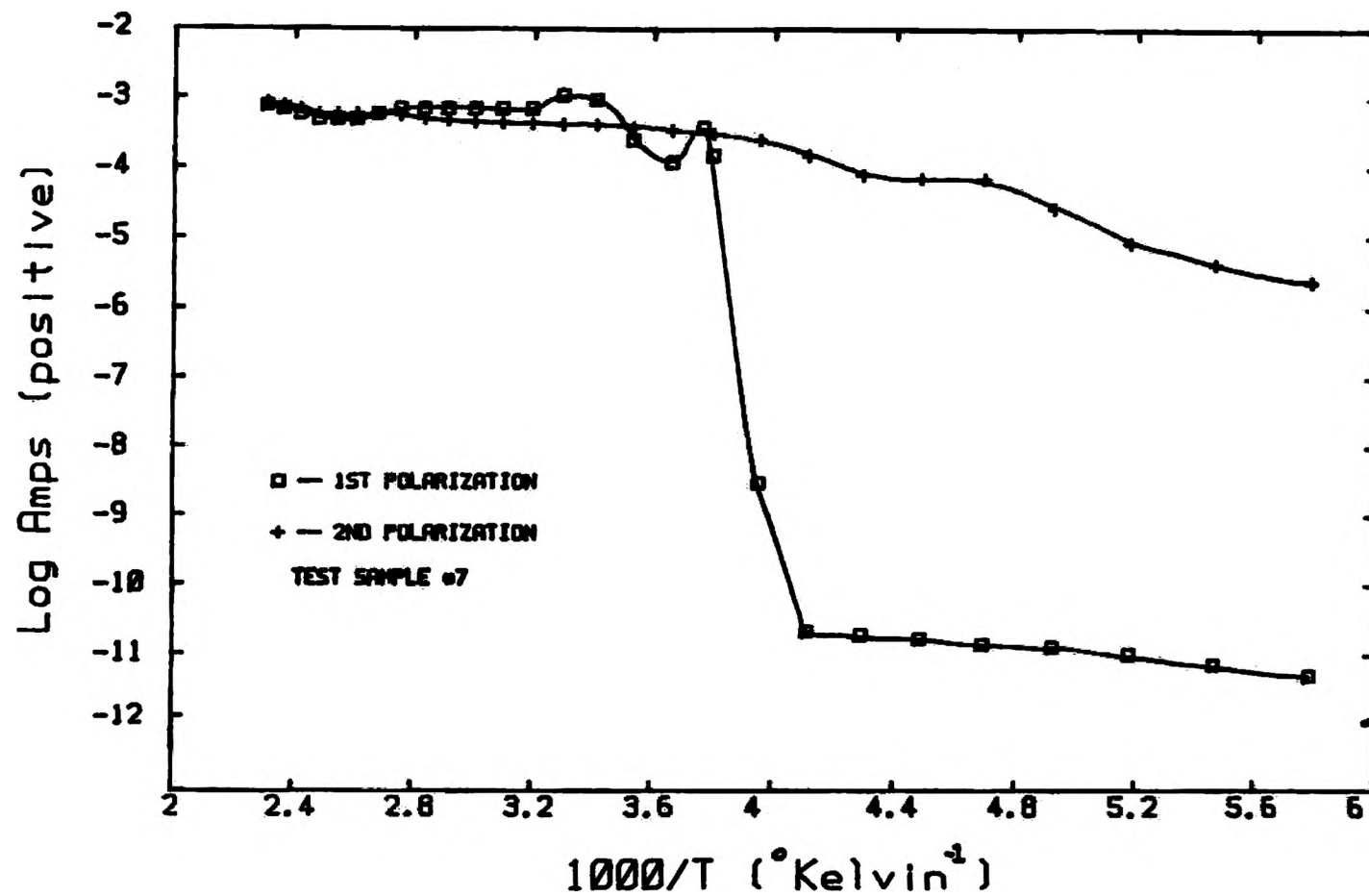


Figure 31. TSPC Graph of BX Multilayer Capacitor (Sample #7) with Field of 7200 V/cm and Heating Rate of 0.07 K/s.

4) The TSPC/TSDC technique appeared to be a good qualitative method to study electrical and material properties of capacitors in conjunction with other capacitor testing methods.

V. CONCLUSION

TSPC/TSDC measurements were used to study the current behavior of BaTiO_3 samples with various Ba/Ti ratios and ceramic multilayer capacitors. The results of these measurements can be concluded as follows:

- 1) The TSPC/TSDC measurements show the affects of varying the Ba/Ti ratio in BaTiO_3 . Changes in the Ba/Ti ratio influence the grain size which in turn affects the current behavior.
- 2) The TSPC/TSDC measurements can identify the structural transformations that occur in BaTiO_3 by the changes in current behavior
- 3) The TSPC/TSDC measurements can determine differences between good and failed capacitors and are sensitivity to changes in capacitor formulation. However, the TSPC/TSDC measurements cannot predict capacitor reliability or predetermine capacitor lifetest results.

REFERENCES

1. J. Keck, "Electrical Degradation of High Purity Barium Titanate," Ph. D. Dissertation, University of Missouri-Rolla, 1976.
2. W.R. Buessem and T.J. Prokopowicz, "Electrode and Material Problems in Ceramic Capacitors," Ferroelectrics, 10, 1976, pp. 225-230.
3. C. Hong and D.E. Day, "Thermally Stimulated Polarization and Depolarization Current (TSPC/TSDC) Technique for Studying Ion Motion in Glasses," Journal of Material Science, 14, 1979, pp. 2493-2499.
4. R. Chen, "Methods for Kinetic Analysis of Thermally Stimulated Processes," Journal of Material Science, 11, 1976, pp. 1521-1541.
5. K. Shindo, "Thermally Stimulated Currents in Dielectrics," Mem. Shiga University, 27, 1977, pp. 1-8.
6. C. Hong and D.E. Day, "Thermally Stimulated Currents in Sodium Silicate Glasses," Journal of the American Ceramic Society, 64, #2, 1981, pp. 61-68.
7. A.K. Agarwal and D.E. Day, "Polarization and Conduction Mechanisms in Mixed-Alkali Glasses," Journal of the American Ceramic Society, 65, #5, 1982, pp. 231-237.
8. C. Bucci and R. Fieschi, "Ionic Thermocurrents in Dielectrics," Physical Review, 148, #2, 1966, pp. 816-823.
9. W.S. McKeever and D.M. Hughes, "Thermally Stimulated Currents in Dielectrics," Journal of Physics D; Applied Physics, 8, 1975, pp. 1520-1529.
10. T. Hino, "Thermally Stimulated Characteristics in Solid Dielectrics," IEEE Transactions on Electrical Insulation, EI-15, #3, 1980, pp. 301-311.
11. F.J. Morin and J.R. Oliver, "Energy Levels of Iron and Aluminum in Strontium Titanate," Physical Review B, 8, #12, 1973, pp. 5847-5854.
12. J.D. Siegwarth and A.J. Morrow, "Low Temperature Polarization in Impure Strontium Titanate Ceramics," Journal of Applied Physics, 47, #11, 1976, pp. 4784-4790.
13. N.N. Lebedeva, et. al., "Photoluminescence, Thermoluminescence, and Thermally Stimulated Conductivity of Strontium Titanate Single Crystals," Soviet Physics, Solid State, 19, #12, 1977, pp. 2152-2153.

14. A.G. Chynoweth, "Dynamic Method for Measuring the Pyroelectric Effect with Special Reference to Barium Titanate," Journal of Applied Physics, 27, #1, 1956, pp. 78-84.
15. A.G. Chynoweth, "Surface Space-Charge Layers in Barium Titanate," Physical Review, 102, #3, 1956, pp. 705-714.
16. W.D. Kingery, Introduction to Ceramics, John Wiley and Sons, New York, 1976, pp. 913-974.
17. W.J. Merz, "The Electric and Optical Behavior of Barium Titanate Single Domain Crystals," Physical Review, 76, 1949, pp. 1221-1225.
18. F. Jona and G. Shirane, Ferroelectric Crystals, Pergamon Press, New York, 1962, pp. 1-27, 108-215.
19. S. Wang, Solid State Electronics, McGraw-Hill, New York, 1966, pp. 391-452.
20. T.F. Brennan, "Ceramic Capacitor Insulation Resistance Failures Accelerated at Low Voltages," IEEE Transactions on Electrical Devices, ED-26, #1, 1979, pp. 102-108.
21. A.M. Holliday, "Unstable Insulation Resistance in Ceramic Capacitors," Symposium on Capacitor Technologies, Application and Reliability, June, 1981, pp. 27-31.
22. G.J. Ewell and D.A. Demeo, "Electrical Parameters of Capacitors Failing the 85 C/85% rh/1.5 VDC Test," Proceedings of the 2nd Capacitor and Resistor Technology Symposium, 1982, pp. EI 1-6.
23. R.C. Chittick, et. al., "Non-Destructive Screening for Low Voltage Failure in Multilayer Ceramic Capacitors," Proceedings of the 3rd Capacitor and Resistor Technology Symposium, March 8-10, 1983, pp. 61-69.
24. K. Sato, et. al., "Mechanism of Ceramic Capacitor Leakage Failure Due to Low DC Stress," IEEE Proceedings of the 18th International Reliability Physics Symposium, 1980, pp. 205-212.
25. W.H. Payne, "MLC Ceramic Dielectrics and Their Role in Reliability," The Reliability of Multilayer Ceramic Capacitors, National Materials Advisory Board (NSF), March 29-31, 1982, pp. 67-90.
26. D.A. Payne, "Concerning the Physics of Failure of Barium Titanate Capacitors," Proceedings of the Sixth Annual Reliability Physics Symposium, Los Angeles, CA, 1967.

27. M. Pechini, U.S. Patent #3330697, July, 1967.
28. H.U. Anderson and D.E. Day, "Reliability Studies of Ceramic Capacitors," Office of Naval Research Report, July, 1983.
29. E. Fatuzzo and W.J. Merz, Ferroelectricity, John Wiley and Sons, New York, 1967, pp. 9-11, 190-234.
30. B. Jaffe, et. al., Piezoelectric Ceramics, Academic Press, New York, 1971, pp. 53-90.
31. C.A. Miller, "Hysteresis Loss and Dielectric Constant in Barium Titanate," British Journal of Applied Physics, 18, 1967, pp. 1689-1697.
32. H.T. Martirena and J.C. Burfoot, "Grain-size Effects on Properties of Some Ferroelectric Ceramics," Journal of Physics C: Solid State Physics, 7, 1974, pp. 3182-3192.
33. W.R. Buessem, L.E. Cross, and A.K. Goswami, "Phenomenological Theory of High Permittivity in Fine-Grained Barium Titanate," Journal of the American Ceramic Society, 49, #1, 1966, pp. 33-36.
34. W.R. Buessem, L.E. Cross, A.K. Goswami, "Effect of Two Dimensional Pressure on the Permittivity of Fine- and Coarse-Grained Barium Titanate," Journal of the American Ceramic Society, 49, #1, pp. 36-39, 1966.
35. G.H. Jonker and W. Noorlander, "Grain-Size of Sintered Barium Titanate," Science of Ceramics, Vol. 1, Academic Press, New York, 1962, pp. 255-264.
36. K. Kinoshita and A. Yamaji, "Grain-Size Effects on Dielectric Properties in Barium Titanate," Journal of Applied Physics, 47, #1, 1976, pp. 371-373.
37. V.F. Capozzi, "Multilayer Ceramic Capacitor Materials and Manufacture," Oxy Metal Industries Corporation, Nutley, NJ.

VITA

Patrick Donald Martin was born on October 21, 1958 in Los Angeles, California. His primary education was at St. Thomas the Apostle School in Florissant, Missouri. He graduated from Rosary High School, located in Spanish Lake, Missouri in June 1977. He entered the University of Missouri-Rolla in August 1977 and graduated with a Bachelor of Science Degree in Ceramic Engineering in May 1981.

After employment as a Process Engineer at AVX Ceramics Corporation, in Myrtle Beach, South Carolina, he returned to the University of Missouri-Rolla to pursue graduate studies in August 1982.

APPENDIX

ADDITIONAL ILLUSTRATIONS

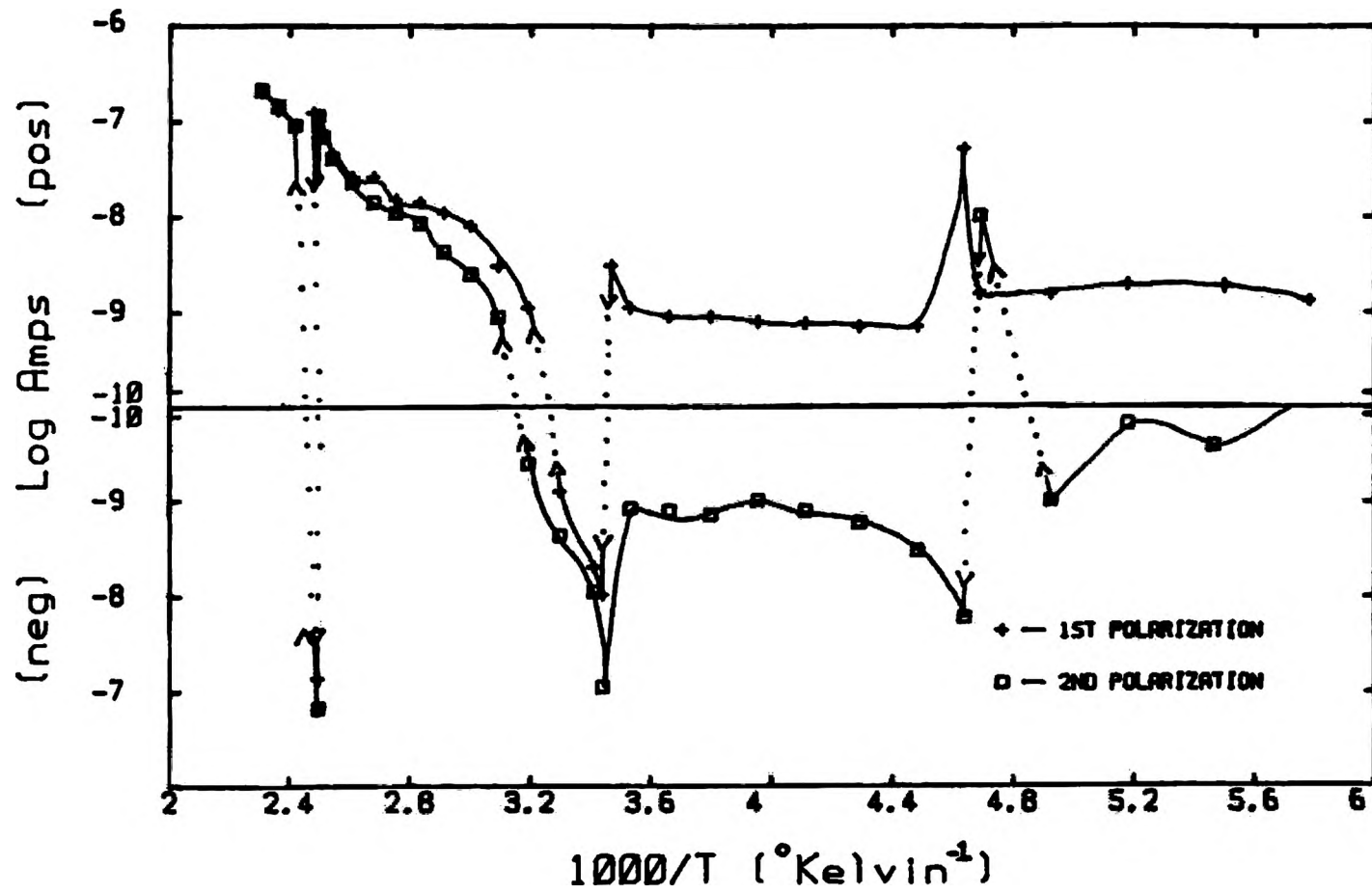


Figure 32. TSPC Graph of Barium Titanate (Ba/Ti = 0.96) with Field of 250 V/cm and Heating Rate of 0.07 K/s.

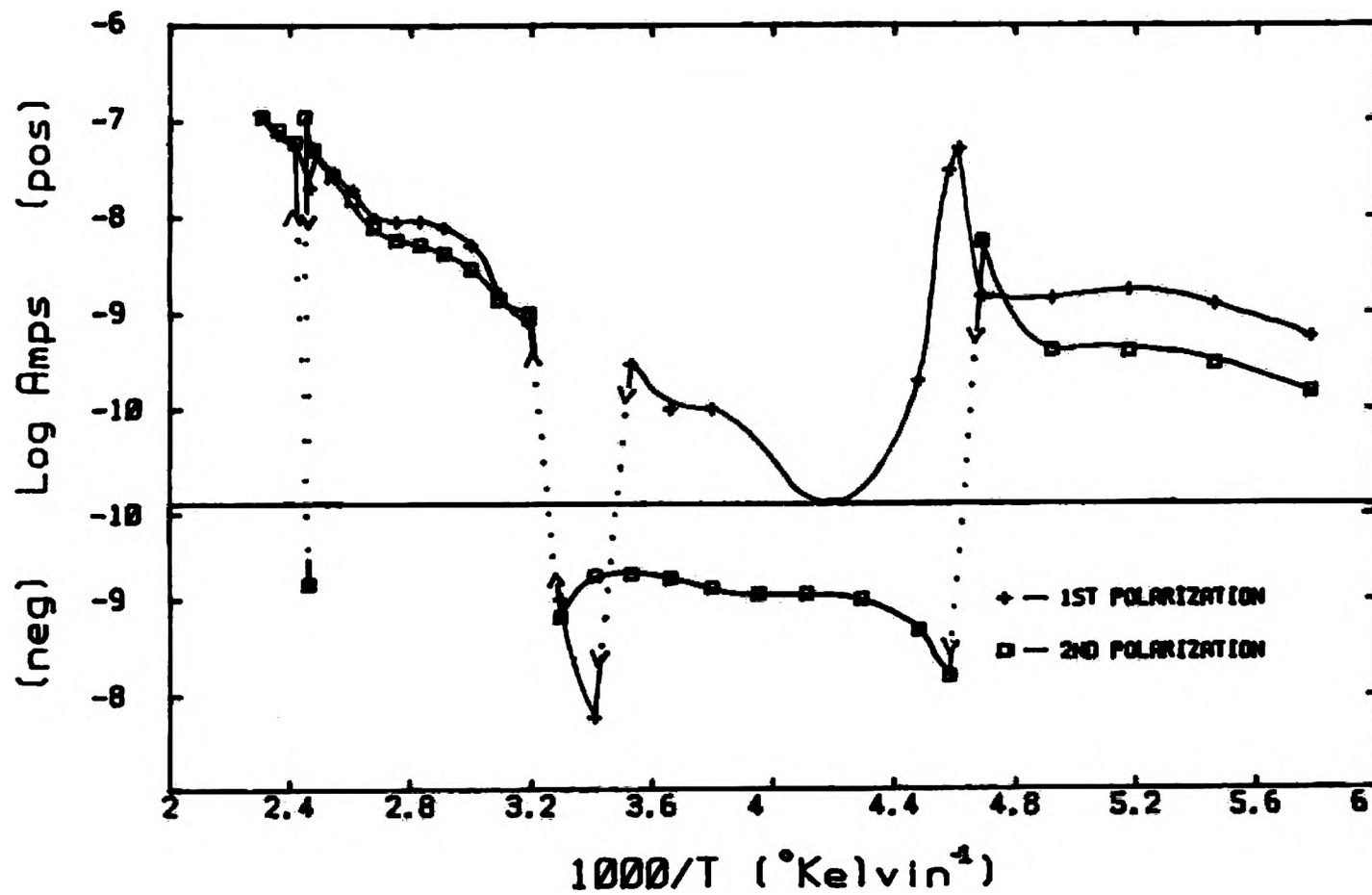


Figure 33. TSPC Graph of Barium Titanate (Ba/Ti = 0.97) with Field of 250 V/cm and Heating Rate of 0.07 K/s.

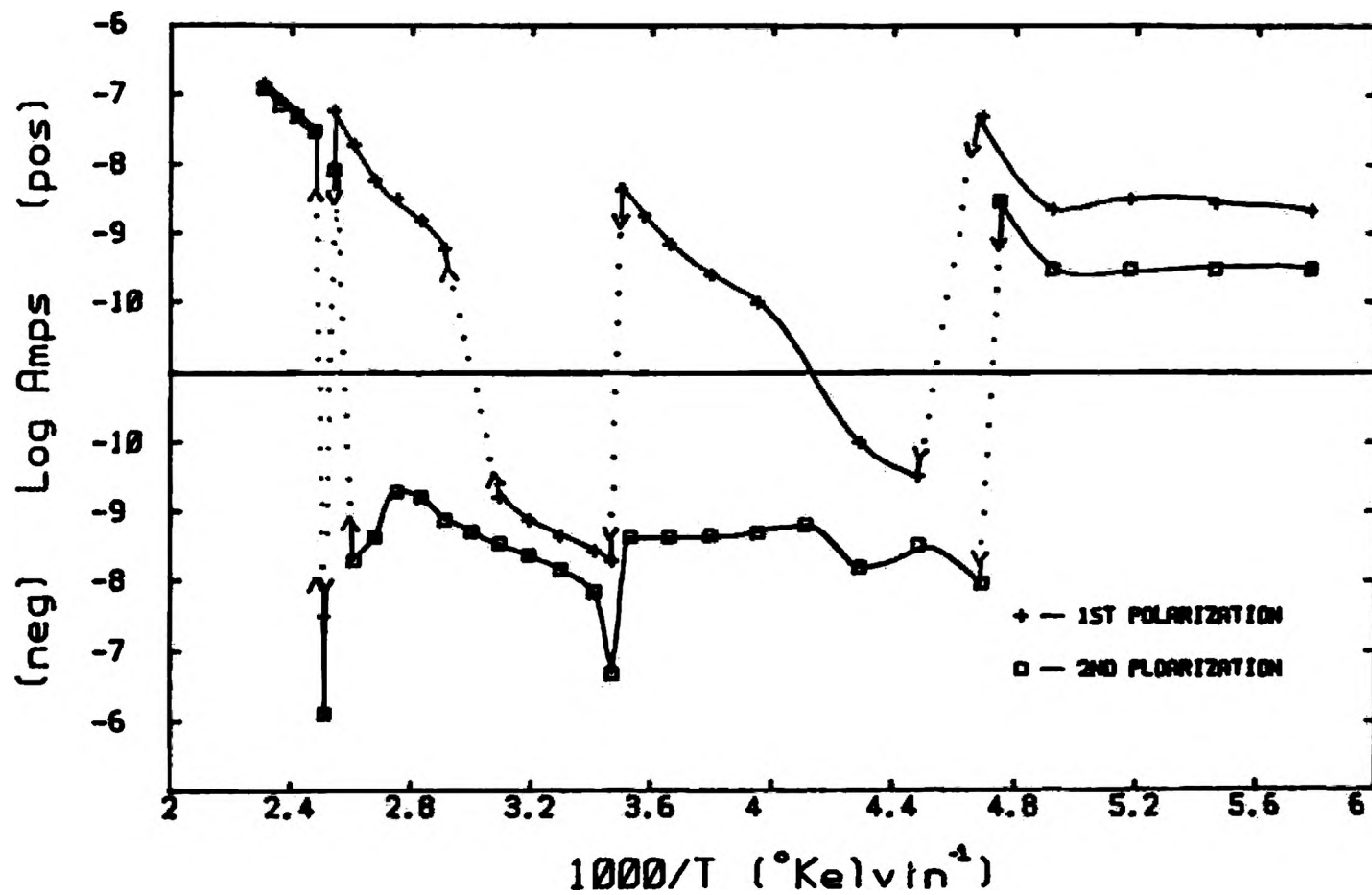


Figure 34. TSPC Graph of Barium Titanate (Ba/Ti = 0.99) with Field of 250 V/cm and Heating Rate of 0.07 K/s.

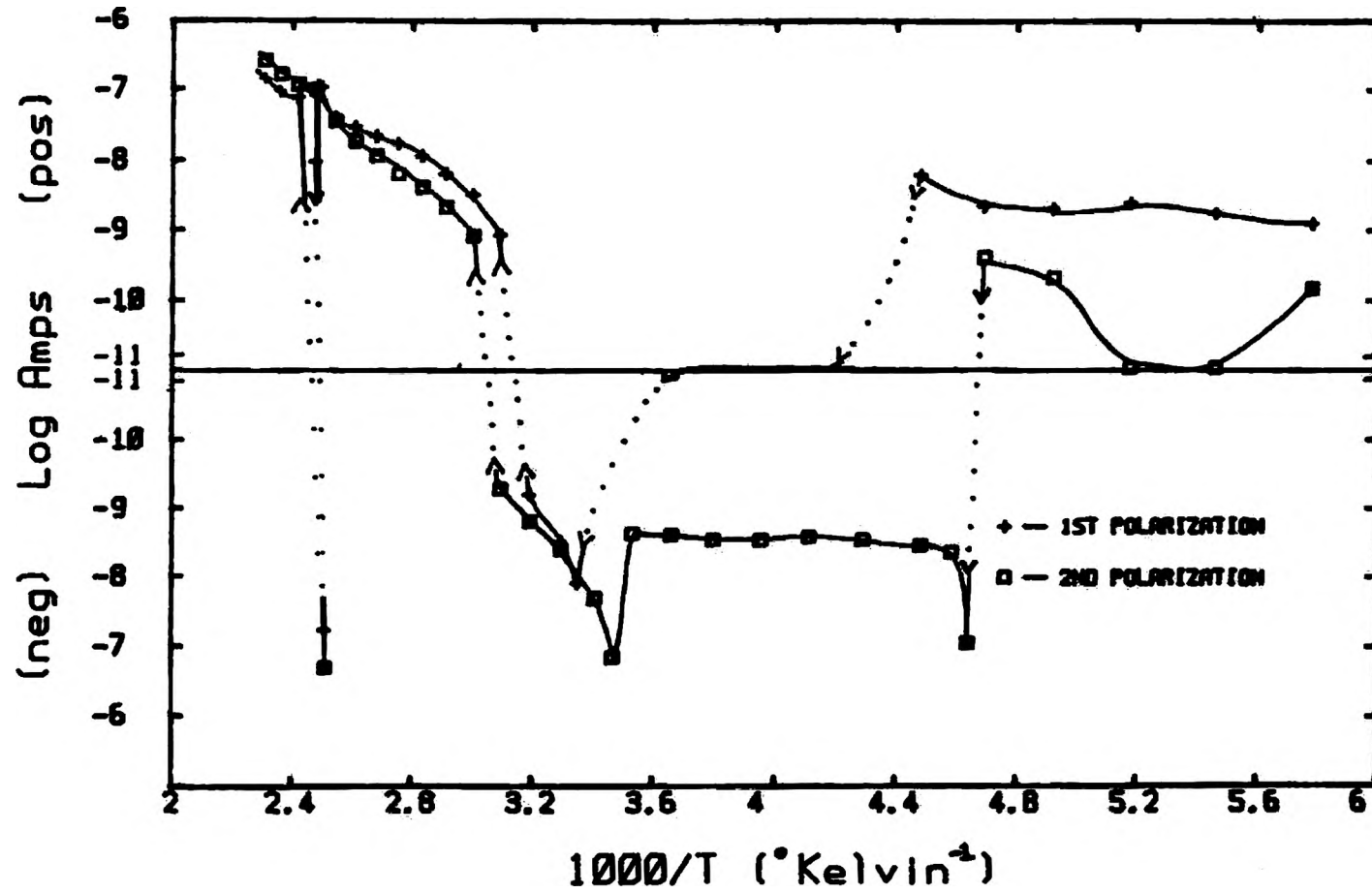


Figure 35. TSPC Graph of Barium Titanate (Ba/Ti = 0.995) with Field of 250 V/cm and Heating Rate of 0.07 K/s.

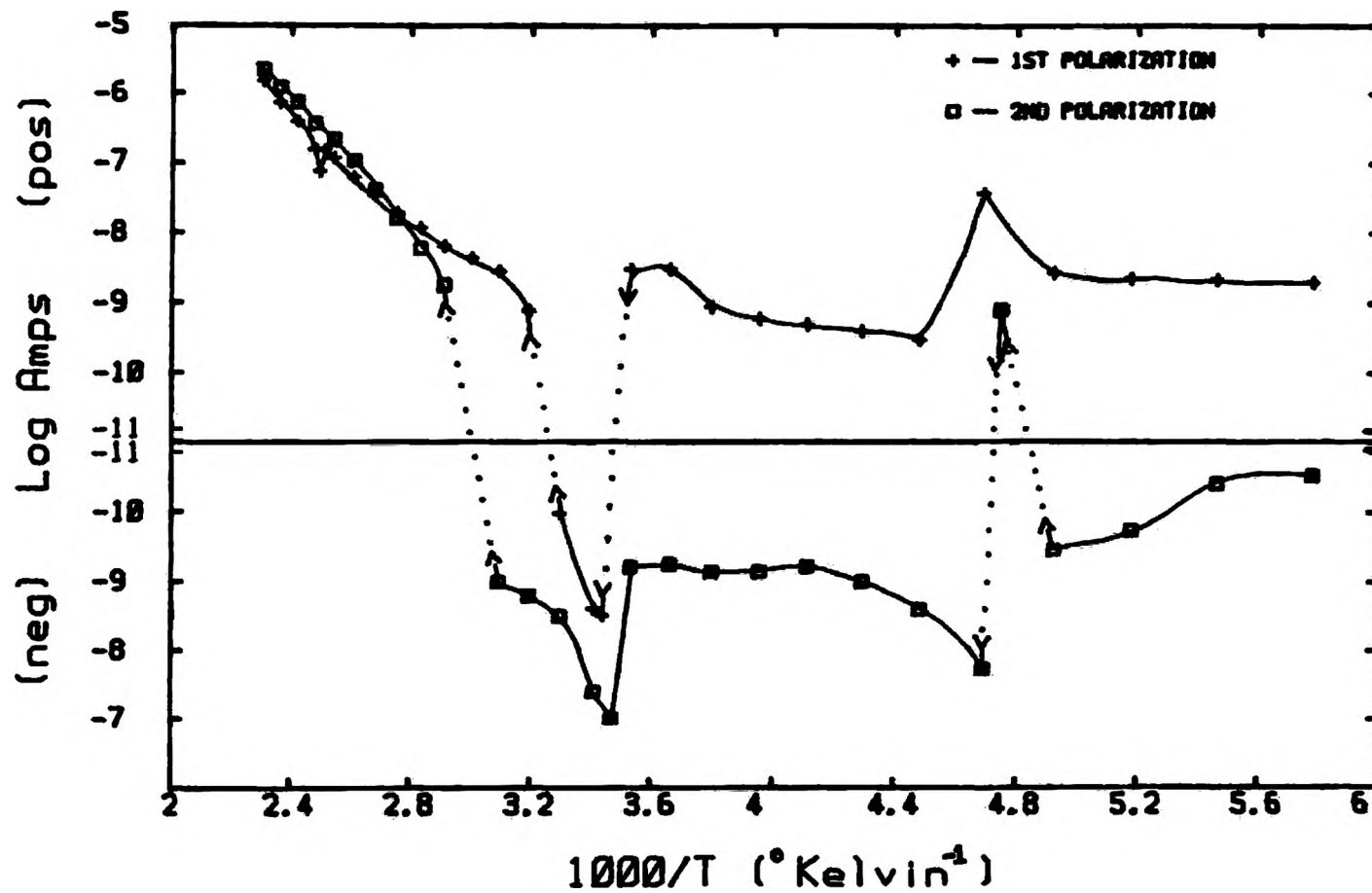


Figure 36. TSPC Graph of Barium Titanate (Ba/Ti = 1.005) with Field of 250 V/cm and Heating Rate of 0.07 K/s.

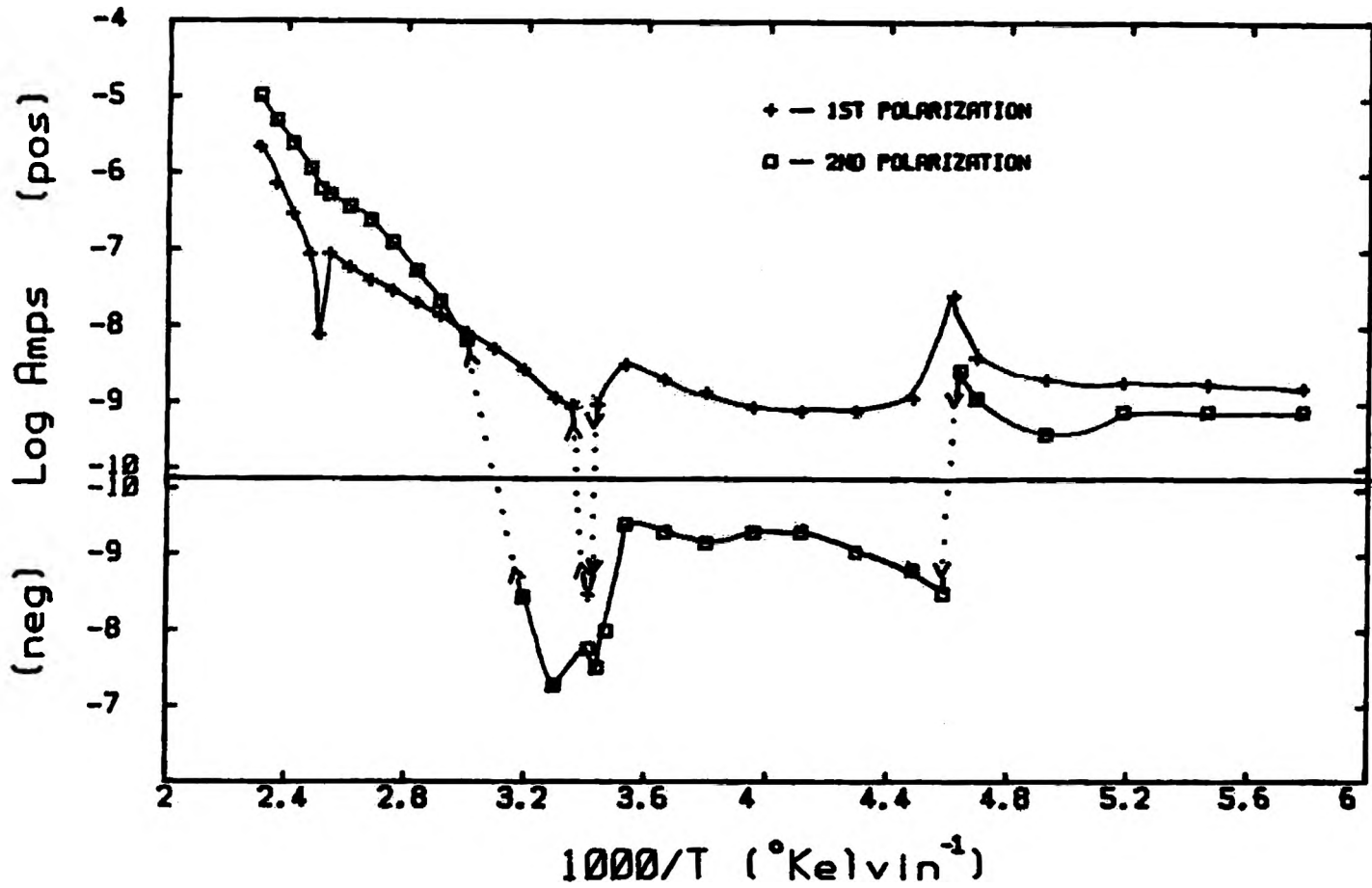


Figure 37. TSPC Graph of Barium Titanate (Ba/Ti = 1.01) with Field of 250 V/cm and Heating Rate of 0.07 K/s.

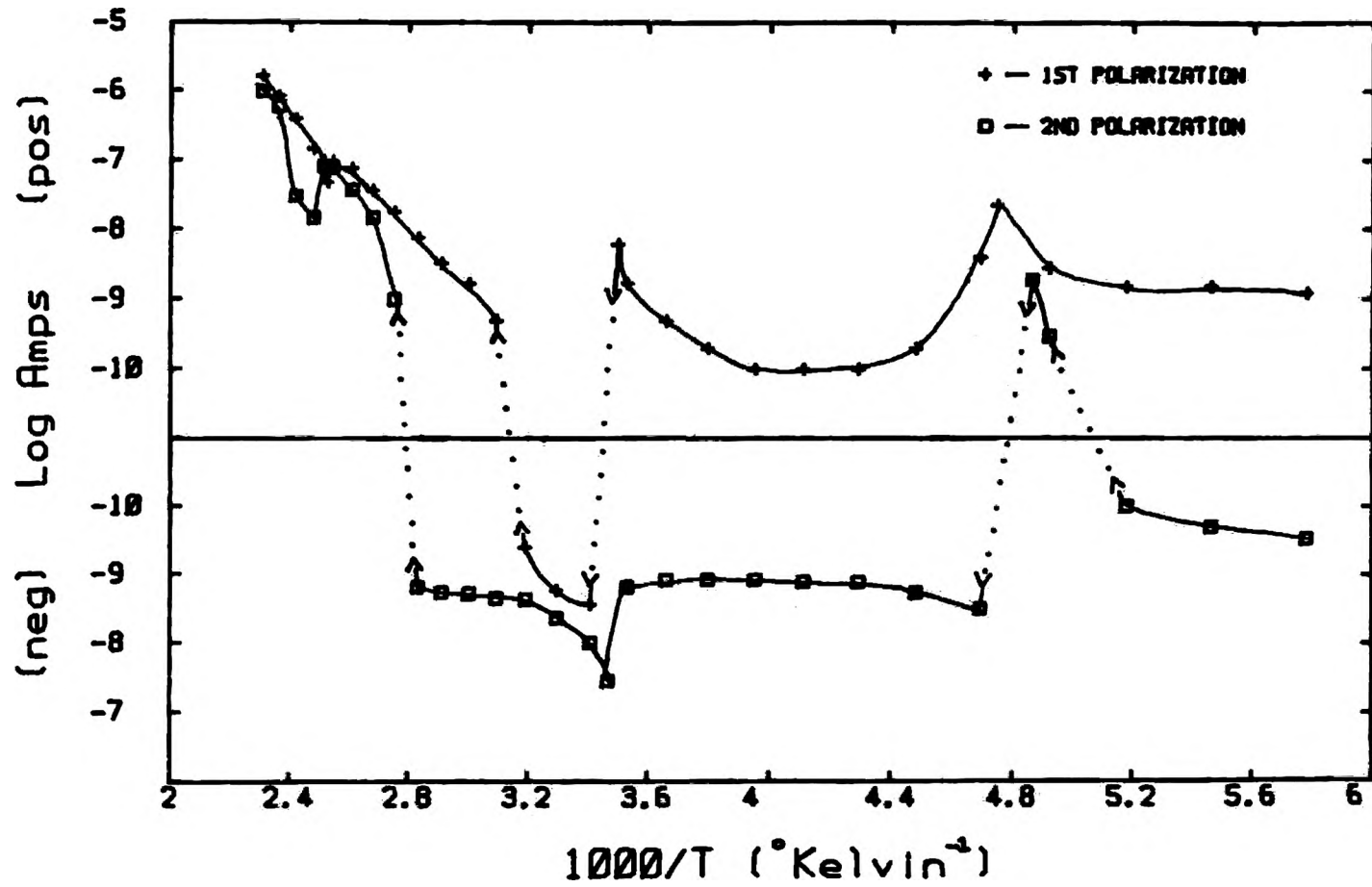


Figure 38. TSPC Graph of Barium Titanate (Ba/Ti = 1.03) with Field of 250 V/cm and Heating Rate of 0.07 K/s.

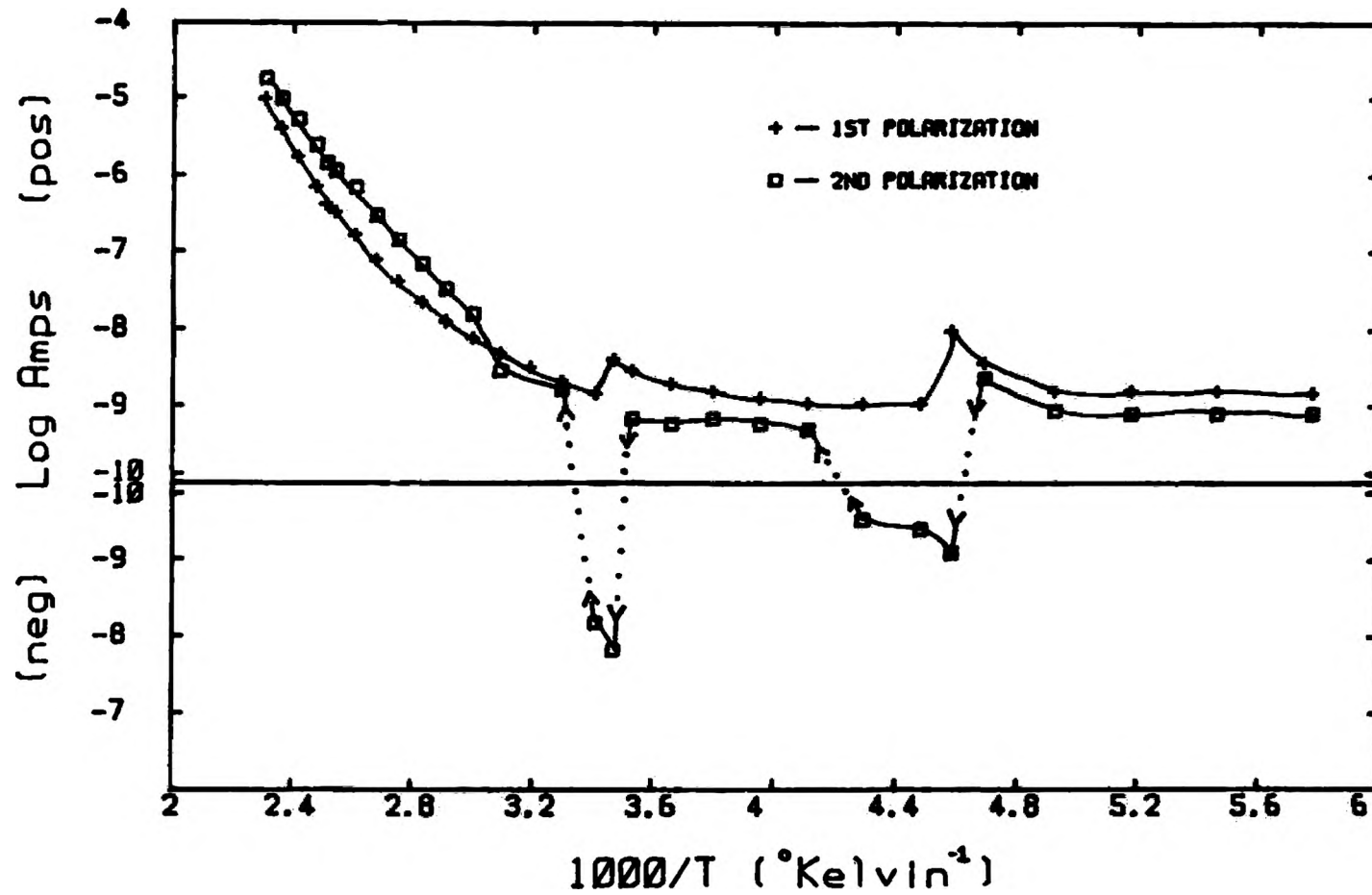


Figure 39. TSPC Graph of Barium Titanate ($\text{Ba/Ti} = 1.04$) with Field of 250 V/cm and Heating Rate of 0.07 K/s.

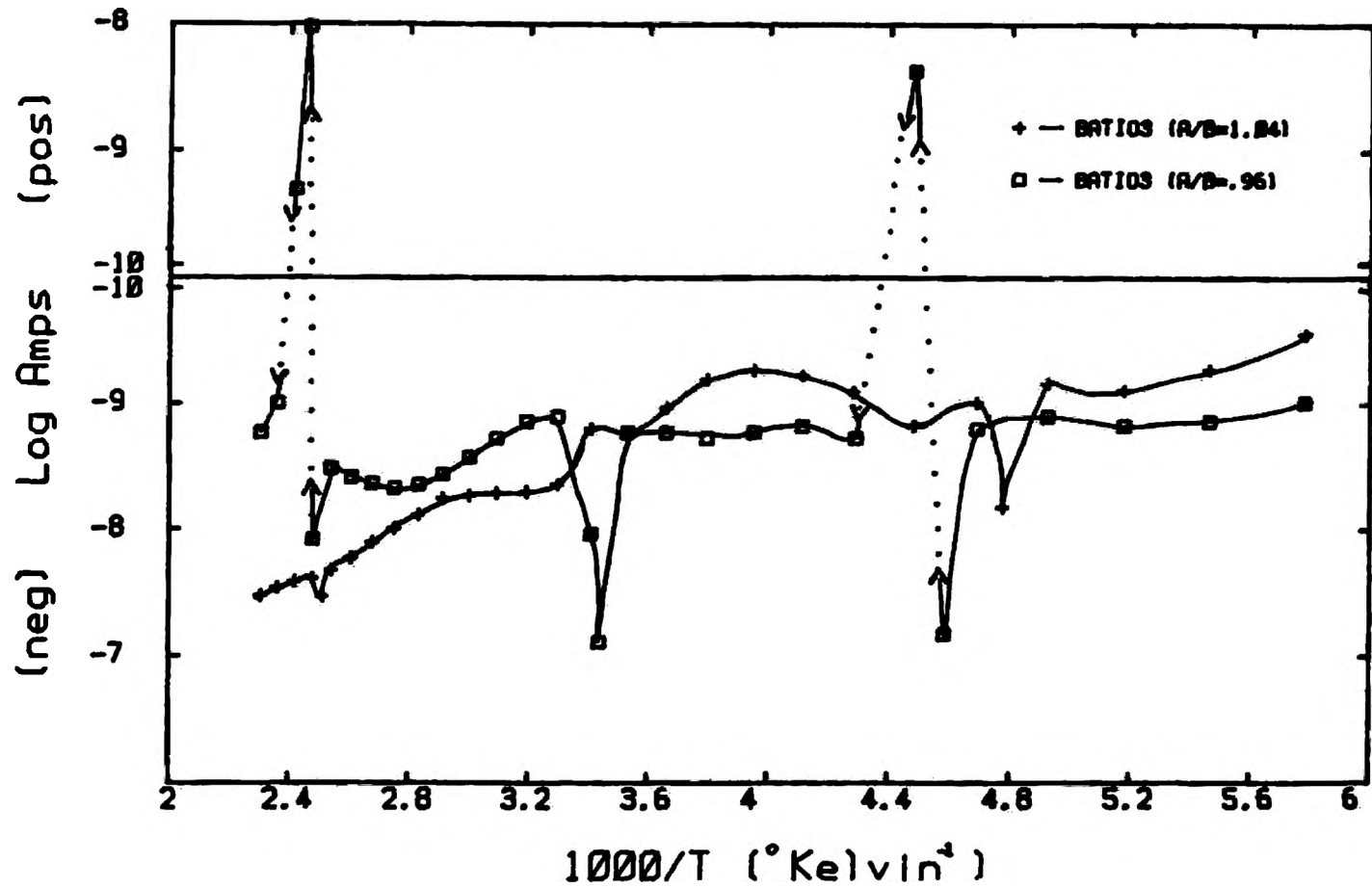


Figure 40. TSDC Graph of Barium Titanate (Ba/Ti = 1.04 and 0.96) with No Field and Heating Rate of 0.07 K/s.

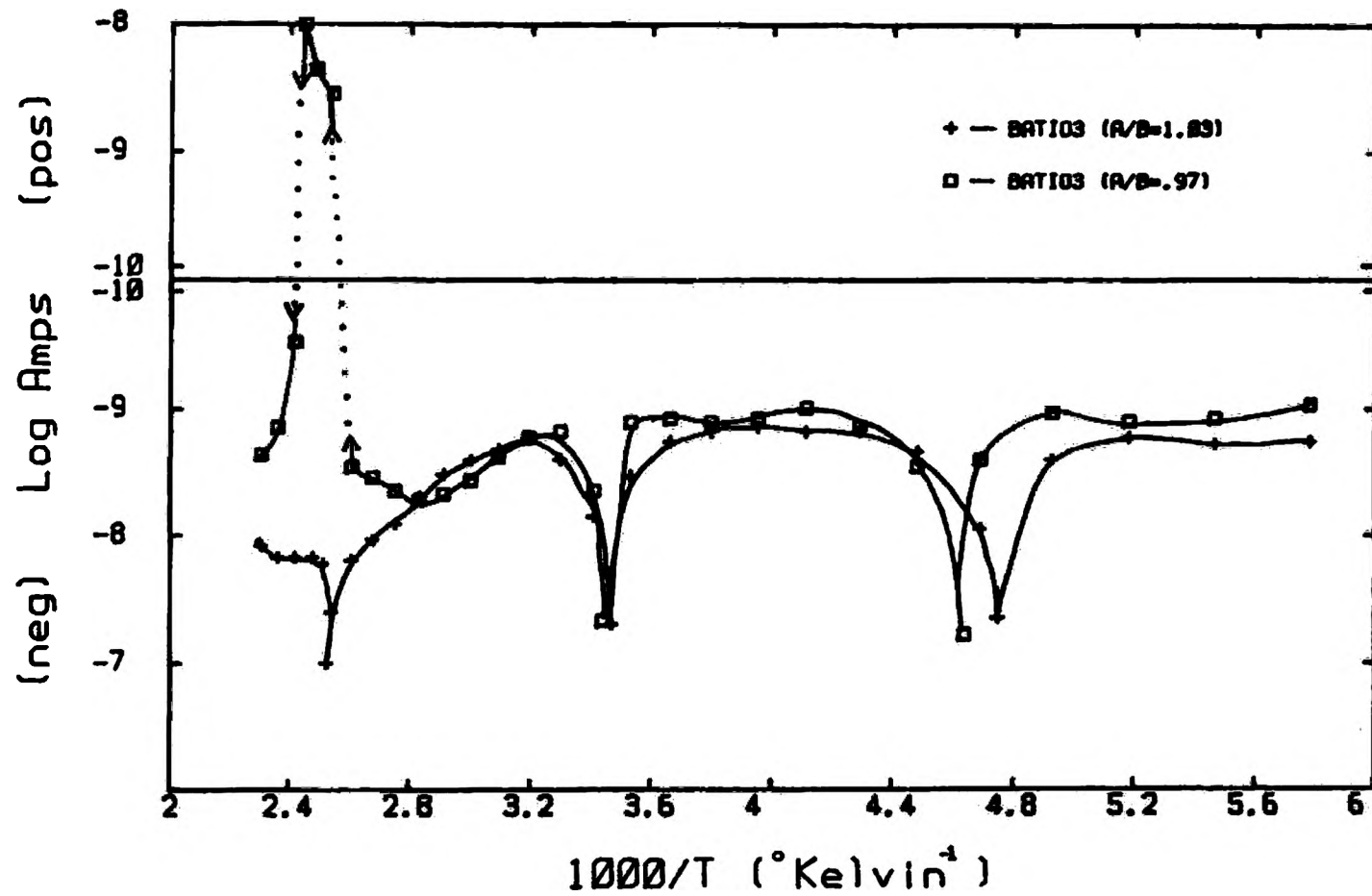


Figure 41. TSDC Graph of Barium Titanate (Ba/Ti = 1.03 and 0.97) with No Field and Heating Rate of 0.07 K/s.

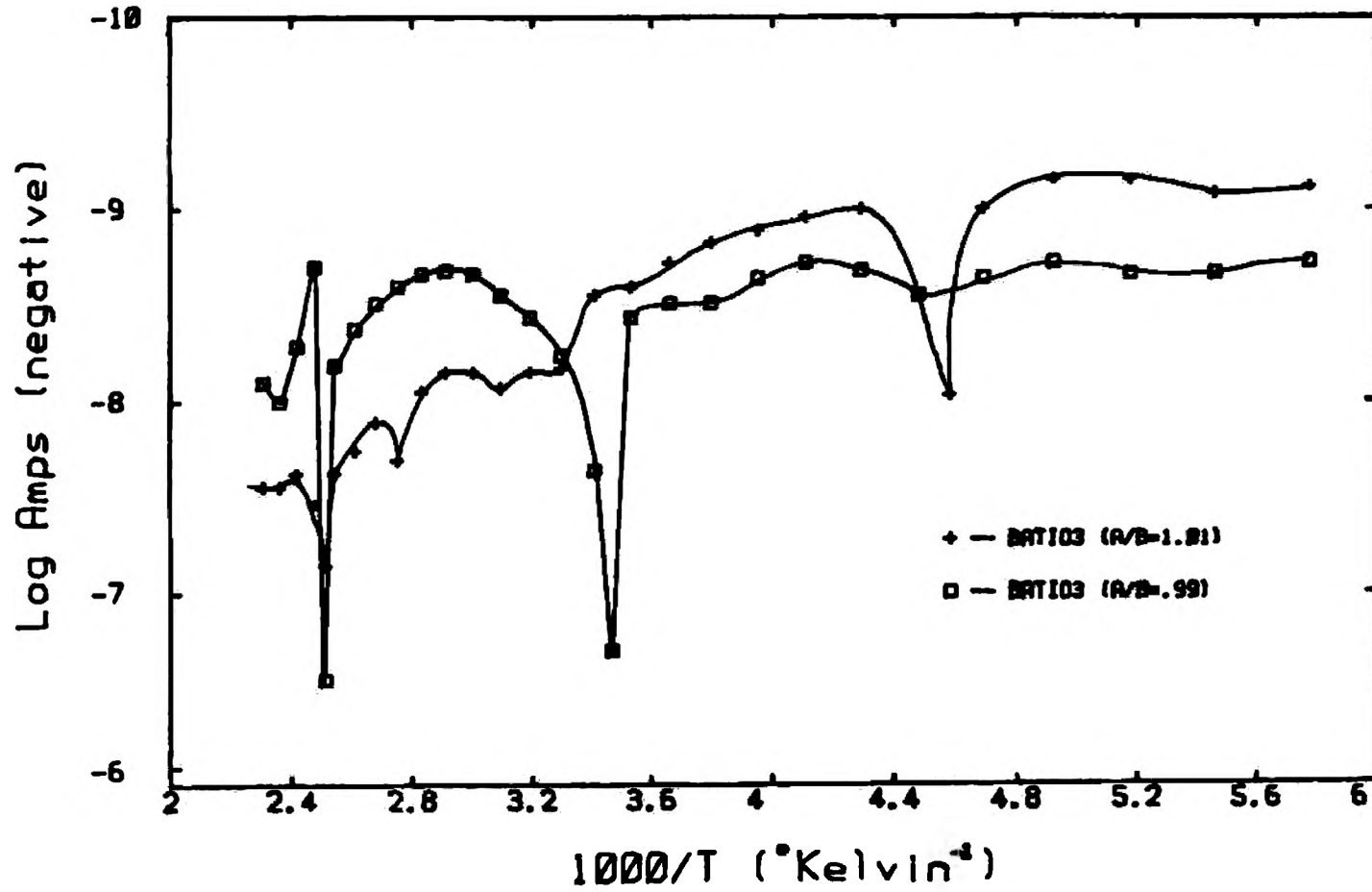


Figure 42. TSDC Graph of Barium Titanate (Ba/Ti = 1.01 and 0.99) with No Field and Heating Rate of 0.07 K/s.

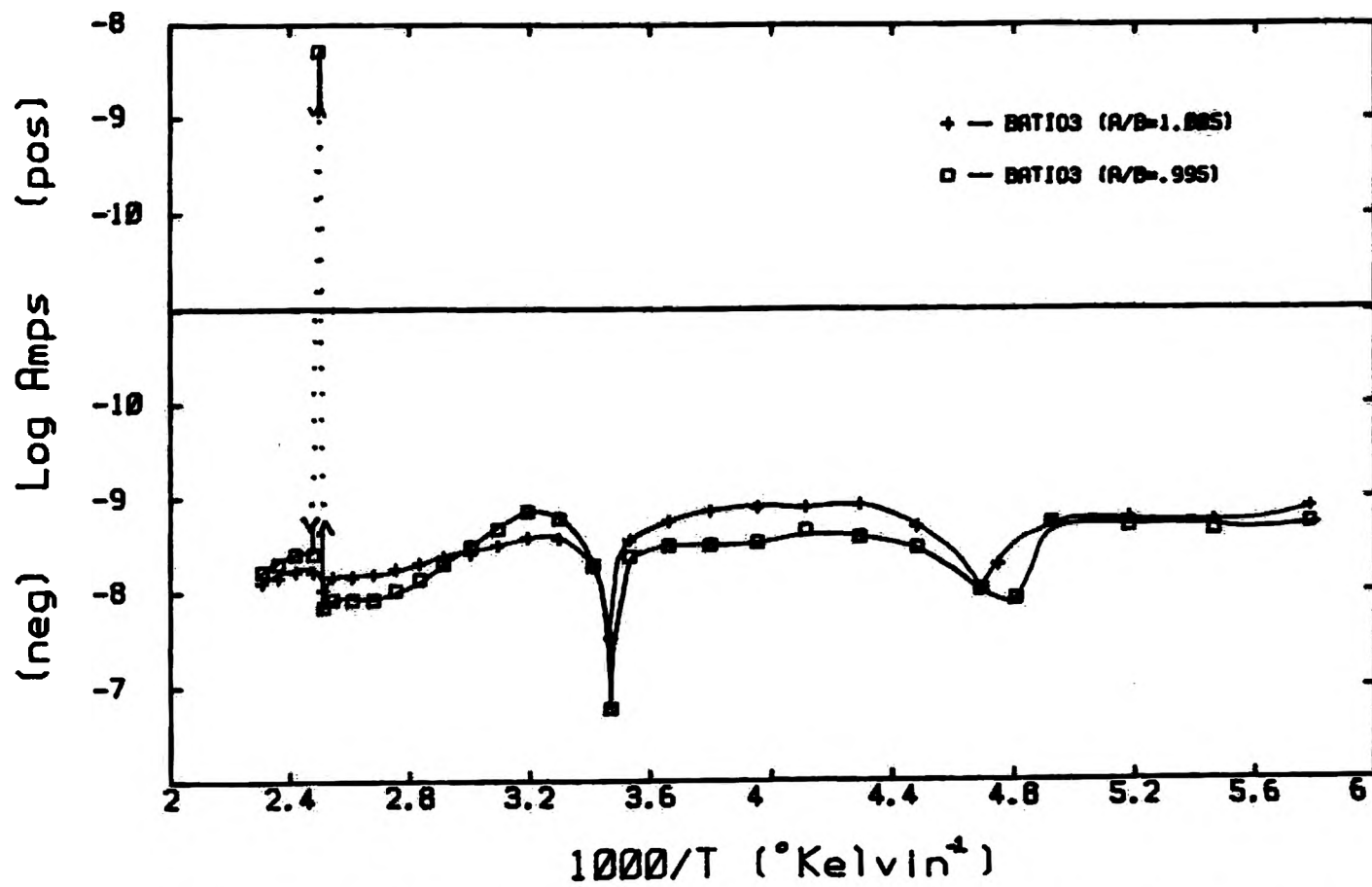


Figure 43. TSDC Graph of Barium Titanate (Ba/Ti = 1.005 and 0.995) with No Field and Heating Rate of 0.07 K/s.